Secretory Leukocyte Protease Inhibitor: a potential target to improve immune response in ovarian cancer

By Maryam ECHAIBI

Thesis submitted to the University of Ottawa in partial fulfillment of the requirement for the M.Sc. degree in Cellular and Molecular Medicine

Department of Cellular and Molecular Medicine
Faculty of Medicine
University of Ottawa

Table of Contents

Abstract

Understanding the communication between cancer cells and immune cells is crucial, particularly in ovarian cancer, given its aggressive and heterogeneous nature. This interaction becomes even more complex when cancer cells undergo epithelial-to-mesenchymal transition (EMT), which enhances their invasive capabilities. In this study, we analyzed cell-cell communication in 34 high-grade serous ovarian cancer single-cell RNA-sequencing datasets, focusing on three distinct EMT phenotypes: epithelial, partially mesenchymal, and mesenchymal. Our findings revealed a significant interaction mediated by the Secretory Leukocyte Protease Inhibitor (SLPI), a small, secreted protein highly expressed in ovarian cancer cells, particularly in the mesenchymal state, with CD4 receptors on immune cells. The functional consequences of this interaction are not well understood. To address this, we first identified the pathways regulating SLPI expression by comparing its baseline levels in genetically defined mouse ovarian cancer cell lines to non-cancerous cell lines. SLPI expression was found to be highly variable and primarily regulated by the MEK/ERK signaling pathway. Additionally, we explored the immune functions of SLPI both *in vitro* and *in vivo*, finding that SLPI is associated with an increased presence of immune cells expressing the immune checkpoint molecules PD-1 and its ligand PD-L1, particularly in CD4+ T cells. These results suggest that SLPI should be investigated further as a potential target to improve immune response in ovarian cancer.

Acknowledgments

The completion of this project would not have been possible without the support of many individuals. First and foremost, I would like to express my heartfelt gratitude to my primary supervisor, Dr. Barbara Vanderhyden. Her unwavering support, insightful guidance, and continuous encouragement throughout this research journey have been pivotal. From day one, she provided me with the academic freedom to explore new techniques and expand my critical thinking, while offering constructive feedback that transformed my weaknesses into strengths. I am truly fortunate to have had the opportunity to learn under her mentorship. I would also like to extend my sincere thanks to my co-supervisor, Dr. Arvind Mer, who was always available to answer my questions and guide me through the bioinformatic complexities of this project. His insights and support have been greatly appreciated. My deep appreciation also goes to my colleagues in the Vanderhyden lab for their unwavering support. Particularly, I would like to thank Dr. Edward Yakubovich, a former PhD student, who mentored me in bioinformatics, and Vincent Miranda, who generously taught me essential lab techniques. I am also grateful to Dr. Kristianne Galpin, Dr. Galaxia Rodriguez, and Sara Asif for their indispensable contributions especially in immunology, each of which played a crucial role in the success of this project. Special thanks are also due to Dr. John Abou-Hamad for his valuable support in Western blotting techniques and for his patience in answering my endless questions. Lastly, I thank Elizabeth Macdonald for always being present for me and being my go-to “first-aid” person in the lab. Her valuable time and support, especially with respect to anything related to animal work. Last but not least, I am very grateful for my parents for their continuous support. Their belief in me has been the bedrock upon which I have built my academic pursuits. Without their guidance and sacrifices, this achievement would not have been possible. Thank you for always being there for me, every step of the way.

List of Tables

List of Figures

List of Abbreviations

AKT	Protein Kinase B
BRCA1/2	Breast Cancer gene 1/2
CA-125	Cancer Antigen 125
CAFs	Cancer-Associated Fibroblasts
CCC	Clear Cell Carcinoma
Ccl5	Chemokine (C-C Motif) Ligand 5
CCNE1	Cyclin E1
CTLA-4	Cytotoxic T-Lymphocyte-Associated Protein 4
Cxcl1	Chemokine (C-X-C Motif) Ligand 1
DC	Dendritic Cell
E/M	Epithelial/Mesenchymal Hybrid State
EC	Endometrioid Carcinoma
ECM	Extracellular Matrix
EGF	Epidermal Growth Factor
EMT	Epithelial-to-Mesenchymal Transition
EMT-TF	EMT-Transcription Factors
EOC	Epithelial Ovarian Cancer
EPI	Epithelial
ERK	Extracellular Signal-Regulated Kinase
FOXO/FOXA	Forkhead Box O/A
GDP	Guanosine Diphosphate
GM-CSF	Granulocyte-Macrophage Colony-Stimulating Factor
GTP	Guanosine Triphosphate
HE4	Human Epididymis Protein 4
HGSC	High-Grade Serous Carcinoma
HIF	Hypoxia-Inducible Factor
IB	Immunoblotting
IFNγ	Interferon Gamma

IL-4	Interleukin-4
Il-6	Interleukin-6
IP	Intraperitoneal
LAG3	Lymphocyte Activation Gene 3
LGSC	Low-Grade Serous Carcinoma
M1	Pro-inflammatory Macrophages
M2	Anti-inflammatory Macrophages
MAPK	Mitogen-Activated Protein Kinase
MC	Mucinous Carcinoma
MEK	Mitogen-Activated Protein Kinase Kinase
MES	Mesenchymal
MMP	Matrix Metalloproteinase
mTOR	Mechanistic Target of Rapamycin
MYC	Myelocytomatosis Oncogene
NF1	Neurofibromin 1
NK	Natural Killer Cells
OSE	Ovarian Surface Epithelium
PCOS	Polycystic Ovary Syndrome
PD-1	Programmed Cell Death Protein 1
PDK1	Phosphoinositide-Dependent Kinase 1
PD-L1	Programmed Death-Ligand 1
PI3K	Phosphoinositide 3-Kinase
PIP2	Phosphatidylinositol 4,5-Bisphosphate
PIP3	Phosphatidylinositol 3,4,5-Trisphosphate
PTEN	Phosphatase and Tensin Homolog
RAF	Rapidly Accelerated Fibrosarcoma
RAS	Rat Sarcoma Viral Oncogene
SCCOHT	Small Cell Carcinoma of the Ovary, Hypercalcemic Type
scRNA-seq	single-cell RNA-sequencing
SD	Standard Deviation

SEM	Standard Error of the Mean
SLPI	Secretory Leukocyte Protease Inhibitor
SMAD	Mothers Against Decapentaplegic Homolog
SNAIL	SNAI1 Zinc Finger Protein
STIC	Serous Tubal Intraepithelial Carcinoma
TAM	Tumor-Associated Macrophages
TGFβ	Transforming Growth Factor Beta
TIM3	T-Cell Immunoglobulin and Mucin-Domain Containing-3
TLR	Toll-Like Receptor
TME	Tumor Microenvironment
TP53/P54	Tumor Protein 53 / Phosphorylated 53
TWIST	Twist Family BHLH Transcription Factor
VEGF	Vascular Endothelial Growth Factor
ZEB	Zinc Finger E-Box Binding Homeobox

Chapter 1: Introduction

1.1 Ovarian Cancer

1.1.1 Development of ovarian cancer

Cancer is a natural process characterized by abnormal cellular division, which can occur in any part of the human body and result from hereditary genes or mutations. Cancer cells exhibit distinct behaviors, defined by 10 hallmarks: evasion of growth suppressors, avoidance of immune destruction, resistance to cell death, activation of invasion and metastasis, induction of angiogenesis, tumor-promoting inflammation, enabling replicative immortality, promotion of genomic instability and mutation, sustained proliferative signaling, and disruption of metabolic pathways[1,2]. These hallmarks offer a foundational framework for understanding the complex biology of cancer. Therefore, researchers and clinicians can better navigate the pathways that drive cancer research and clinical practice by examining each hallmark individually and exploring their interactions. However, this approach should be personalized for each type of cancer and its subtypes, as the hallmarks are highly variable.

Gynecologic cancer, unique to women, targets the reproductive organs[3]. There are five main types: cervical, ovarian, uterine, vaginal, and vulvar cancer[3]. Among these, uterine cancer is the most predominant in Canada, with an estimated 8,600 women diagnosed in 2024[4]. Ovarian cancer is the second most frequently diagnosed gynecological cancer, with an estimated 3,000 cases in 2024, and about 2,000 expected deaths[5]. On the scale of all cancers, ovarian cancer is the fourth leading cause of cancer-related deaths among women, responsible for 5% of these deaths

compared to breast cancer (13%), the first most responsible of cancer-related deaths among women[6]. Although a 2.6% decrease in the incidence of ovarian cancer was observed from 2014 to 2024, the 5-year overall survival rate is only 45%[7].

The low survival rate of ovarian cancer is largely attributed to late diagnosis, as the disease often presents with few or no symptoms in its early stages[8]. Over the years, extensive research has focused on identifying risk factors for ovarian cancer, aiming to identify women at higher risk and encourage them to undergo regular check-ups for early detection or consider prophylactic oophorectomy. Several hypotheses have been proposed to explain the risk factors associated with ovarian cancer. One prominent theory is the "incessant ovulation" hypothesis, which suggests that increased ovulation leads to more frequent ruptures and repairs of the ovarian surface epithelium, thereby increasing the risk of DNA damage and, subsequently, cancer development[9]. Therefore, factors associated with a decrease in ovulation rate, such as use of oral contraceptives, were associated with protective strategies for ovarian cancer. Conversely, late menopause, which prolongs the fertile period and therefore increases the lifetime number of ovulations, contributes to ovarian cancer risk[9].

Family history and inherited genetic predispositions are also associated with a higher probability of developing ovarian cancer[9]. For example, the Breast Cancer 1 and 2 (*BRCA1* and *BRCA2*) genes encode for proteins that are responsible for homologous DNA repair. They are also the most altered cancer predisposition genes in breast and ovarian cancers. Women with germline mutations in these genes face a significantly higher risk of developing tumors, with the likelihood increasing notably between the ages of 35 and 45[10]. Additionally, mutations in other genes, such as *SMARCA4*, have been linked to a rare type of ovarian cancer called small cell carcinoma of the ovary hypercalcemic type (SCCOHT)[10].

Epidemiological studies have identified several other factors related to an increased risk of ovarian cancer, including polycystic ovarian syndrome (PCOS), endometriosis, obesity, and smoking[11,12]. On the other hand, the use of oral contraceptives has been shown to reduce the risk of ovarian cancer by 40% to 50%, even among women with heightened risk, making it a significant protective measure[12].

1.1.2 Subtypes of ovarian cancer

Ovarian cancer can be classified into three main types: epithelial, germ cell, and sex-cord stromal cancer[13]. More than 90% of diagnosed patients have an epithelial ovarian cancer (EOC) type, and it is thus the most common type[14]. Germ cell and sex-cord stromal cancers are rare cases that account for up to 5%[14]. Epithelial ovarian cancer is divided into 5 subtypes: High-grade serous carcinoma (HGSC), endometrioid carcinoma (EC), clear cell carcinoma (CCC), low-grade serous carcinoma (LGSC), and mucinous carcinoma (MC)[15]. They can be differentiated based on histology and mutations in specific proteins[15]. For instance, the CTNNB1 gene is highly mutated in the EC subtype and is thus used as its marker during immunohistochemistry[15,16].

HGSC is the most aggressive subtype of EOC for several reasons. It accounts for nearly 75% of all EOC diagnoses, whereas EC constitutes about 10% of EOC cases, and CCC is found in only 5% to 10% of diagnosed patients[14,16]. The less common EOC subtypes, LGSC and MC, each occur in less than 5% of EOC patients[17,18]. HGSC has a heterogenous morphology, histologically, where tumor cells have abnormal cell nuclei in different sizes and shapes with an abundance of proliferation[19]. The tissue of origin for HGSC was long believed to be the ovarian surface epithelium (OSE) or ovarian inclusion cysts derived from it. However, recent studies have revealed that premalignant lesions arise in the epithelium of the distal fallopian tube. These lesions, known

as serous tubal intraepithelial carcinomas (STIC), share common gene mutations and other similarities with HGSC, and thus are now suggested to develop into HGSC, which subsequently spreads to the ovary[20]. Genetically, HGSC is characterized by somatic mutations in *TP53*, the gene coding for the tumor suppressor protein p53[21], in approximately 97% of cases[22]. These mutations lead to the dysfunction of p53, a crucial protein that plays a key role in regulating DNA repair and initiating apoptosis when DNA damage is irreparable[22]. In addition to *TP53* mutations, HGSC frequently exhibits mutations in homologous repair genes such as *BRCA1* and *BRCA2*, along with amplification of oncogenes like *MYC* and Cyclin E1 (*CCNE1*), and deletions of tumor suppressor genes such as Neurofibromatosis type 1 (*NF1*) and the Phosphatase and tensin homolog (*PTEN*)[23]. These alterations lead to the activation of multiple signaling pathways that promote tumor growth.

1.1.3 Oncogenic signaling pathways

Cancer cells can express their hallmarks through the activation of multiple pro-tumorigenic signaling pathways. This thesis focuses on three key pathways: the phosphoinositide 3-kinase (PI3K)/AKT signaling pathway, the rapidly accelerated fibrosarcoma (RAF)/mitogen-activated protein kinase (MAPK) pathway, and the transforming growth factor (TGF)-β signaling[24] (**Figure 1).**

In the PI3K/Akt pathway, activation of PI3K leads to the phosphorylation of phosphatidylinositol-4,5-bisphosphate (PIP2) resulting in the production of phosphatidylinositol-3,4,5-trisphosphate (PIP3), that activates the phosphoinositide-dependent kinase-1 (PDK1)[25]. PDK1 will then activate the AKT protein, a serine and threonine kinase also known as protein kinase B, that promotes tumor cell survival by interacting with downstream effectors[25]. AKT substrates are numerous and can be activated like mTOR complex, responsible for the regulation

of tumor growth and metabolism, or inhibited like the Forkhead box Os (FOXOs), a subgroup of the FOX transcription factor family that regulates gene expression and cell survival[25]. Activation of the PI3K/AKT pathway can be induced by growth factors such as epidermal growth factor (EGF) and vascular endothelial growth factor (VEGF) or by Toll-like receptors (TLRs) when binding to specific ligands in immune cells[25]. Mutations in PTEN, which is responsible for blocking the PI3K/AKT pathway by catalyzing the conversion of PIP3 to PIP2, inhibit its function and maintain the activation of the PI3K/AKT pathway[25,26].

The second important signaling pathway for tumor growth is the RAF/MAPK pathway. The Rat sarcoma virus (RAS) protein is the upstream protein of the RAF/MAPK pathway, which regulates the response to various stimuli. Phosphorylation of growth factor receptors leads to activation of the RAS protein by interchanging guanosine-diphosphate (GDP) to guanosine-triphosphate (GTP) bound molecules[26]. This enables RAS to activate the downstream RAF proteins, leading to the phosphorylation of MAPK kinase (MEK) and subsequently activating the MEK-extracellular signal-related kinase (ERK) pathway[26]. ERK protein then activates various transcription factors in the nucleus to regulate the expression of genes responsible for proliferation and cell survival in cancer[26].

Both PI3K/AKT and MAPK pathways can be activated through the non-canonical signaling pathway of TGFβ[27]. TGFβ has multiple receptors that can also lead to signaling through a canonical pathway involving the receptor-regulated SMAD proteins (SMAD1, 2, 3, 5, 8, 9)[27]. Both canonical and non-canonical signaling can occur at the same time but while the interplay between the two is not yet clear, it is thought that the cellular context, the type of the receptor and the external signals can push the TGFβ towards activating one of the two[28].

These three key signaling pathways, but especially TGFβ signaling promote proliferation and metastasis through a specific process called epithelial-to-mesenchymal transition (EMT).

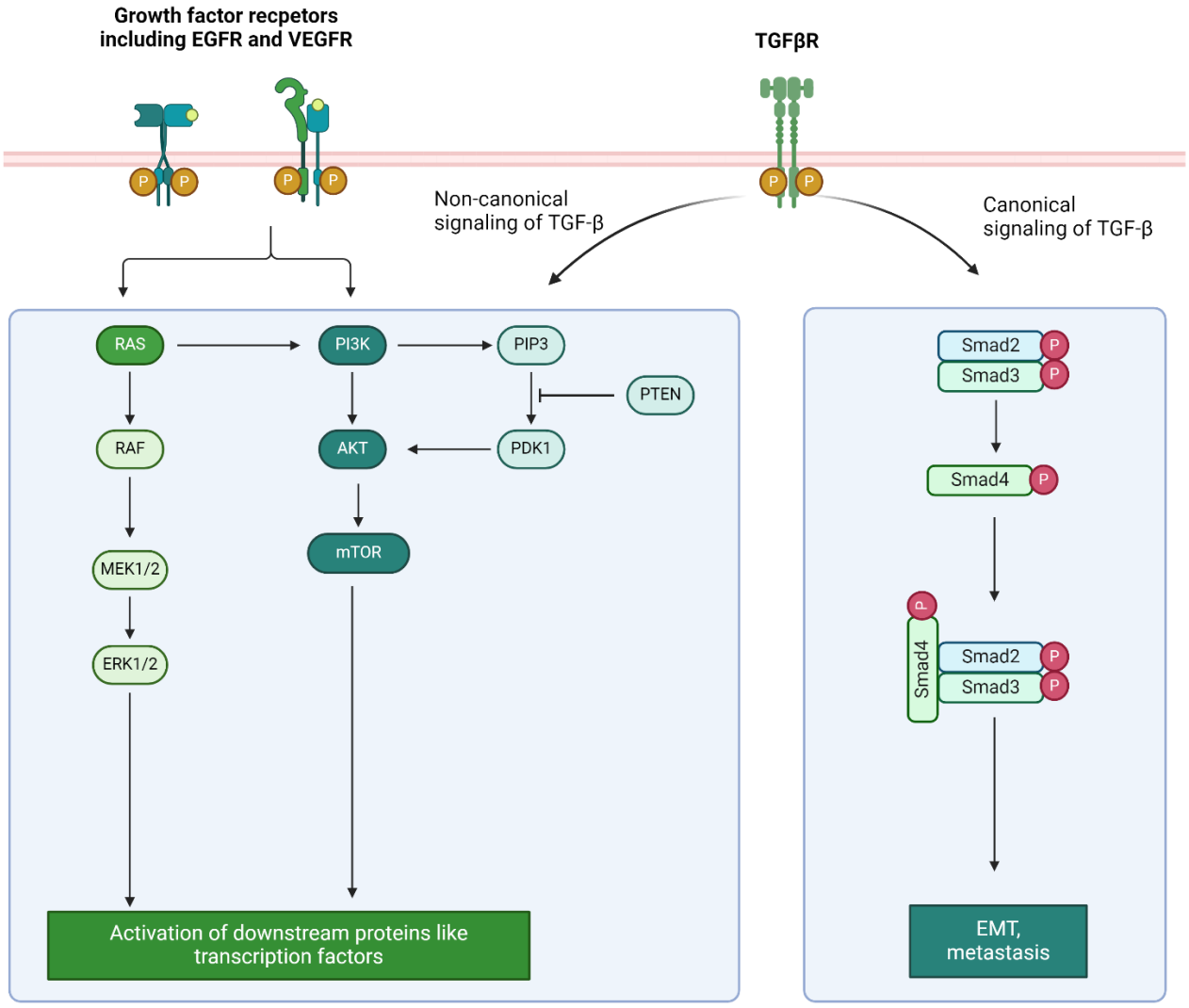

Figure 1. Schematic representation of the oncogenic pathways*. The binding of growth factors like EGF and VEGF leads to the activation of the MEK/ERK and PI3K/AKT pathways, which are also induced during the non-canonical signaling of TGFβ. The SMAD pathway represents the canonical signaling of TGFβ. This figure was created by Biorender, and inspired from Lei et al., 2022*[29].

1.2 Epithelial-to-mesenchymal transition

EMT is a biological process that normally occurs during embryonic development, where polarized epithelial cells transform into mesenchymal cells with an elongated morphology, enabling them to migrate[30]. Cancer cells use this process to promote survival, tumor growth, and metastasis, by losing cell-cell adhesion properties, gaining motility, and reorganizing the cytoskeleton[30]. The regulation of this process depends on and is influenced by secreted cytokines and growth factors present in the tumor microenvironment. TGFβ, for example, is a highly produced protein by various types of cells within the microenvironment including cancer cells and fibroblasts[31]. Following its interaction with specific receptors, it can activate various EMT transcription factors (EMT-TFs) through either the canonical or non-canonical signaling pathway[27]. Activated EMT-TFs include the Snail family zinc finger transcriptional factors (SNAIL), Twist family transcriptional factor (TWIST), and zinc finger E-box binding homeobox (ZEB)[32]. These EMT-TFs decrease the expression of epithelial markers like E-cadherin and cytokeratins and increase mesenchymal markers like N-cadherin, Vimentin, Fibronectin, Snail, and Slug[32].

In ovarian cancer, metastasis happens primarily within the peritoneal cavity where cancer cells survive in a malignant intra-abdominal fluid called ascites[33]. Once cancer cells undergo EMT, they detach from the primary site as single cells or as small clusters called spheroids and disseminate throughout the peritoneal cavity[33]. The preferred site for ovarian cancer metastasis is the omentum, a visceral adipose tissue formed from a fold of the peritoneum surrounding the stomach and other organs in the abdomen[34]. This tissue is rich in adipocytes, which have been proven to interact with cancer cells leading to the formation of “cancer-associated adipocytes”, which can release factors that promote tumor growth[35]. Several studies have demonstrated that EMT is linked to chemoresistance, largely due to the tumor microenvironment's heterogeneity

created by the mesenchymal phenotype of cancer cells and the plasticity of the EMT process, along with the feedback loop between immunosuppression and EMT[36,37]. This shows the importance of understanding the immune system in cancer research to facilitate the development of better therapies.

1.3 The tumor microenvironment (TME)

1.3.1 Characteristics of the tumor microenvironment

The complexity of the TME is a key factor contributing to the heterogeneity of ovarian cancer. Generally, the TME is composed of various types of cells including cancer cells, fibroblasts, endothelial cells, and immune cells[38]. Each one of these cell types can exhibit different phenotypes and distinct mutations, leading to the release of different factors which can be anti- or pro-tumorigenic within the same TME[39]. Cancer-associated fibroblasts (CAFs), for example, are derived from tissue-resident fibroblasts and are known to be activated within the TME[40]. They contribute to tumor growth through the secretion of cytokines and chemokines, like CXCL1, CCL5, and IL-6, and EMT-promoting factors, notably TGFβ[40]. CAFs were also found to secrete extracellular (ECM) matrix components, including the remodeling enzymes matrix metalloproteinases (MMPs) that degrade E-cadherin, and VEGF which promotes angiogenesis[38]. ECM plays an important role in regulating the function of many cell types, but the abnormal ECM deposition in cancer facilitates the tumor cells to proliferate and invade the microenvironment[41]. Angiogenesis is another pro-tumorigenic process through which new blood vessels generate from pre-existing vasculature. It is a hypoxia-dependent process that activates in response to hypoxia-inducible factors (HIFs), enabling tumor growth and survival within the TME[41]. The majority of

these processes are stimulated or enhanced by EMT and dominate the microenvironment, allowing the tumors to develop resistant mechanisms against first-line immune responses and therapies[42].

1.3.2 The immune system of the tumor microenvironment

The immune system within the TME comprises two primary cell types: myeloid-derived and lymphoid-derived cells. CD45 is the major transmembrane glycoprotein expressed in these cells and is therefore used as an initial marker to differentiate immune cells from other cell types[43]. Lymphoid lineage cells encompass T cells, B cells, and natural killer (NK) cells, each defined by specific markers[44]. T cells, for example, are identified by their expression of the CD3 transmembrane antigen associated with the T-cell receptor (TCR), whereas NK cells are detected through their expression of CD56 marker[45,46]. In contrast, myeloid lineage cells are known to be negative for both T cell, B cell, and NK cell markers, and include monocytes, macrophages, dendritic cells (DCs), and granulocytes[44]. Each of these immune cells can differentiate into various subtypes, exhibiting either anti-tumor or pro-tumor phenotypes. For example, monocytes serve as precursors to tumor-associated macrophages (TAMs), which can polarize into either classically activated macrophages (M1) in the presence of interferon-γ (IFNγ) and granulocyte-macrophage colony-stimulating factor (GM-CSF) or alternatively activated macrophages (M2) in response to cytokines secreted by malignant cells including IL-4, IL-6, and VEGF[47,48]. The presence of M1-TAMs in the tumor microenvironment is linked to a pro-inflammatory response, characterized by the phagocytosis of malignant cells, leading to anti-tumor effects[48]. In contrast, M2-TAMs are associated with a poor prognosis as they promote metastasis and exhibit an anti-inflammatory response, which supports tumor progression[48]. DCs are also divided into multiple subtypes including classic DCs 1 and 2, plasmacytoid DCs, and monocyte-derived DCs, which can exhibit

various immune responses depending on the changes occurring within the TME[49]. Similarly, lymphocytes, specifically T cells, exist in 2 main subtypes CD4+ and CD8+ T cells. They recognize tumor-associated antigens (TAAs) present on malignant cells and antigen-presenting cells (APCs) including macrophages and DCs in order to exhibit their cytotoxic function[40]. The interplay between CD4+ and CD8+ T cells is crucial for the antitumoral response since the activation and proliferation of CD8+ T cells depend on multiple factors, including cytokines secreted by CD4+ T helper (Th) cells[40].

Infiltration of immune cells within the TME is an important factor determining the fate of deficient cells, such as cancer cells and CAFs. This outcome depends mainly on the location of the T cells, referred to as tumor-infiltrating lymphocytes (TILs) within the TME. TILs are used to assess immune infiltration in tumors, primarily due to their prognostic potential in various cancers and the ability to be modulated for therapeutic purposes, compared to other immune cells like macrophages which may be more challenging to use given the heterogeneity of their phenotypes[50,51]. Tumors can be classified as infiltrated, when TILs are present between other cell types of the TME, where they exhibit their cytotoxicity and contribute to tumor-killing by secreting the antitumoral cytokine such as IFNγ and tumor necrosis factor alpha (TNF-α), ensuring a better prognosis[40,52]. Conversely, tumors can be immune-excluded and immune-desert when TILs are distant from malignant cells usually due to tumor stroma[52,53]. Other immune characteristics remain important for the functioning of immune cells, notably the expression of exhaustion markers that lead to immunosuppression and tumor growth.

1.3.3 Immunosuppression

Therapeutic strategies have been developed over the years to ensure a better prognosis for the patients and, if possible, eliminate tumor development. The primary treatment for ovarian

cancer patients when first diagnosed is surgical debulking, aiming to remove the whole tumor mass[54]. When residual disease is larger than 1 cm, patients undergo platinum and/or taxane-based chemotherapies for a certain number of cycles depending on their stage[54]. However, recurrence of tumors and/or resistance to chemotherapies are common and prevent the recovery from the disease. In the majority of cases, this is mainly due to the production of immunosuppressive factors by both cancer cells and immune cells[55].

Immunosuppression within the tumor microenvironment can be initiated by a chronic inflammation manifesting through the secretion of anti-tumor cytokines or the expression of specific molecules and markers on cells, both of which contribute to an environment that prevents the immune system's ability to target and eliminate cancer cells[56]. Inhibitory cytokines, such as TGF-β, IL-10, IL-4, and IL-13, create a suppressive environment, while pro-inflammatory cytokines, including IL-1, IL-15, TNF-α, and IFN-γ, can also be present but are often counteracted by the dominant suppressive signals[57]. These factors contribute to an increase in the expression of immune checkpoint markers within the TME. Programmed cell death ligand 1 (PD-L1) is an example of checkpoint molecules expressed by cancer cells and APCs, including B cells, DCs, and macrophages[55]. PD-L1 expression allows cancer cells to evade T cell cytotoxicity by interacting with programmed cell death protein 1 (PD-1), the receptor on T cells. This results in the inhibition of T cell function within the TME and the acquisition of an exhaustion phenotype, leading to reduced effectiveness in combating the tumor[55]. Lymphocyte activation gene-3 (LAG-3) is another immune checkpoint molecule expressed on T cells and NK cells, acting as an inhibitor of immune responses[55]. Both PD-1 and LAG-3 are often co-expressed on CD8+ T cells in human ovarian tumors, resulting in impaired production of key cytokines like IFN-γ and TNF-α and reduced cytotoxic activity[58]. Other immune checkpoint molecules, such as TIM-3(T-cell immunoglobulin

and mucin-domain containing 3) and CTLA-4 (cytotoxic T-lymphocyte associated protein 4), also contribute to T cell exhaustion and immune suppression in EOC[59].

Significant efforts have been made to develop therapies targeting these molecules, known as immune checkpoint inhibitors (ICIs)[60]. In ovarian cancer, ICIs have been used as single-agent therapy targeting one specific immune checkpoint molecule like anti-PD-L1 drugs, dual-agent therapy targeting two immune checkpoint molecules like combination of anti-PD and CTLA-4, or in combination with other targeted therapies like PARP inhibitors[60–62]. Promising results have been observed in mouse models, but clinical results still show tumor recurrence and resistance in EOC patients[60]. Ongoing research continues to focus on enhancing existing therapies and developing new treatments that target the molecular mechanisms contributing to resistance in EOC to improve treatment outcomes and enhance the quality of life for patients.

1.4 Rationale

The HGSC tumor microenvironment remains a complex and shifting domain and many studies have tried to elucidate the factors and processes contributing to its phenotype. The ability of cancer cells to transition from an epithelial to mesenchymal phenotype creates an obstacle to treatments, such as immunotherapies, targeting specific aspects of the TME. This is thought to be mainly due to the crosstalk between cancer cells at different EMT states and immune cells that aim to suppress cytotoxicity. Therefore, this study aims to investigate this interaction during the EMT process. In the course of this work, the expression of a promising molecule called secretory leukocyte protease inhibitor (SLPI) was found to change during EMT. SLPI is a small, secreted protein that positively correlates with and belongs to the protein family of a common biomarker of ovarian cancer, HE4[63]. SLPI is characterized by its immunoregulatory role in normal conditions,

but its role in ovarian cancer is unknown. Therefore, we hypothesize that SLPI secretion is associated with an aggressive phenotype of ovarian cancer, leading to increased proliferation and immune escape or promotion of a pro-tumorigenic TME.

1.5 Objectives

1) Determine how the EMT state of ovarian cancer cells affects their communication with the immune cells in the TME by analyzing single-cell RNA sequencing (scRNA-seq) datasets of either primary or metastatic tumors from ovarian cancer patients.
2) Investigate the expression profile of SLPI in datasets of human and mouse ovarian cancer tumors or cells and identify processes that regulate its expression.
3) Determine the effects of recombinant SLPI on the activation of immune cells *in vitro*, particularly the CD4+ cells that are shown to interact with SLPI based on the scRNA-seq analysis.
4) Examine the impact of SLPI expression on the tumor microenvironment *in vivo* by using a knockout and an overexpression model.

Chapter 2: Materials and Methods

2.1 Single-cell RNA sequencing analysis and data processing

Publicly available datasets for primary and metastatic ovarian cancers were used to explore the impact of EMT status on immune cells. Omental metastatic ovarian cancer samples had been collected from 6 different patients and sequenced using a high-throughput single-cell RNA sequencing (scRNA-seq) technique called Drop-seq. Details about the sequencing process are described in the original paper published by Olalekan et al., 2021[64] and the dataset is located in the Gene Expression Omnibus (GEO) repository with the identifier GSE147082. The primary HGSC dataset was generated by combining 28 scRNA-seq datasets from four different studies. Six cases were published by Geistlinger et al., 2020[65], another 6 were published by Quian et al.,2020[66] and 15 were available from Hornburg et al., 2021[67]. One unpublished scRNA-seq dataset was sequenced by a former PhD student in the lab, Dr. David Cook.

Analysis of the scRNA-seq datasets was performed using Seurat v3[68] package in R. Functions in this package were used to eliminate doublets, for normalization, scaling, and dimensionality reduction. A specific function in the Seurat package "FindClusters" was used to generate clusters of cell populations within the TME. Immune cells were labeled first using a multimodal reference for peripheral blood mononuclear cells (PBMCs)[69]. Cancer cells were labeled manually using known markers including EpCam, Krt19, Elf3, and Amhr2. Similarly, Col1a1 and Col1a2 markers were used to label fibroblasts, Cldn5 and Cdh5 for endothelial cells, and Acta2 for smooth muscle cells. Following the basic analysis, the 6 omental metastatic datasets were integrated into one Seurat dataset using the IntegrateData function[68] to ensure that their characteristics were aligned within their group. Prior to using it for visualization, the integrated

data was also processed using functions in the Seurat pipeline. Similar steps were followed for the 28 primary HGSC datasets.

2.2 EMT scoring of cancer cells

The EMT status of cancer cells in both primary and omental datasets was based on a module-driven EMT scoring strategy for cancer cells. The initial step for our scoring strategy was to calculate the average expression levels of EMT genes per cell based on a published module of conserved EMT signature genes[70] using the AddModuleScore function provided by the Seurat package. Thresholds defining the limits between each EMT state were calculated using the following formula:

$$\text{EMT score} = \text{mean (scores)} \pm \text{SD (scores)}$$

Cancer cells were labeled as epithelial (EPI), mesenchymal (MES), or partially mesenchymal (E/M) for their EMT status as follows:

$$\textbf{EPI}_{\textbf{score}} \leq mean(scores) - SD(\text{scores}) < \textbf{E/M}_{\textbf{score}} < mean(scores) + SD(\text{scores}) \leq \textbf{MES}_{\textbf{score}}$$

2.3 Ligand-receptor analysis

Ligand-receptor (LR) interactions were predicted using the liana_wrap function from the LIANA package[71] that combines 12 databases and 6 methods for inferring cell-cell communication from single-cell transcriptomic data. In this study, the OmniPath database was used with 5 methods (SingleCellSignalR (sca), NATMI, logFC, Connectome and Cellchat) for the LR analysis. The interactions identified by each method were combined using the liana_aggregate function**.** Additional packages like circlize[72] were used for visualization purposes. Represented data was selected based on the aggregate rank value which can be interpreted as an adjusted p-value[71].

2.4 Bulk RNA sequencing analysis

The Vanderhyden lab recently published bulk RNA sequencing data of all murine ovarian cancer cells[73] available in our lab and was used to determine the levels of SLPI. Cells of this dataset all had similar passage numbers. Log normalized distribution of all the genes was performed before the visualization that was done using ggplot2 package.

2.5 SLPI overexpression and knockout in mouse ovarian cancer cells

For the *in vitro* investigations, five murine HGSC cell lines were used representing the two known cells of origin for HGSC, two different strains of mice, and carrying clinically relevant mutations. ID8 and STOSE cells were derived from spontaneously transformed OSE cells and MOE and KPCA.B cell lines were derived from mouse oviductal epithelial cells. The cell lines used in this study were ID8 with *Trp53-/-;* MOE cells with $Pten^{shRNA}$, MOE cells with both $Pten^{shRNA}$ and $KRas^{G12V}$ mutation; STOSE cells; and KPCA.B. ID8 and KPCA.B cells lines were derived from C57BL/6 mice and all other cell lines were derived from FVB/n mice. OVE4 and MOSE cells are non-cancerous cell lines derived from FVB/n mouse oviductal epithelium and OSE, respectively, and were used as controls. KPCA.B cells were kindly provided by Dr. David Pépin[74].

To generate cells overexpressing SLPI with their proper control, KPCA.B and ID8 *Trp53-/-* cells were transduced with a lentiviral vector encoding *Slpi* generated by the Genomic Engineering and Molecular Biology (GEMb) core facility in the Faculty of Medicine at the University of Ottawa. These cells are referred to in this thesis as KPCA.B-$Slpi^{OE}$ and ID8 *Trp53-/-*$Slpi^{OE}$ and their vector-only controls as KPCA.B-$Slpi^{EV}$ and ID8 *Trp53-/-*$Slpi^{EV}$. For the knockout model, three single guide RNAs (sgRNA) targeting SLPI coded by the Gene ID 20568 were cloned in

pLentiCRISPRv2 and transduced in MOE *Pten*^{shRNA}*KRas*^{G12V} cells. A sgRNA control vector containing a Renilla sequence that does not target mammalian genomes was generated to control the Cas9 expression as well as the transduction process. These cells are referred to as MOE *Pten*^{shRNA}*KRas*^{G12V}*Renilla* in this thesis. In the overexpression and knockout models, the selection post-infection was done using a concentration of 8µg/mL and 10µg/mL of puromycin, respectively (Fisher Scientific, #A11138-03). The culture media for all the cell lines described above as well as their mutations and/or genetic alterations are summarized in **Table 1**.

Table 1: Cell line information and culture media for murine HGSC models.

Cell type[Reference]	Known Mutations	Culture Media*
ID8 *Trp53-/-*[75]	*Trp53*$^{-/-}$,	DMEM + 4% FBS + 1x ITSS
ID8 *Trp53-/-Slpi*^{OE}	*Trp53*$^{-/-}$, *Slpi*^{OE}	
ID8 *Trp53-/-Slpi*^{EV}	*Trp53*$^{-/-}$	
MOSE[76]	None	αMEM + 4% FBS + 1x ITSS + 2µg/mL EGF
STOSE[77]	None	
MOE *Pten*^{shRNA} (78)	*Pten*^{shRNA}	αMEM + 4% FBS + 1x ITSS + 2µg/mL EGF + 18.2ng/mL β-Estradiol
MOE *Pten*^{shRNA} *KRas*^{G12V} (78)	*Pten*^{shRNA}, *KRas*^{G12V}	
MOE *Pten*^{shRNA}*KRas*^{G12V} *Slpi-/-*	*Pten*^{shRNA}, *KRas*^{G12V}, *Slpi*$^{-/-}$	
MOE *Pten*^{shRNA}*KRas*^{G12V} *Renilla*	*Pten*^{shRNA}, *KRas*^{G12V}	
OVE4[79]	None	
KPCA.B[74]	*Trp53*$^{-/-R172H}$, *Ccne1*^{OE}, *Akt2*^{OE}, *KRAS*^{G12V}	DMEM + 4% FBS+ 1x ITSS + 2µg/mL EGF + 1x Penicillin-Streptomycin (Thermo Fisher, #15140122)
KPCA.B-*Slpi*^{OE}	*Trp53*$^{-/-R172H}$, *Ccne1*^{OE}, *Akt2*^{OE}, *KRAS*^{G12V}, *Slpi*^{OE}	
KPCA.B-*Slpi*^{EV}	*Trp53*$^{-/-R172H}$, *Ccne1*^{OE}, *Akt2*^{OE}, *KRAS*^{G12V}	

* *DMEM* (Corning, #10-013-CV) and αMEM *(Gibco, #12571-063) are media solutions, to which additional products may be added including Fetal Bovine Serum (FBS) (Gibco, #12483-020),*

Insulin-Transferrin-Selenium (ITSS) (Gibco #41400045 or Sigma, #I1884), murine EGF (R&D systems, #2028-EG-200) and/or β-Estradiol (Sigma, #E2257). *All the cells were incubated at 37°C and 5% carbon dioxide (CO_2).*

2.6 Proliferation assay

After modifying the MOE *Pten*^{shRNA}*KRas*^{G12V}, ID8-Trp53-/-, and KPCA.B cell lines and validating their SLPI expression levels, we assessed their proliferation. The modified cells were seeded in 6-well plates at densities of 0.15 x 10^5 cells/well for ID8-Trp53-/-, 0.25 x 10^5 cells/well for MOE *Pten*^{shRNA}*KRas*^{G12V}, and 0.20 x 10^5 cells/well for KPCA.B. Two technical replicates were prepared for each of the four biological replicates. Cell densities were optimized prior to the experiment to prevent over-confluency by 96 hours. Plates for each time point were prepared on day 0 and incubated under standard growth conditions (37°C and 5% CO2). Cells were collected at 24-, 48-, 72-, and 96-hours using trypsin (Corning, #25-052-CI) and counted with the Vi-CELL™ cell viability analyzer. Manual counts using a hemacytometer were performed to validate the accuracy of the Vi-CELL™ readings.

2.7 Treatment with TGFβ

To induce EMT *in vitro*, ID8 Trp53-/-, MOE *Pten*^{shRNA}, MOE *Pten*^{shRNA}*KRas*^{G12V}, and STOSE cells were seeded in 6-well plates on day 0 at a density of 0.15 x 10^5 cells/well, 0.25 x 10^5 cells/well, 0.25 x 10^5 cells/well and 0.20 x 10^5 cells/well, respectively. This density was optimized to avoid over-confluency by the collection day. After 24 hours, cells were treated for 72 hours with 10ng/mL of TGFβ1 (R&D Systems, #240-B-010), or with dimethyl sulfoxide (DMSO) at a 1:1000 ratio as a control, then collected for RNA extraction.

2.8 Treatment with Inhibitors

MOE *Pten*^{shRNA}*KRas*^{G12V} cells were used to study the effect of the inhibition of KRAS downstream pathways on the levels of SLPI. Cells were seeded at 1.5 x 10^5 cells/well in a 6-well

plate 24h hours prior to the treatment to allow them to adhere. Inhibitors of MEK (Selleckchem, Mirdametinib (PD0325901, #S1036) and AKT (Selleckchem, MK-2206, #S1078) were added at a concentration of 10nM, 500nM, 1μM and 10 μM. DMSO was added at a 1:1000 ratio to another well as a control. After 24 hours of incubation, cells were collected for RNA and protein collection

2.9 RNA extraction and reverse transcription polymerase chain reactions

To assess changes in the expression of the genes of interest, RNA was extracted using RNAeasy Mini Kits (Qiagen, #74106), following the manufacturer's protocol. For each sample, RNA concentrations were assessed using NanoDrop, and used for cDNA synthesis that was prepared using the Lunascript RT Supermix (New England Biolabs, #M3010X). The relative expression of the genes of our interest was assessed using primers listed in **Table 2**. *Ppia* and *36B4* were used as housekeeping genes for immune cells and *Ppia*, *Hprt1,* and *β-Actin* for the cancer cells to normalize the expression of the target genes across samples.

Table 2: Murine qPCR primer oligonucleotide sequences from 5' to 3'. *All primers were validated to ensure that they target their respective genes with efficiency and specificity.*

Gene of interest	Forward Primer	Reverse Primer
Slpi	CCATTCGCAAACCAGTGTGG	AGTTTCCAGAGCACACCGAG
Vim	CGGAAAGTGGAATCCTTGCAGG	AGCAGTGAGGTCAGGCTTGGAA
Cdh2	CCTCCATGTGCCGGATAG	CACCAGAAGCCTCCACAGAC
Sani2	TGCAAGATCTGTGGCAAGG	CAGTGAGGGCAAGAGAAAGG
Ifn-γ	TTGCCAAGTTTGAGGTCAACAA	CGCTTCCTGAGGCTGGATTC
Il-4	ACCCCCAGCTAGTTGTCATC	ACTCTCTGTGGTGTTCTTCGT
Il-21	AGGACCCTTGTCTGTCTGGT	GCTCACAGTGCCCCTTTACA
Il-6	CGGAGAGGAGACTTCACAGA	ATTTCCACGATTTCCCAGAG
Il-10	TGAATTCCCTGGGTGAGAAGC	CATTCATGGCCTTGTAGACACC

Tgfβ	ACGTGGAAATCAACGGGATCA	GTTGGTATCCAGGGCTCTCC
Ppia	AGGGTGGTGACTTTACACGC	GATGCCAGGACCTGTATGCT
β-Actin	CCTTCCTTCTTGGGTATGGA	ACGGATGTCAACGTCACACT
Hprt1	TCAGTCAACGGGGGACATAAA	GGGGCTGTACTGCTTAACCAG
36B4	TGACATCGTCTTTAAACCCCG	TGTCTGCTCCCACAATGAAG

2.10 Protein extraction and western blot

Cell pellets from each experiment were washed twice with phosphate-buffered saline (PBS), then lysed with a mix of RIPA buffer (Thermo Fisher, #89901), protease inhibitor (Sigma-Aldrich, #P8340) and phosphatase inhibitor cocktail (Sigma-Aldrich, #P0044) on ice for 15 minutes. Samples were then centrifuged at 15,000rpm for 15 minutes at 4 ºC, from which supernatant was collected and quantified using the Bio-Rad Protein Assay Dye Reagent concentrate diluted in water at a ratio of 1:5. A mixture of the concentrated protein, water and loading buffer with 2-mercaptoethanol (Sigma-Aldrich, #M7522) was prepared for each sample to have an equal amount of protein, and were then boiled for 5 min. For ERK, pERK, AKT, and pAKT proteins, NuPage 4-12% Bis-Tris gel (Thermo Fisher, #NP0336BOX) was transferred onto a PVDF membrane (Millipore). After blocking using bovine serum albumin (BSA) (Bioshop, #ALB001) for 1 hour, membranes were probed for ERK2 (Santa Cruz, 1:2000, #SC-154), phospho-ERK (Tyr 204; Santa Cruz, 1:2000, #SC-7383), AKT (Cell Signaling, 1:1000, #9272) and phospho-AKT (Ser473; Cell Signaling, 1:1000, #9271) antibodies overnight at 4 ºC. Prior to adding the secondary antibodies, membranes were washed in TBST three times for 5 minutes. Anti-mouse (Abcam, 1:10000, #ab6728) or anti-rabbit (Jackson Immunoresearch, 1:10000, #711-035-152) secondary antibodies were incubated with the membranes for 1 hour at room temperature. Antibodies to β-actin (Sigma,

1:10000, #a2228) were used as a loading control and the membrane was incubated for 1 hour at room temperature.

Because SLPI is a secreted protein, visualization of SLPI protein was enhanced by blocking secretion. Cells were seeded in a 6-well dish and allowed to adhere overnight. They were then treated with the BD GolgiPlug™ Protein Transport Inhibitor, Brefeldin A, (BD Biosciences, #555029) at a 1:1000 ratio or DMSO, according to the manufacturer's protocol, for 12 hours. Protein was collected and lysed in RIPA buffer with protease and phosphatase inhibitors as indicated above. Protein lysate was run on a 15% acrylamide tris-glycine and transferred to a PVDF membrane. The membrane was then incubated in an SLPI antibody (R&D Systems, 1:1000, #AF1735) overnight followed by an anti-goat secondary (Santa Cruz, 1:10000, #sc-2354) antibody for 1 hour.

For all western blots, β-actin was used as a loading control and was incubated with antibodies (Sigma, 1:10000, #a2228) for 1 hour at room temperature. Membranes were developed using Clarity Western ECL substrate (Bio-Rad) and imaged using the ChemiDoc system (Bio-rad).

2.11 T cells isolation

CD4+ T cells were isolated from the spleen and lymph nodes of 8–10 week-old female FVB/N mice (Charles River laboratories, strain #207) and purified using the EasySep Mouse CD4+ T cell isolation kit (Fischer Scientific, #NC0471206) following the manufacturer's protocol. CD8+ T cells were isolated from the spleen and lymph nodes of 8-10 week-old female OT-1 mice (The Jackson Laboratory, #003831) kindly provided by Dr. Rebecca Auer's laboratory. CD8+ T cells were purified using the EasySep™ Mouse CD8+ T cell isolation kit (Stem Cell Technologies, #19853) following the manufacturer's protocol. Before the isolation of both CD4+ and CD8+ T cells, the spleen and lymph nodes were disassociated and purified by the removal of erythrocytes

using ACK Lysis Buffer (Thermo Fisher, #A10492-01). The culture medium for the T cells cells was RPMI with 10% FBS, 1X penicillin/streptomycin (Thermo Fisher, #15140122), 10mM HEPES (Thermo Fisher, #BP310-500), and 55 μM 2-mercaptoethanol.

2.12 *In vitro* recombinant SLPI treatment

Isolated T cells were seeded in a 12-well plate at 1 x 10^6 cells/well. For T cell activation, wells were precoated with 2μg of αCD3 (Fisher Scientific, #5012341) and αCD28 (Fisher Scientific, 501129711) antibodies. For CD8+ T cells form OT-1 mice, another activation condition used 0.5μM of ovalbumin (OVA) peptide SIINFEKL (Canpeptide, #QCP191007-5) to the culture conditions. Naïve CD4+ and CD8+ T cells were maintained in the normal culture conditions but with added 10ng/mL of mouse recombinant IL-7 (Cell Signaling, #64063S) to maintain them in the naïve state and ensure their survival. Recombinant mouse SLPI (Abbexa, #abx069004) was added to the culture medium for 72 hours at various concentrations as noted in the Results section.

2.13 Flow cytometry of *in vitro* samples

Single-cell suspensions of the *in vitro* treated T cells were washed using PBS for extracellular staining. All samples were first stained for cell viability discrimination for 15 minutes followed by Fc-blocking (BD Biosciences, CD16/CD32, #553142). Samples were then fully stained for the target proteins indicated in **Tables 3 and 4** for 20 minutes, fixed in 1% paraformaldehyde (PFA), and stored overnight at 4ºC. All antibodies were optimized by titration and diluted in PBS + 2%FBS buffer except for the Zombie NIR™ which was diluted in PBS only. Data acquisition from the samples was done using a Cytek™ Aurora Spectral flow cytometer and analysis was performed using FlowJo software (v10.10.0).

Table 3: Summary of the fluorophore-conjugated flow cytometry antibodies used to analyze specific targets in CD4+ treated T cells.

Target	Fluorochrome	Dilution	Company and Catalogue #
Viability	Zombie NIR™	1:1000	Biolegend Cat# 423106
LAG3	BUV805	1:200	BD Biosciences Cat# 748540
CD62L	BUV737	1:200	BD Biosciences Cat# 612833
PD-L1	BUV395	1:200	BD Biosciences Cat# 745616
CD25	BV786	1:200	BD Biosciences Cat# 564023
PD-1	PE	1:200	Biolegend Cat#135206
CD4	PERCP	1:200	Biologend Cat#100538
CD69	NIR-685	1:200	Biolegend Cat# 104557

Table 4: Summary of the fluorophore-conjugated flow cytometry antibodies used to analyze specific targets in CD8+ treated T cells.

Target	Fluorochrome	Dilution	Company and Catalogue #
Viability	Zombie NIR™	1:1000	Biolegend Cat# 423106
LAG3	BV786	1:200	BD Biosciences Cat# 740959
CD62L	BUV737	1:200	BD Biosciences Cat# 612833
PD-L1	BUV395	1:200	BD Biosciences Cat# 745616
CD25	BV605	1:200	BD Biosciences Cat# 563061
PD-1	PE	1:200	Biolegend Cat#135206
CD8a	BUV615	1:200	BD Biosciences Cat# 613004
CD69	Spark NIR™ 685	1:200	Biolegend Cat# 104557
CD3	PE-Cy5	1:200	Biolegend Cat#100310

2.14 *In vivo* impact of SLPI

The effect of SLPI on the TME and progression of ovarian tumors was tested in two sets of experiments to evaluate the effects on overall survival and on the immune profile in the TME. For all experiments, the animals were housed in the Animal Care and Veterinary Services (ACVS) facilities at the University of Ottawa, where they were given standard chow and water ad libitum and monitored daily. The Animal Care Committee approved the experimental protocols that have met or exceeded the ethical standards set by the Canadian Council for Animal Care. Criteria used to determine the humane endpoint include slow mobility, the presence of abdominal distension due to ascites, the presence of an obvious tumor mass by palpation, hunched back, and/or squinting eyes.

2.14.1 Survival Study

To assess the impact of SLPI on the rate of tumor progression and survival in mice, 3 different syngeneic models of intraperitoneal (IP) ovarian cancer were used. The MOE *Pten*^{shRNA}*KRas*^{G12V} model (Parental, Slpi-/-, and Renilla control) was used to assess the effects of SLPI knockout, and 5 x 10^6 cells were injected IP into six 9-weeks old female FVB/N mice for Slpi-/- and the Renilla control, and three for the parental cell line. ID8-*Trp53-/-Slpi*^{OE}, ID8-*Trp53-/-Slpi*^{EV}, KPCA.B (Parental), KPCA.B-*Slpi*^{OE} and KPCA.B-*Slpi*^{EV} cells were used to assess the effect of overexpression of SLPI and 5 x 10^6 cells were injected IP into 6 9-weeks old female C57BL/6 mice (The Jackson Laboratories, #000664) for each group. Cells were resuspended in 100µL of PBS for injection. The mice were monitored daily and euthanized using CO_2 when they reached a humane endpoint. The results of the study are presented in Kaplan-Meier plots.

2.14.2 Tumor collection and flow cytometry for TME assessment

To assess the effects of overexpression or knockout of SLPI on the TME, MOE *Pten*^{shRNA}*KRas*^{G12V} and KPCA.B-derived cell lines were used to generate orthotopic ovarian tumors

in syngeneic mice. Intrabursal (IB) surgery was performed to inject 0.15 x 10^6 cells under the bursal membrane as previously described[77]. For MOE *Pten*^{shRNA}*KRas*^{G12V}, the experimental groups included 5 mice for the parental cell line, 6 for the *Slpi*-/- cell line, and 9 for the Renilla control cells. For the KPCA.B model, the experimental groups included 3 mice for the parental cell line, 6 for the empty vector control (*Slpi*^{EV}), and 6 for the *Slpi*^{OE} cells.

Six days before the humane endpoint, mice were euthanized, and tumors were collected and disassociated for flow cytometry analysis. The disruption process started by first cutting the tumors into small pieces using a razor blade in 2.5 mL of digestion solution from the Tumor Dissociation Kit (Miltenyi Biotec, #130-096-730) and the gentleMACS Octo Dissociator with heaters (protocol tumor 37ºC_m_TDK_1) following the manufacturer's protocol. Ascites fluid was also collected and, if absent, a peritoneal wash (PW) was performed by intraperitoneal injection of 5mL of PBS-EDTA 2mM and abdominal massage. Single cells were generated by filtering the fluids through a 70µm filter. To remove erythrocytes from the samples, cells were resuspended in ACK Lysis Buffer for an average of 3 minutes.

Single-cell suspensions were stained for viability for 15 minutes followed by Fc-blocking (BD Biosciences, #553142) for 5 minutes. Samples were then stained for extracellular targets shown in **Table 5** and incubated at room temperature for 20 minutes. Prior to intracellular staining, cells were incubated with fixation/permeabilization buffers (eBioscience™, #00-5523-00) for 45 minutes. After this, samples were incubated with the antibodies of intracellular targets, indicated in **Table 5,** at room temperature for 20 minutes. All samples were fixed in 1% PFA and stored overnight at 4ºC. Data was acquired using a CytekTM Aurora Spectral flow cytometer and analyzed using FlowJo software (v10.10.0).

Table 5: Fluorophore-conjugated flow cytometry antibodies used to analyze specific targets in TME. *The dilution of all antibodies was optimized by titration. The fixable viability was diluted in PBS, extracellular antibodies in PBS + 2%FBS and intracellular antibodies in the permeabilization buffer.*

Target	Fluorochrome	Dilution	Company and Catalogue #
Viability	BV510	1:1000	BD Biosciences Cat# 564406
Extracellular antibodies			
CD3e	BV650	1:100	BD Biosciences Cat# 564378
CD45	PerCP-Cy5.5	1:200	BD Biosciences Cat# 550994
CD4	APC-H7	1:200	BD Biosciences Cat# 560181
CD8	PE-Cy7	1:200	BD Biosciences Cat# 552877
CD25	BV421	1:200	BD Biosciences Cat# 563061
CD11c	BUV563	1:200	BD Biosciences Cat# 749040
CD11b	BUV661	1:200	BD Biosciences Cat# 612977
F4/80	BV421	1:200	BD Biosciences Cat# 565411
PD-1	BV785	1:200	Biolegend Cat# 135225
PD-L1	BUV395	1:200	BD Biosciences Cat# 568308
Intracellular antibodies			
T-Bet	PE-CF594	1:150	BD Biosciences Cat# 562467
GATA3	APC	1:150	Biolegend #653805
RORγt	BB515	1:150	BD Biosciences Cat# 567175
FoxP3	PE	1:150	Biolegend #126404

2.15 Statistical Analysis

All statistical analyses were performed using GraphPad Prism (v10.0.1) software. The student's T-test was used when comparing two groups, and one-way ANOVA with Tukey's multiple comparison method was used to compare three or more groups. Two-way ANOVA and Log-Rank (Mantel-Cox) tests were used to compare different groups of the survival study. Where applicable, results are presented as mean +/- SD. Figures were made using either the ggplot2 (3.5.1) visualization package in R Studio or the Prism software. Statistical significance was set at $p \leq 0.05$ for all results. Non-significant results are identified with either nothing or "ns", depending on the experiment.

Chapter 3: Results

3.1 Discovery of the ligand-receptor interaction SLPI-CD4

Processing the primary and omental tumor scRNA-seq datasets showed, after clustering, the presence of similar cell populations (**Figure 2A**) with differences in their abundance (**Figure 2B-C**). In both primary and omental tumors, cancer cells with the partially mesenchymal phenotype (E/M) were the most abundant (30% in the omental and 24% in the primary tumors), followed by fibroblasts which were the second most abundant cell type (25% in the omental and 20% in the primary tumors), but the metastatic tumors had more of these cells than the primary tumors. Epithelial (EPI) and mesenchymal (MES) cancer cells were equally abundant and each formed 5% to 6% of the total population. When comparing immune cell populations, the abundance in primary vs. metastatic tumors becomes different. For instance, B cells were the most abundant immune cell population in the omental tumors at 8%, followed by CD4+ T cells at 7%, then monocytes at 5%, with only 3% of cells being CD8 T cells and DCs. However, in the primary tumors, monocytes were the most abundant immune cell type with 13.6% of the cell population, followed by CD8+ T cells at 9.6%, CD4+ T cells at 8.3%, and finally B cells and DCs at an abundance of 3% each. NK cells were the least abundant immune cell type in both the primary and omental tumors with a percentage of around 2%. In total, immune cells comprise 27.65% of the omental tumors and 39.73% of the primary tumors. This affects the ratio of immune to non-immune cells, specifically cancer cells, which is higher in the primary tumors (immune: cancer cells; 39.72%:34.42%) compared to the metastatic tumors (immune: cancer cells; 27.56%:42.62%, **Figure 2B-C**).

After having identified the main cell populations of each type of tumor, we used the LIANA pipeline[71] to identify the predominant interactions between cancer cells and immune cells. In both primary and metastatic tumors, the cancer cells with a mesenchymal phenotype had the strongest

interaction with immune cells (**Figure 3A-B**), especially with monocytes/macrophages. Based on this finding, we looked deeper into the ligands and receptors contributing to the strength of this interaction and, out of the top significant ones, the interaction between the ligand SLPI and the receptor CD4 was the strongest (**Figure 3C**). This interaction was notable not only because of its magnitude but also because of its specificity. This was quantified on a dot plot (**Figure 3D**) showing the specificity and magnitude of the interactions based on the cancer cell EMT phenotype. Interestingly, the SLPI-CD4 interaction was observed to be more specific with the mesenchymal cancer cells than the partially mesenchymal cancer cells, and there was no specific interaction with epithelial cancer cells. After assessing the level of expression of SLPI in the same tumors, we found that the main reason behind these differences was due to the high expression of SLPI in mesenchymal cancer cells and its absence in epithelial cancer cells (**Figure 4A-B**). Therefore, our initial results suggested that SLPI-CD4 interaction could be a key player in the progression of ovarian cancer and a possible therapeutic target.

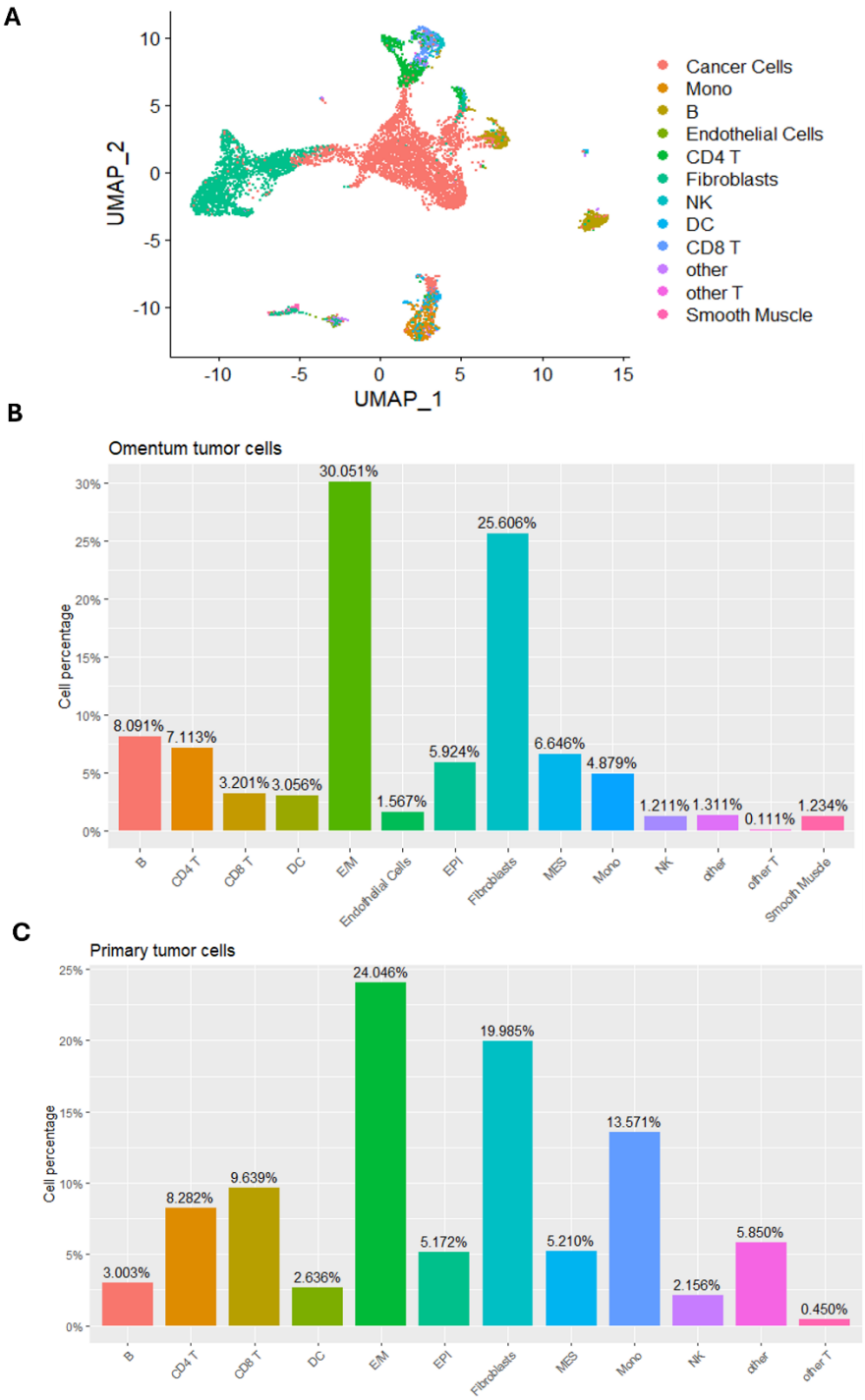

Figure 2. Cell clustering of ovarian tumor samples sequenced using scRNA-seq. *(A) Labelled UMAP representing an overall clustering of cell populations present in the metastatic ovarian cancer. (B) Percentages of cell populations in the dataset from metastatic ovarian cancer based on an integration of the 6 datasets. (C) Percentages of cell populations in the dataset from primary HGSOC based on integration of the 28 datasets. Immune cells include monocytes (mono), natural*

killer (NK) cells, dendritic cells (DC), B cells, CD8 T cells and CD4 T cells. Epithelial cancer cells (EPI), mesenchymal cancer cells (MES) and partially mesenchymal cancer cells (E/M).

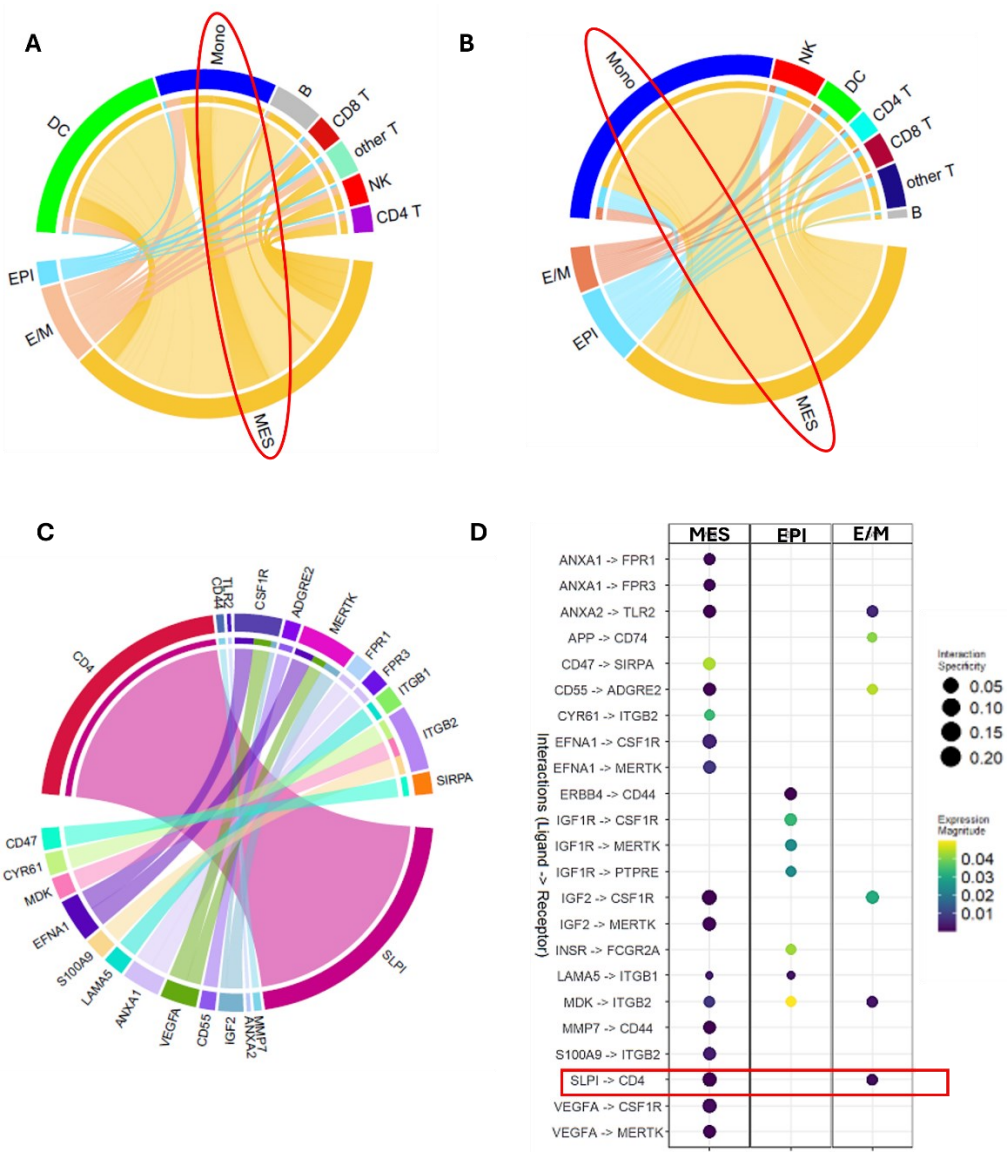

Figure 3. Interactions between ligands produced by cancer cells and receptors expressed on immune *cells in ovarian tumors. (A) Circos plot showing an overview of ligand-receptor interactions between cancer cells and immune cells in primary ovarian tumors. (B) Circos plot showing an overview of ligand-receptor interactions between cancer cells and immune cells in metastatic ovarian tumors. (C) Circos plot showing ligand-receptor interactions between cancer cells and monocytes in the metastatic tumors. (D) Dot plot representing ligand-receptor interactions between cancer cells based on their EMT phenotype and monocytes in the metastatic tumors. For metastatic tumors, only 30 ligand-receptor (LR) interactions were significant to an aggregate-rank value < 0.05 and thus represented in the two plots. For primary tumors, out of 300 LR significant interactions. Epithelial cancer cells (EPI), mesenchymal cancer cells (MES) and partially mesenchymal cancer cells (E/M).*

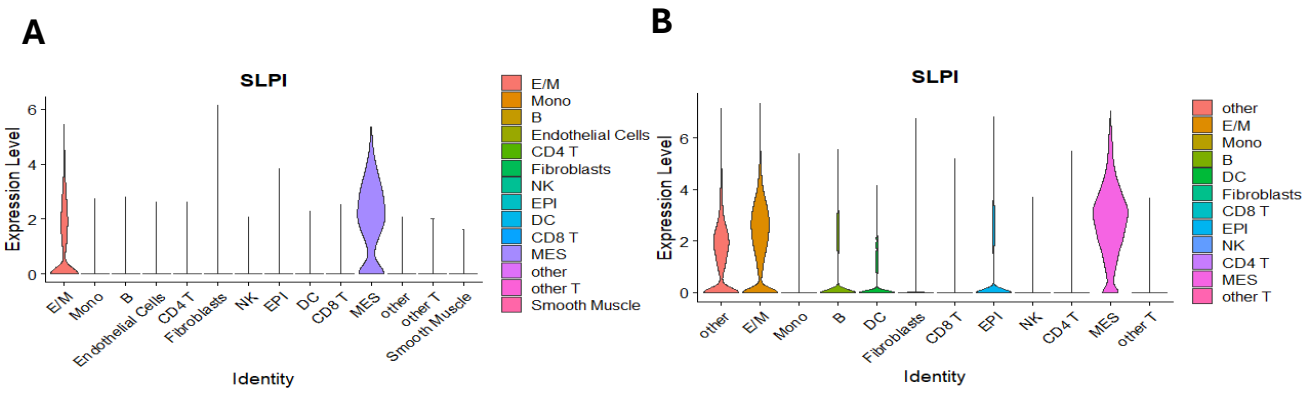

Figure 4. Level of expression of SLPI in cell populations present in human datasets corresponding to *(A) metastatic and (B) primary ovarian cancers. Cancer cells are referred by their EMT phenotype: epithelial cells (EPI), mesenchymal cells (MES) and partially mesenchymal cancer cells (E/M)).*

3.2 Assessing the baseline level of SLP in ovarian cancer cell lines

The RNA sequencing dataset of ovarian cancer cell lines from Cook et al., 2023[73] provided a resource for our assessment of *Slpi* expression levels in mouse models. The analysis revealed variable expression levels of *Slpi* in different ovarian cancer cell lines (**Figure 5A**). Notably, the ID8 models exhibited relatively low *Slpi* expression, whereas the MOE and STOSE models expressed almost 4 times higher levels of *Slpi.* The non-cancerous OVE16 and OVE4 models displayed expression patterns akin to the tumorigenic cell lines derived from them, although *Trp53* mutation in those models does cause a modest increase in *Slpi* expression in some cases (**Figure 5A**). This baseline data guided the selection of cell lines for further investigation into SLPI's role in ovarian cancer. We chose STOSE and MOE $Pten^{shRNA}KRas^{G12V}$ cells due to their elevated SLPI expression, which was also higher than their respective non-cancerous control/parental lines MOSE and OVE4 at both the RNA and protein levels (**Figure 5B-C**). Conversely, ID8-*Trp53-/-* was selected as a negative control due to its low SLPI expression (**Figure 5A**). The mRNA and protein quantifications (**Figure 5B-C**) were consistent with the RNA-seq results, confirming differential baseline SLPI expression across various cancer cells. This variability prompted our subsequent investigation into possible underlying reasons, which is the focus of the next section.

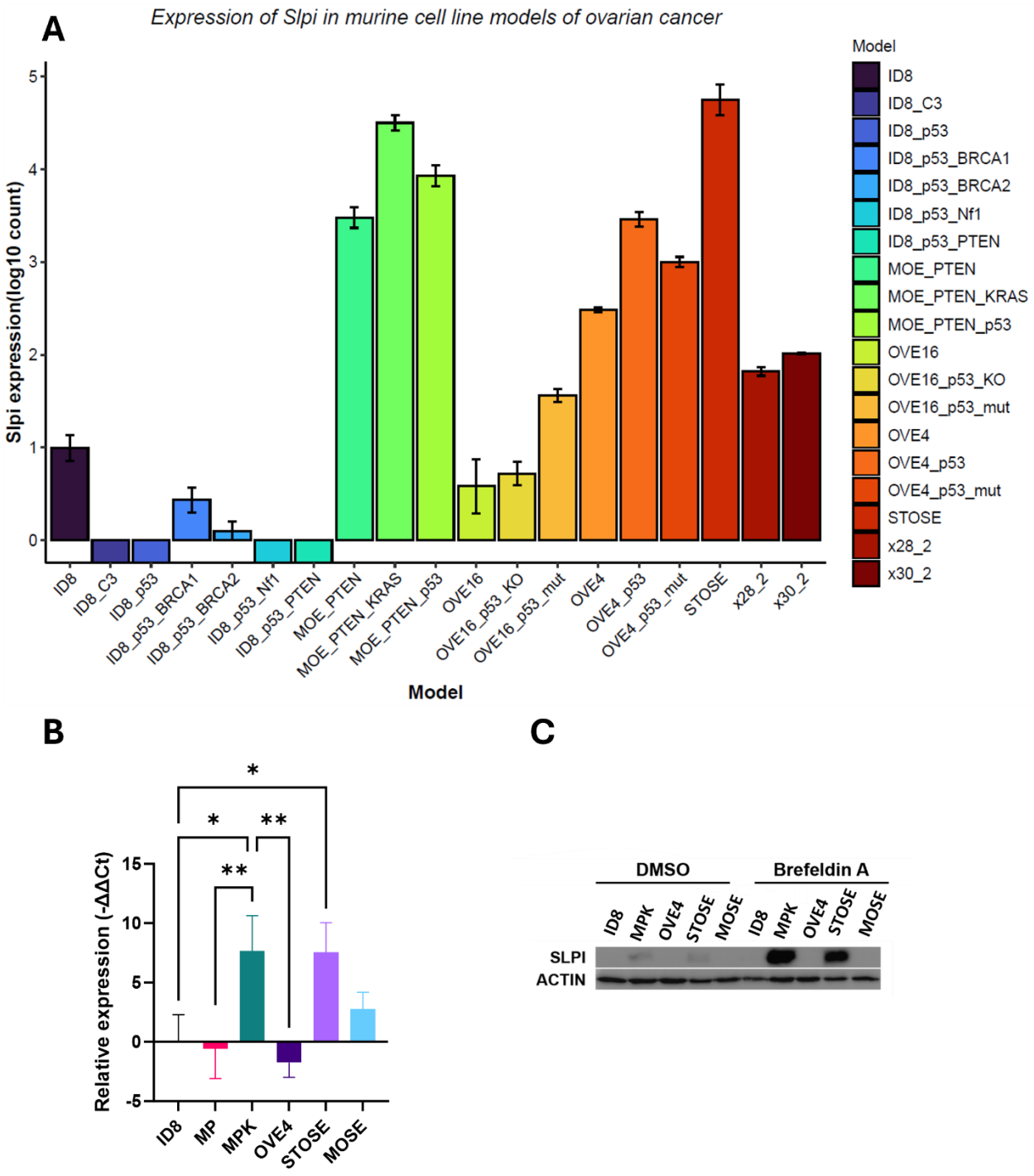

Figure 5. Different mouse ovarian cancer cell lines show different levels of expression of SLPI. *(A) Relative expression levels of SLPI were extracted from RNA-seq datasets[73] of the cell lines (n=3/cell line) and shown as mean+/- SD. (B) When quantified by RT-qPCR, cell lines chosen from the plot in (A) (n=3/cell line) show levels of Slpi expression that are consistent with the results*

*from the RNA-seq analysis. (C) Protein levels of SLPI in a subset of the cells presented in (B). In B, statistical analysis was done using one-way ANOVA and the p-value was less than 0.01 or 0.05 (indicated respectively as ** and *); n=3, showing mean +/- SEM. Abbreviations of the figures ID8, MP and MPK refer to respectively ID8-Trp53-/-, MOE Pten^{shRNA} and MOE Pten^{shRNA}KRas^{G12V}.*

3.3 Assessing the relationship between SLPI and EMT

The results of scRNA sequencing analysis indicated that mesenchymal cancer cells exhibited the strongest interaction between SLPI and CD4 compared to the epithelial and partially mesenchymal cancer cells (**Figure 3C-D**). Since TGFβ is known to be an inducer of EMT-like phenotypes[80], it was used as a treatment to explore the relationship between SLPI and EMT. Following a 72h TGFβ treatment of ID8-*Trp53-/-,* MOE *Pten^{shRNA},* MOE *Pten^{shRNA}KRas^{G12V,}* and STOSE, the morphology of all these cells was changed to become more elongated and depolarized compared to their respective controls (**Figure 6A)**, a common phenotype of EMT, validating the effects of the treatment. Some of the classical EMT markers, specifically Vimentin (*Vim*), Slug (*Snai2*), and N-cadherin (*Cdh2*), were also used to assess the induction of the EMT phenotypes. MOE *Pten^{shRNA}* and MOE *Pten^{shRNA}KRas^{G12V}* both displayed a significant increase or trends towards an increase of all these markers (**Figure 6C and 6D**). In contrast, ID8-*Trp53-/-* showed a rising trend in Slug only, whereas the levels of other markers did not change (**Figure 6B**). Similarly, no markers changed in STOSE cells (**Figure 6E**). Surprisingly, none of the cell lines showed a significant increase in *Slpi* mRNA levels, although ID8-*Trp53-/-* showed a positive trend. In contrast, MOE *Pten^{shRNA,}* and MOE *Pten^{shRNA}KRas^{G12V}* both showed a significant decrease in *Slpi* mRNA levels, and there was no effect on STOSE cells. These results suggest that, despite the expression of *SLPI* in mesenchymal cancer cells in human tumors, TGFβ-induced EMT in mouse ovarian cancer cell lines is not sufficient to upregulate SLPI expression.

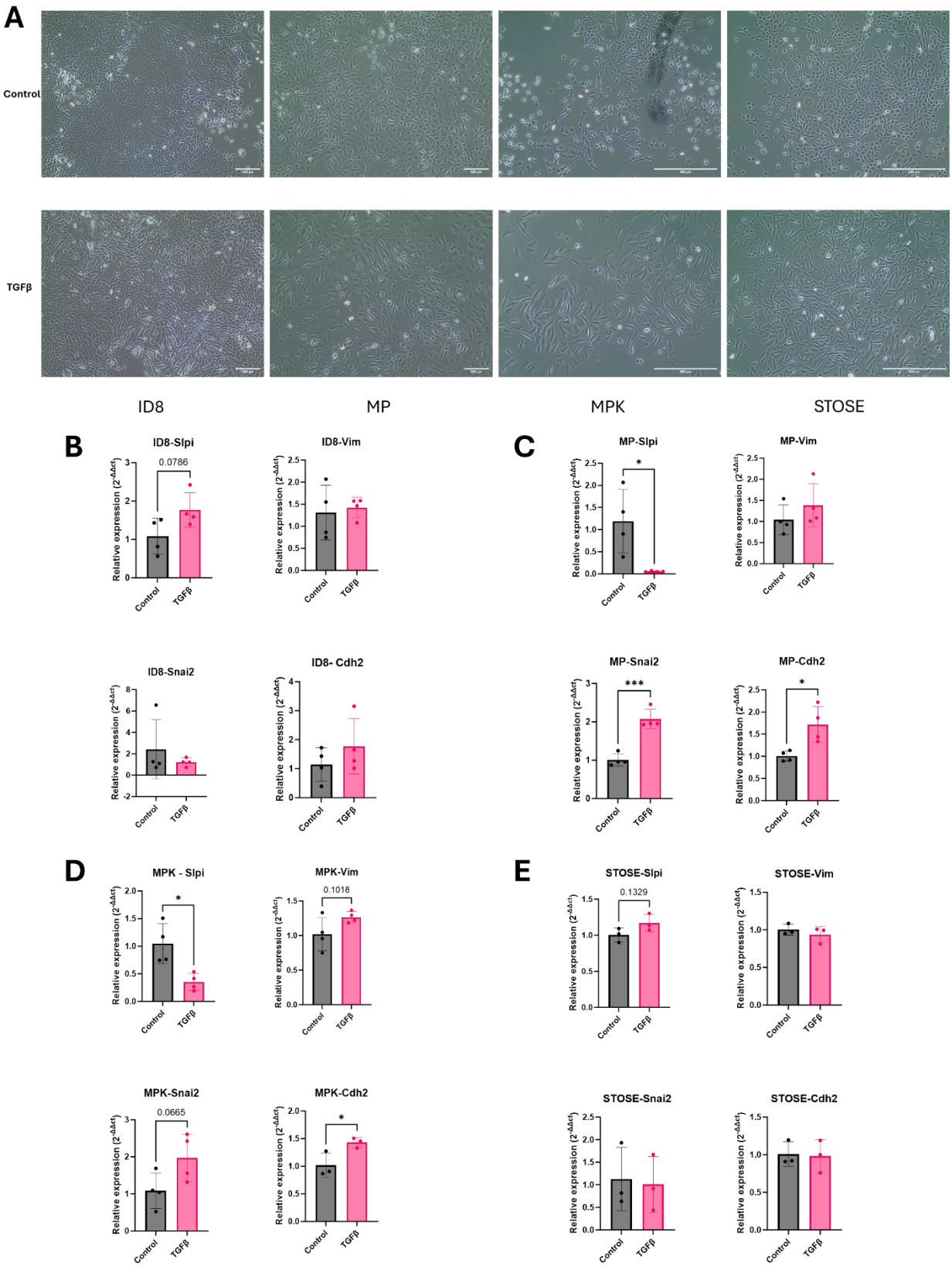
A
Control
TGFβ
ID8
MP
MPK
STOSE
B
ID8-Slpi
0.0786
ID8-Vim
ID8-Snai2
ID8- Cdh2
C
MP-Slpi
*
MP-Vim
MP-Snai2
***
MP-Cdh2
*
D
MPK - Slpi
*
MPK-Vim
0.1018
MPK-Snai2
0.0665
MPK-Cdh2
*
E
STOSE-Slpi
0.1329
STOSE-Vim
STOSE-Snai2
STOSE-Cdh2
Relative expression (2-ΔΔct)
Control
TGFβ

Figure 6. TGFβ treatment changes significantly the level of expression of Slpi mRNA in mouse ovarian cancer cell lines. *A) Images of non-treated (top row) and TGFβ-treated cells showing morphological changes. Scale bar = 500μm. B-E) Panels showing the mRNA levels of SLPI, Vimentin, Slug, and N-cadherin in (B) ID8-Trp53-/-, (C) MOE Pten^{shRNA}, (D) MOE Pten^{shRNA}KRas^{G12V}, and (E) STOSE cells. Statistical analysis was done using one-way ANOVA and the p-value was less than 0.001, 0.01 or 0.05 indicated respectively as ***, ** and *. Panels show mean +/- SD with n=4 for each cell line except STOSE cells that are represented by n=3 and Cdh2 for MPK. Abbreviations of the figures ID8, MP and MPK refer to respectively ID8-Trp53-/-, MOE Pten^{shRNA} and MOE Pten^{shRNA}KRas^{G12V}.*

3.4 Assessing the relationship between SLPI and KRAS mutation

Examining the level of SLPI in the various mouse cell lines, we observed that the addition of the *Kras* mutation in MOE *Pten^{shRNA}* caused an increase in *Slpi* expression in MOE *Pten^{shRNA}KRas^{G12V}*, which was confirmed to be a significant increase when tested by qPCR (**Figure 7A**). To explore that further, we examined TCGA datasets of ovarian cancers with *KRAS* mutation compared to non-mutants and observed a similar trend in which *KRAS* mutants showed a higher level of *SLPI* expression (**Figure 7B**). This led to the hypothesis that KRAS activation can regulate the expression of SLPI.

Activation of KRAS leads to increased signaling of two primary downstream signaling pathways, MAPK (RAF/MEK/ERK) and PI3K/AKT. We therefore blocked the phosphorylation of ERK and AKT using pathway specific inhibitors in cells with constitutive KRAS activity (MOE *Pten^{shRNA}KRas^{G12V}*). *Slpi* mRNA levels decreased significantly (**Figure 7D**) with increasing concentrations of the ERK inhibitor, which was confirmed to decrease the level of pERK (**Figure 7E**). The AKT inhibitor reduced the phosphorylation of AKT (**Figure 7G**) but did not affect the level of *Slpi* transcripts (**Figure 7F**). These results indicate that the expression of *Slpi* associated with KRAS activity is mainly controlled by the MAPK (RAF/MEK/ERK) pathway.

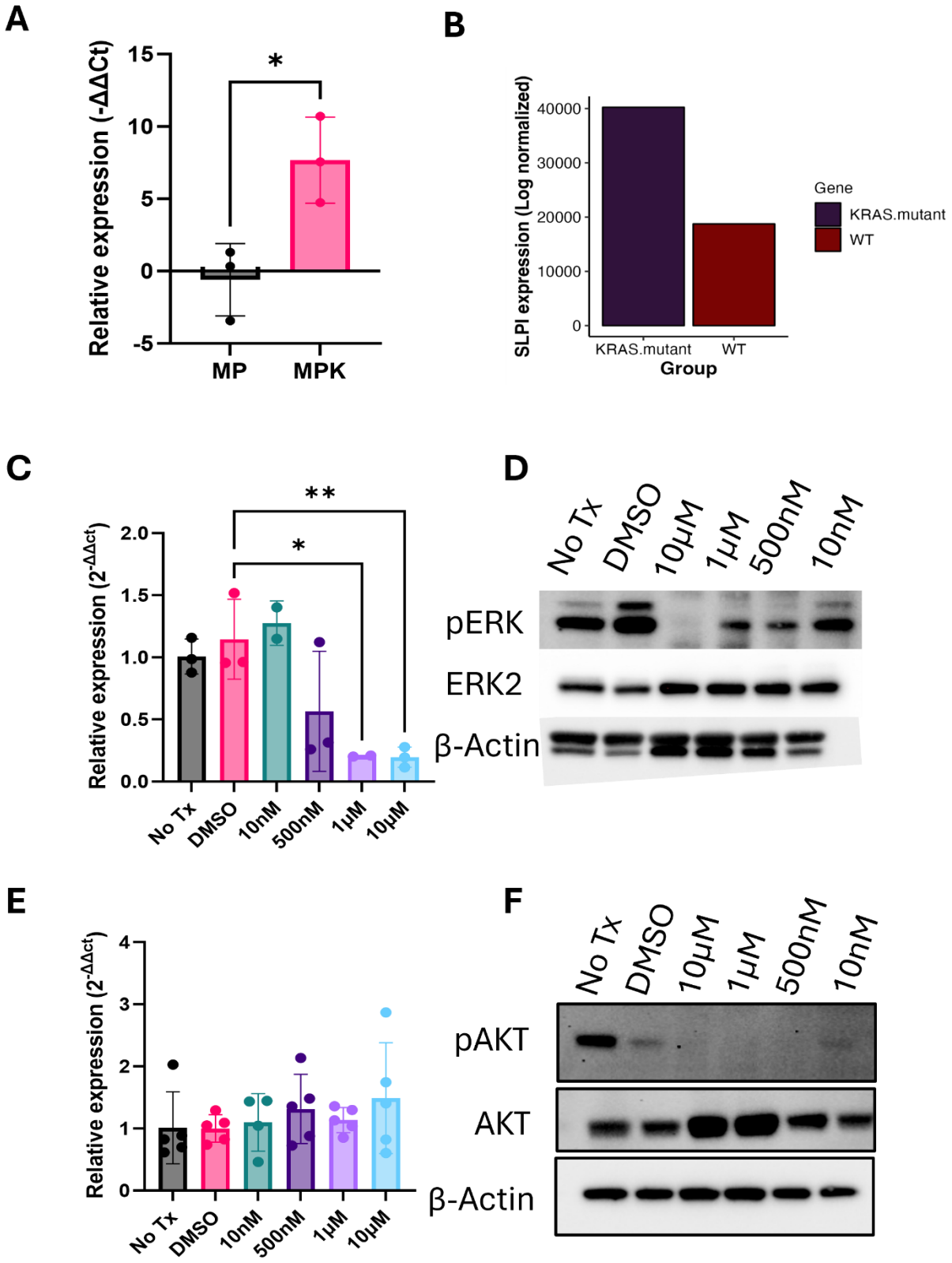
A
Relative expression (-ΔΔCt)
15
10
5
0
-5
*
MP
MPK
B
SLPI expression (Log normalized)
40000
30000
20000
10000
0
KRAS.mutant
WT
Group
Gene
KRAS.mutant
WT
C
Relative expression (2-ΔΔct)
2.0
1.5
1.0
0.5
0.0
**
*
No Tx
DMSO
10nM
500nM
1μM
10μM
D
No Tx
DMSO
10μM
1μM
500nM
10nM
pERK
ERK2
β-Actin
E
Relative expression (2-ΔΔct)
4
3
2
1
0
No Tx
DMSO
10nM
500nM
1μM
10μM
F
No Tx
DMSO
10μM
1μM
500nM
10nM
pAKT
AKT
β-Actin

Figure 7. SLPI expression is controlled by activation of the MEK/ERK pathway. *(A) Relative expression level of SLPI mRNA increases by addition of the KRas mutation in the MPK cell line (B) Ovarian cancer groups with KRas mutation (n=306) from TCGA show increased levels of SLPI compared to non-mutants (WT) (n=3) (C) MEK inhibitor treatment decreases the level of Slpi expression in MOE* $Pten^{shRNA}KRas^{G12V}$ *(n=3) (D) Samples treated with MEK inhibitor show a decrease in the pERK levels. (E) AKT inhibitor treatment does not affect the level of Slpi expression in MOE* $Pten^{shRNA}KRas^{G12V}$*(n=5) (F) Samples treated with AKT inhibitor show a decrease in the pAKT levels. Results were represented as mean +/- SD in (A), (C), and (E). Statistical analysis was done using one-way ANOVA and the p-value was less than 0.01 or 0.05 (indicated respectively as ** and *). Abbreviations of the figures MP and MPK refer to MOE* $Pten^{shRNA}$ *and MOE* $Pten^{shRNA}KRas^{G12V}$*.*

3.5 Assessing the effect of recombinant SLPI on T cells

The effect of SLPI on immune cells, particularly T cells, has been poorly studied. Given the strong interaction between SLPI and CD4+ cells discovered in the scRNA-seq analysis, we evaluated the effects of recombinant SLPI on CD4+ and CD8+ T cells by assessing the expression of activation and immune checkpoint markers under various conditions. Specifically, this analysis aimed to compare the impact of rSLPI on CD4+ cells with its effects on CD8+ cells.

3.5.1 CD4+ T cells

For CD4+ T cells, we examined two conditions. The first was the activated state, where cells were seeded on a pre-coated anti-CD3/CD28 plate and treated with 1µg/mL or 2µg/mL of recombinant SLPI for 72 hours (**Figure 8**). The second was the priming condition, where cells were initially treated with 1µg/mL or 2µg/mL of recombinant SLPI and IL-7 for 24 hours to maintain their naïve state, then washed and transferred to a pre-coated anti-CD3/CD28 plate for an additional 48 hours (**Figure 8**). Naïve CD4+ T cell treatment was excluded as rSLPI did not affect the expression of the markers of interest.

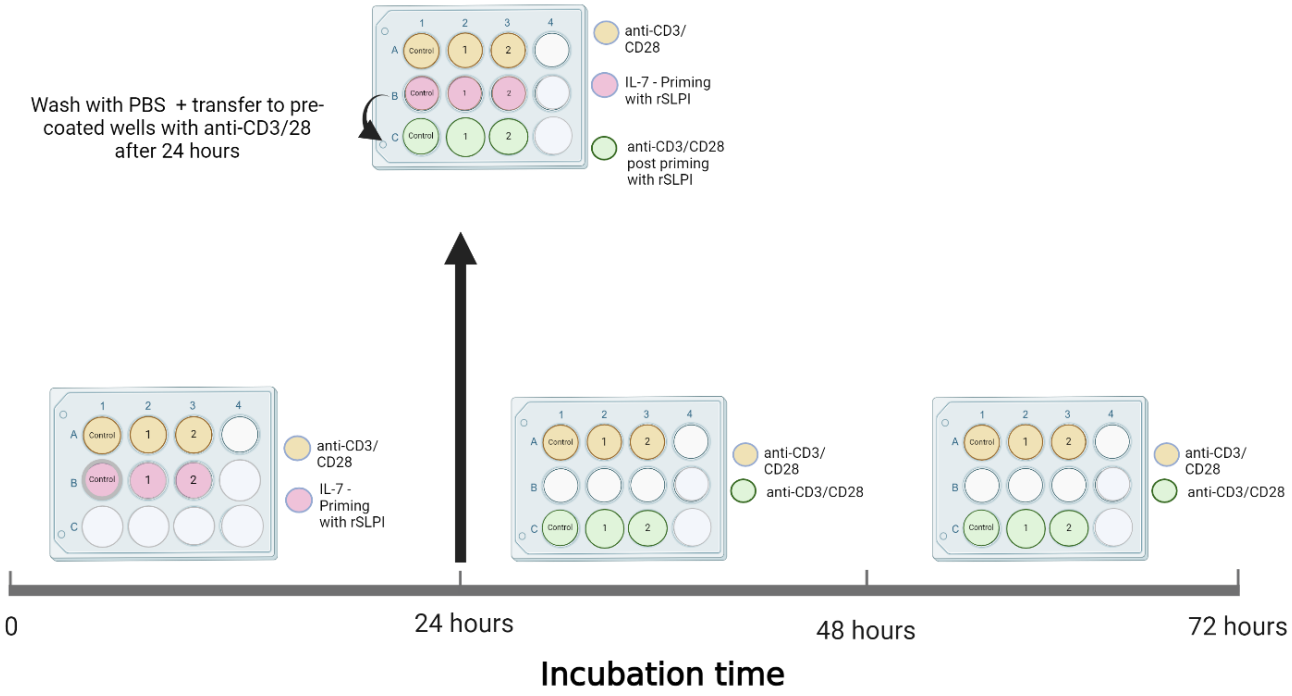

Figure 8. Schematic design of the CD4+ T cell experimental conditions over a 72-hour period. *After isolation, cells were incubated either in wells pre-coated with anti-CD3/CD28 antibodies (Line A of the 12-well plate) for 72 hours, or in IL-7 rich media with no rSLPI (control), 1µg/mL, or 2µg/mL rSLPI (Line B of the 12-well plate) for 24 hours under primed conditions. Subsequently, the primed cells were transferred to Line C wells and incubated for an additional 48 hours (Line C of the 12-well plate). This figure is created with BioRender.*

3.5.1.1 Activation markers

To assess the activation level of CD4+ T cells in both the anti-CD3/CD28 and primed conditions, we measured the expression of the early activation marker CD69 relative to CD25, another activation marker expressed later to enable the proliferation of T cells in response to specifically IL-2 cytokine[81]. In the anti-CD3/CD28 condition, rSLPI treatment increased the percentage of CD69+CD25+ cells from 18.7% in the controls to 55.5% at the 1µg/mL dose and to 77.1% at the 2µg/mL dose (**Figure 9A, top panel**). In the primed condition, the percentage of the CD69+CD25+ population did not change in response to 1µg/mL of rSLPI (Q22: 41.5%) compared to the control (Q22: 40.6%) (**Figure 9A bottom panel**). However, treatment with 2µg/mL of rSLPI

caused a slight shift to 31.3% of CD69+CD25+ T cells (**Figure 9A bottom panel**). When looking at the CD69+CD25- CD4 T cells in the primed condition, a slight increase is observed in their percentage from the control (Q23: 19.2%) to the 1μg/mL treated (Q23: 23.8%) to the 2μg/mL treated condition (Q23: 31.7%) (**Figure 9A bottom panel**). Therefore, the overall percentage of CD69+ (activated) CD4+ T cells has increased with SLPI treatment with no change in the CD25 marker during the primed condition.

CD62L, another marker commonly found in naïve T cells[82], showed consistent results with CD69. In the anti-CD3/28 condition, there was a gradual increase in the percentage of CD62L-CD25+ T cells (Q25) and a corresponding decrease in CD62L+CD25- T cells (Q27). The percentage of CD62L-CD25+ cells increased from 70.8% in the control to 75.7% with 1μg/mL treatment and to 87.4% with 2μg/mL treatment. Conversely, CD62L+CD25- cells decreased from 5.63% in the control to 1.38% with 1μg/mL treatment and 0.56% with 2μg/mL treatment. (**Figure 9B top panel**). In the primed condition, the percentages of CD62L-CD25+ and CD62L+CD25- T cells remained relatively unchanged, with Q25 values around 32% and Q27 values around 24% across all three conditions (**Figure 9B bottom panel**). However, the percentage of the CD62L+CD25+ T cells (Q26) decreased from 30.7% in the control to 28.4% in the 1μg/mL treatment to 23.8% in the 2μg/mL treatment conditions (**Figure 9B bottom panel**). These findings indicate that rSLPI treatment increases these activation markers in CD4+ T cells.

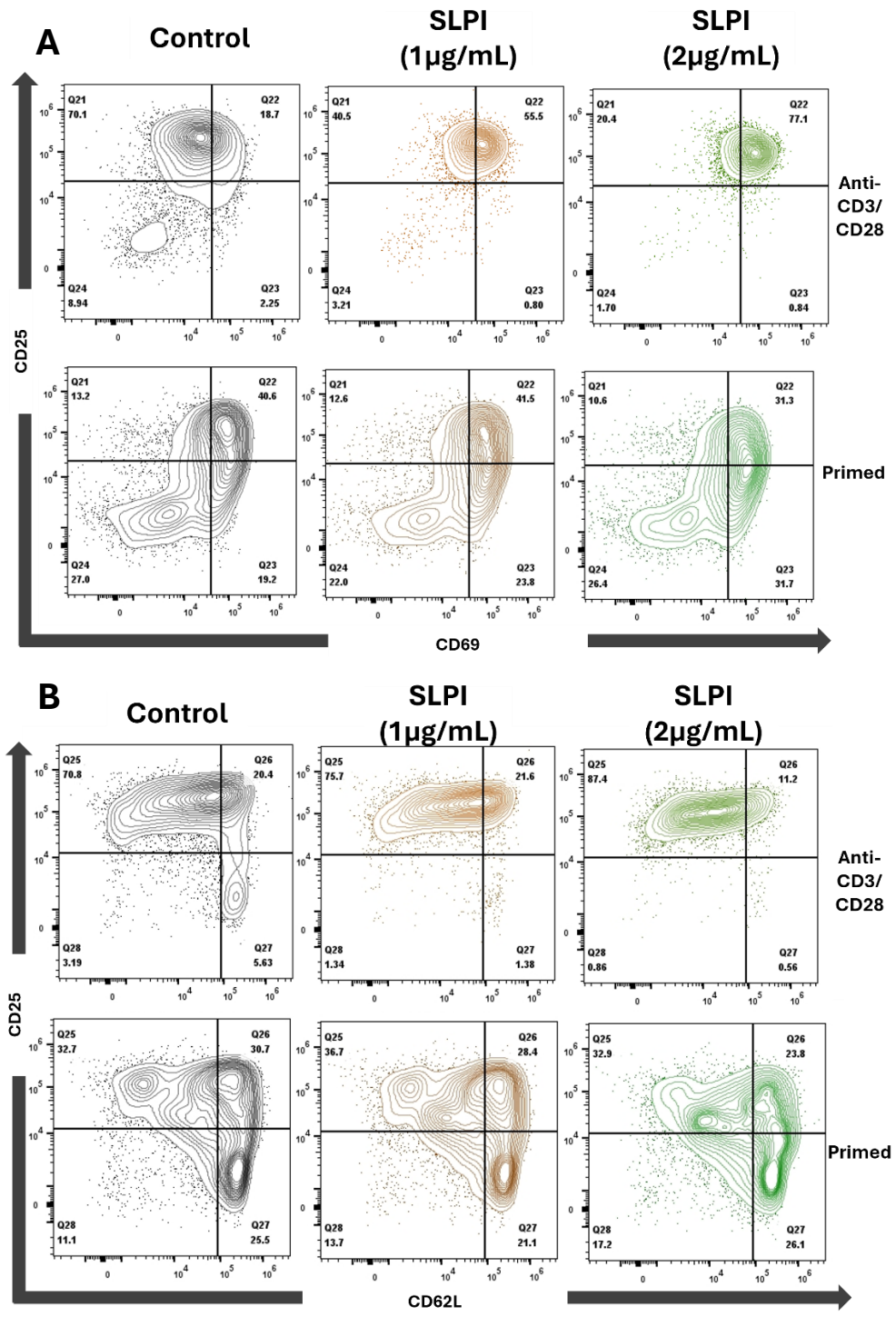

Figure 9. Treatment with recombinant SLPI increased the activation of CD4+ T cells based on the frequency of expression of CD69 and CD62L markers relative to the CD25 marker*. Contour plots showing cell population frequencies based on the expression of A) CD25 and CD69 and B) CD25 and CD62L in CD4+ T cells activated with anti-CD3/CD28 and co-treated with rSLPI for 72h (top) and CD4+ T cells primed with rSLPI then activated with anti-CD3/28 for 48h (bottom). Gating started by isolating lymphocytes, then single cells, followed by dead cell exclusion, and*

then CD4+ cells. FMOs were used for each marker to gate on the true positives. Only one replicate is represented in the figure, but another one showed similar results.

3.5.1.2 Immune checkpoint markers

The phenotypic profile of the cultured CD4+ T cells was next assessed in the two main studied conditions by evaluating the levels of expression of three immune checkpoint markers: PD-1, PD-L1, and LAG3. The PD-1 marker showed a shift in the percentage of PD-1+CD25+ T cells in Q14 that went from 87.8% in the control group to 96.3% and 98.4% respectively in the cells treated with 1µg/mL and 2µg/mL rSLPI during CD3/CD28 activation (**Figure 10A top panel**). These changes observed in Q14 did not occur in the primed condition, but instead, there was a slight shift in the PD-1+CD25- cell population that went from 11.4% in the control group to 13% and 19% respectively in the 1µg/mL and 2µg/mL treated group (**Figure 10A bottom panel**). The PD-L1 marker showed similar trends to the PD-1 marker, especially in the anti-CD3/CD28 condition, where the percentage of PD-L1+CD25+ T cells increased from 17.6% in the control group to 38.5% in the 1µg/mL treated group to 65.3% in the 2µg/mL treated group (**Figure 10B top panel**). The priming of the CD4+ T cells with rSLPI did not affect the proportion of cells expressing PD-L1 (**Figure 10B bottom panel**). Unlike PD-1 and PD-L1, the percentage of LAG3+ cells did not change with the rSLPI treatment in either the anti-CD3/28 or the primed conditions (**Figure 10C**). The only change observed was a decrease in the LAG3-CD25- in Q20 and an increase in the LAG3-CD25+ cell population in the anti-CD3/28 due to the rise in percentage in the CD25 marker (**Figure 10C top panel**). These findings suggest that rSLPI treatment selectively modulates the expression of PD-1 and PD-L1 in CD4+ T cells during CD3/CD28 activation, while LAG3 expression remains unaffected under the same conditions.

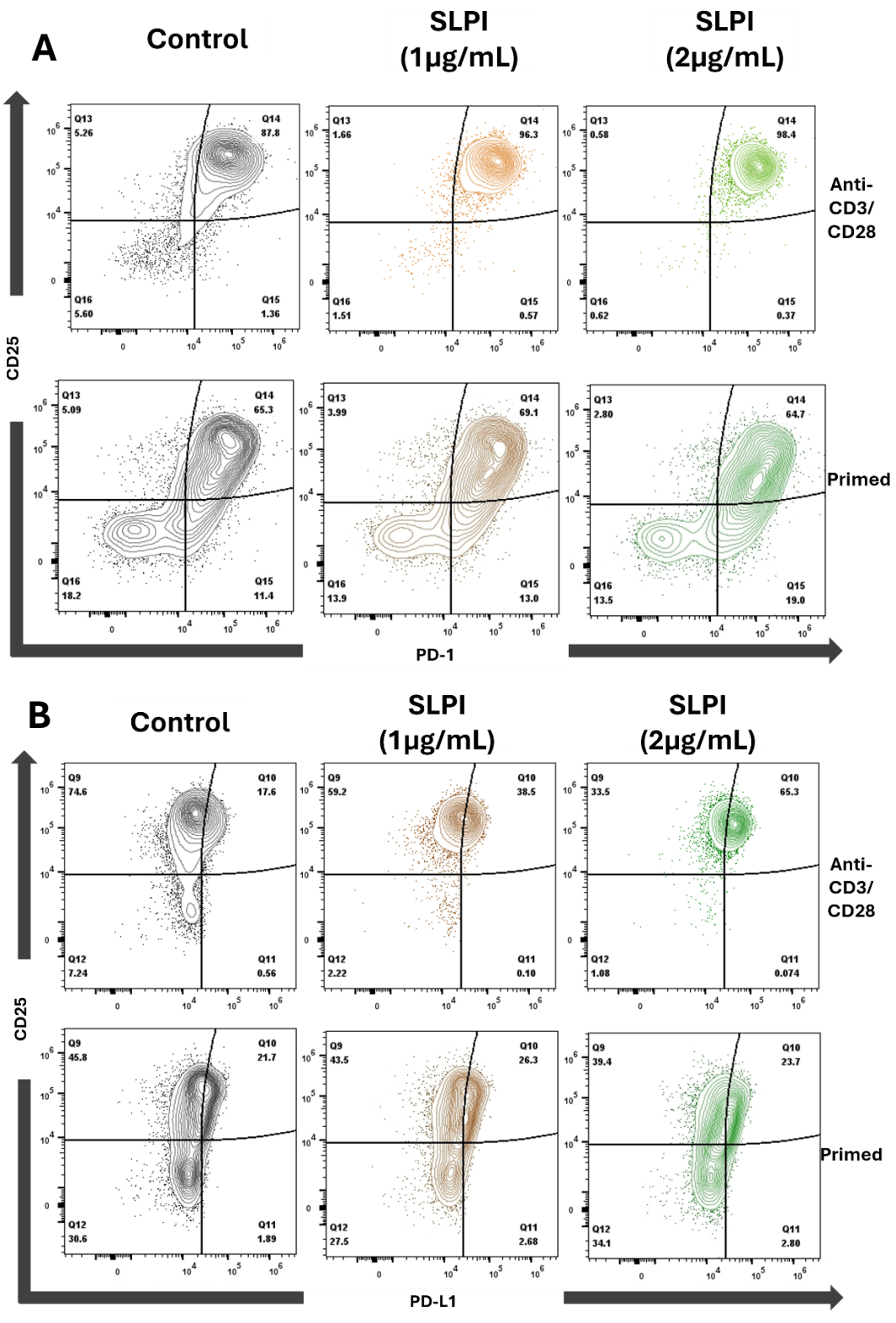
A
Control
SLPI (1µg/mL)
SLPI (2µg/mL)
Anti-CD3/CD28
Primed
CD25
PD-1
Q13 5.26
Q14 87.8
Q16 5.60
Q15 1.36
Q13 1.66
Q14 96.3
Q16 1.51
Q15 0.57
Q13 0.58
Q14 98.4
Q16 0.62
Q15 0.37
Q13 5.09
Q14 65.3
Q16 18.2
Q15 11.4
Q13 3.99
Q14 69.1
Q16 13.9
Q15 13.0
Q13 2.80
Q14 64.7
Q16 13.5
Q15 19.0
B
Control
SLPI (1µg/mL)
SLPI (2µg/mL)
Anti-CD3/CD28
Primed
CD25
PD-L1
Q9 74.6
Q10 17.6
Q12 7.24
Q11 0.56
Q9 59.2
Q10 38.5
Q12 2.22
Q11 0.10
Q9 33.5
Q10 65.3
Q12 1.08
Q11 0.074
Q9 45.8
Q10 21.7
Q12 30.6
Q11 1.89
Q9 43.5
Q10 26.3
Q12 27.5
Q11 2.68
Q9 39.4
Q10 23.7
Q12 34.1
Q11 2.80

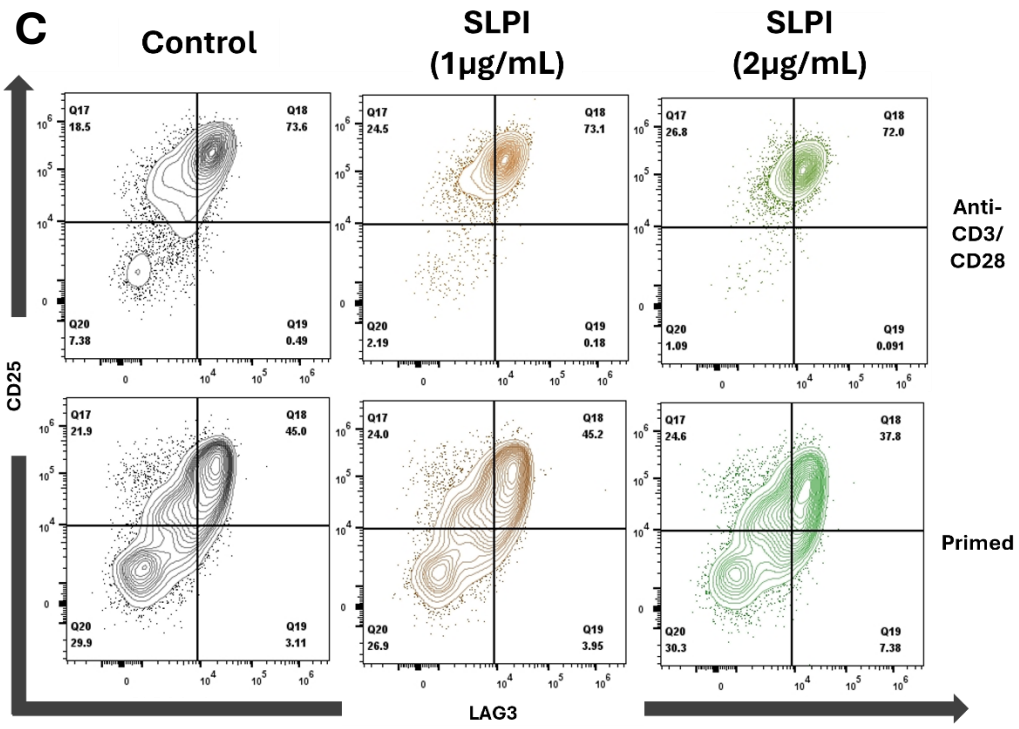

Figure 10. Treatment with recombinant SLPI increased the expression levels of PD-1 and PD-L1 but not LAG3 in CD4+ T cells. *Contour plots showing cell population frequencies based on the expression of A) CD25 and PD-1, B) CD25 and PD-L1, and C) CD25 and LAG3 in CD4+ T cells activated with anti-CD3/CD28 for 72h (top) and CD4+ T cells primed with rSLPI then activated with anti-CD3/28 for 48h (bottom) in control, 1ug/mL treatment with rSLPI and 2ug/mL treatment with rSLPI conditions. Gating started by isolating lymphocytes, then single cells, followed by dead cell exclusion, and then CD4+ cells. FMOs were used for each marker to gate on the true positives. Only one replicate is represented in the figure, but another one showed similar results.*

To complete the profiling of the CD4+ T cells, we collected RNA from both the anti-CD3/28 activated and the naïve (IL-7 treated) T cells after a treatment of 48h with 2µg/mL of rSLPI. To determine if rSLPI causes a pro- or anti-inflammatory stimulus in the TME 6 main cytokines (IFNγ, IL-21, IL-4, IL-6, IL-10, and TGFβ) were assessed via RT-qPCR. In both the activated and naïve conditions, rSLPI did not cause any significant changes in the mRNA levels of these cytokines. However, some of them were trending towards an increase or a decrease. For instance, IL-4 and IL-10 with a p-value of 0.059 and 0.1857 respectively tended to decrease with the addition

of rSLPI in the activating condition (**Figure 11A**). However, the opposite was seen in the naïve condition, where IL-10 (p=0.0971) and TGF-β (p=0.1116) expression tended to further increase. IL-21 showed a trend to decrease when naive CD4+ T cells were treated with rSLPI (p=0.1051) (**Figure 11B**). These findings indicate that, in the naïve state, rSLPI may promote the secretion of immunosuppressive cytokines, particularly IL-10 and TGF-β, and reduce the secretion of pro-inflammatory cytokines like IL-21. IFNγ and IL-6 expression did not show significant changes under the evaluated conditions and due to the high observed variability. However, these results will need a more thorough investigation, especially at the protein level.

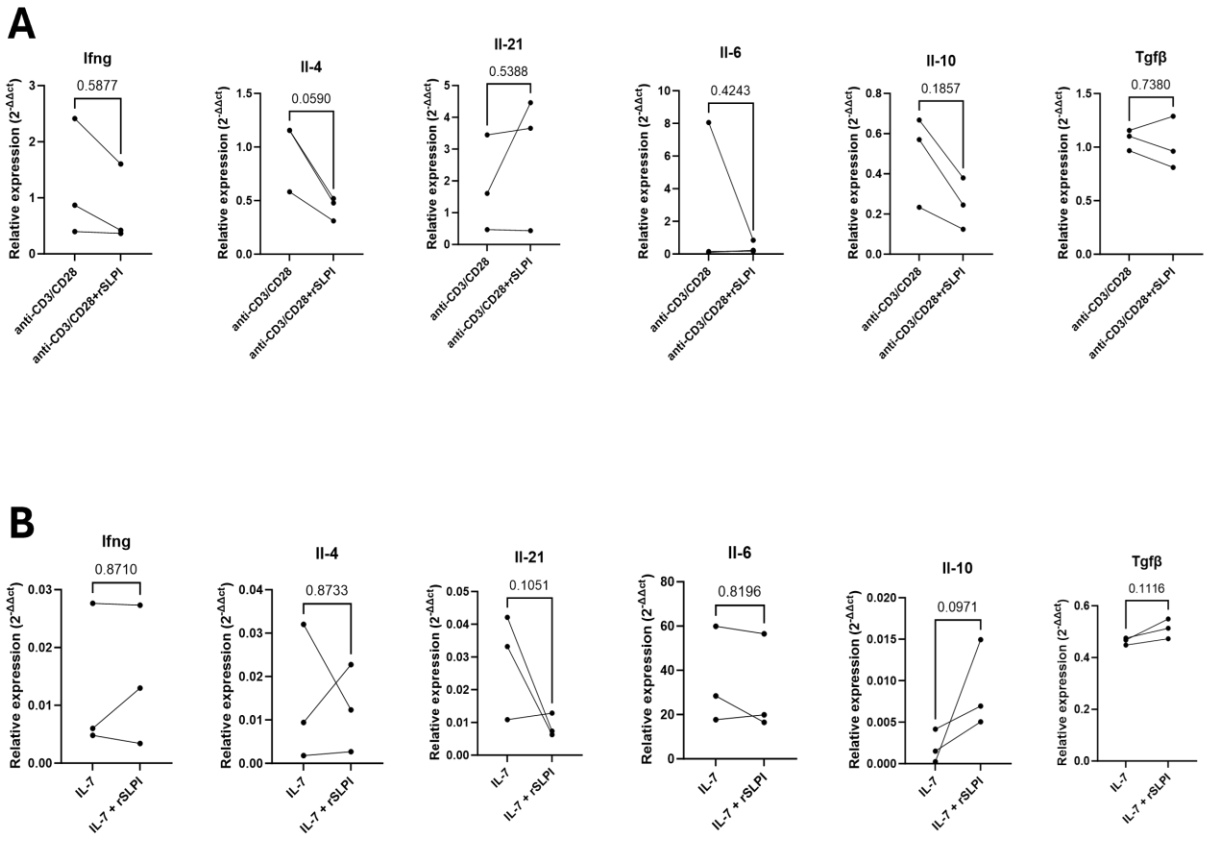

Figure 11. RNA expression levels of some cytokines do not change whereas some trend towards an increase or a decrease *when CD4+ T cells are* ***A)*** *activated with anti-CD3/CD28 and treated with 2µg/mL of rSLPI for 48h or* ***(B)*** *treated with IL-7 and 2µg/mL of rSLPI for 48h. Statistical analysis was done using one-way ANOVA and the p-value is shown for each plot. n=3*

3.5.2 Assessing the effect of recombinant SLPI on CD8+ T cells

For CD8+ T cells, OT-1 T cells were used to examine three conditions: the first one involved activation with anti-CD3/CD28, similar to CD4+ T cells; the second one involved activation with the OVA peptide (cognate peptide for OT-1 CD8+T cells, derived from the ovalbumin which is a protein found in the egg white), and the third condition consisted of naïve cells treated only with IL-7. In all conditions, cells were treated with 1µg/mL or 2µg/mL of recombinant SLPI for 72 hours.

3.5.2.1 Activation markers

To assess the activation of the CD8+ T cells across all the conditions, we focused on three main markers CD25, CD69, and CD62L. In the anti-CD3/CD28 condition, treatment with rSLPI did not cause any significant changes in the CD25 expression (gMFI) nor the frequency of the CD8+CD25+ T cells population (**Figure 13A**). However, in the OVA condition, the addition of 2µg/mL of rSLPI caused a significant increase in the gMFI of CD25 compared to the control with no change in its frequency (**Figure 13B**). The changes of the CD25 marker are important not only because they dictate the activation state in each condition, but also because CD25 is used as a reference to the CD69 and CD62L markers (**Figure 12A-B**). In the anti-CD3/28 condition, the addition of rSLPI did not cause any significant changes in either the gMFI or the frequency of CD69 (**Figure 12A top panel, and 13B**) and CD62L (**Figure 12B top panel, and 13B**) within the CD8+CD25+ T cell population. Similarly, in the OVA condition, rSLPI caused a non-significant shift in both CD69 (**Figure 12A middle panel, and 13B**) and CD62L (**Figure 12B middle panel, and 13B**) markers compared to the control. The naïve condition (IL-7) also showed no significant changes in the frequency of CD69 (**Figure 12A bottom panel**) and CD62L (**Figure 12B bottom**

panel), with a shift of 2% and 3% respectively in the percentage of the CD25+CD69+ and the CD25+CD62L+ populations. In summary, rSLPI treatment significantly increased CD25 expression in CD8+ T cells under the OVA condition, while showing no significant effects in the anti-CD3/CD28 and naïve conditions. The changes in CD69 and CD62L were minor and non-significant across all conditions (**Figure 13**).

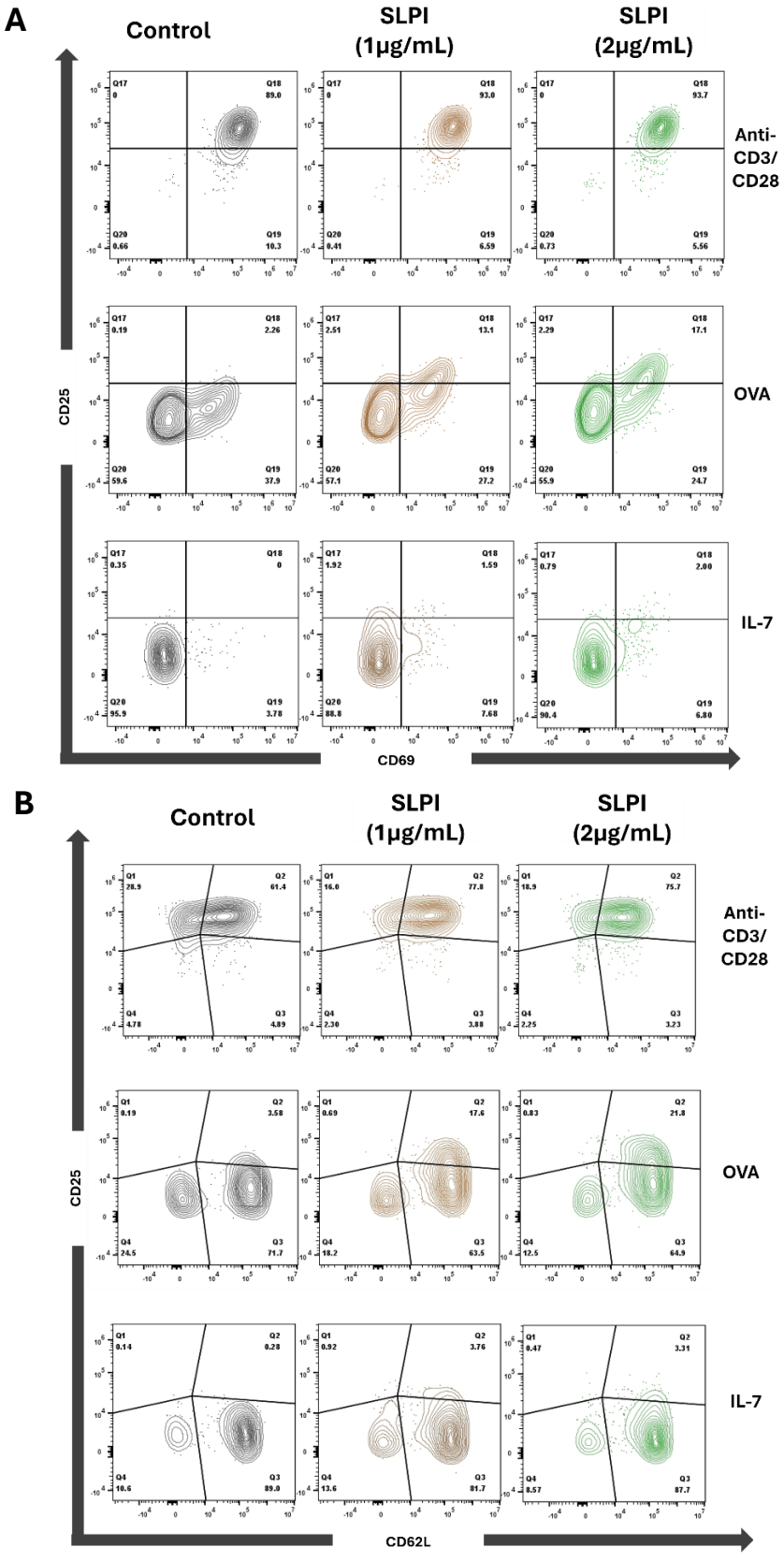
A
Control
SLPI (1μg/mL)
SLPI (2μg/mL)
Anti-CD3/CD28
OVA
IL-7
CD25
CD69
B
Control
SLPI (1μg/mL)
SLPI (2μg/mL)
Anti-CD3/CD28
OVA
IL-7
CD25
CD62L

Figure 12. Treatment with recombinant SLPI induces a shift in the frequency of the activation markers CD69 and CD62L in CD8+ T cells only when stimulated with OVA and rSLPI. *Contour plots showing cell population frequencies based on the expression of (A) CD25 and CD69 and (B) CD25 and CD62L in CD8+ T cells activated with anti-CD3/CD28 for 72h (top), CD8+ T cells stimulated with OVA peptide (middle), and CD8+ T cells maintained in their naïve state using IL-7 (bottom), when co-treated with 0, 1ug/mL or 2ug/mL rSLPI. Gating started by isolating lymphocytes, then single cells, followed by dead cell exclusion, and then CD8+ cells. FMOs were used for each marker to gate on the true positives.*

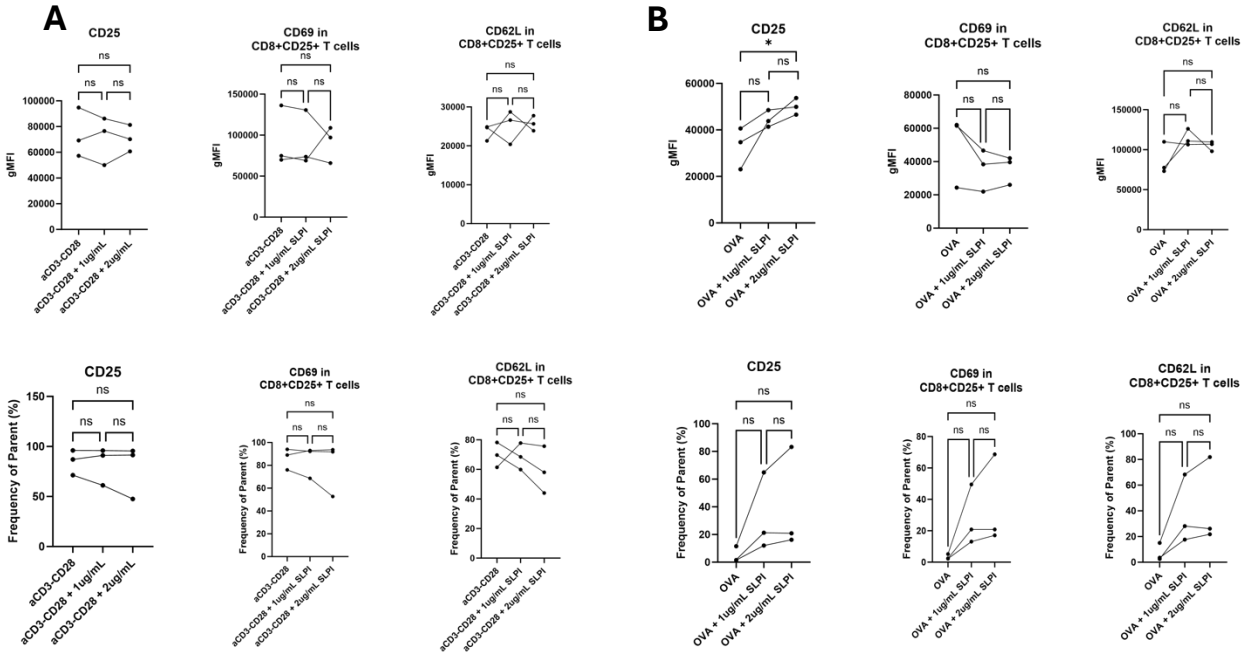

Figure 13. Quantification of the CD8+ T cell populations expressing CD25, CD69, and CD62L markers during the treatment with 1µg/mL and 2µg/mL of rSLPI *presented using their geometric mean fluorescent intensity (gMFI) and their frequency (%) when stimulated with (A) anti-CD3/28 to activate (B) OVA peptide. Statistical analysis was done using one-way ANOVA and the p-value is shown as * when $p<0.05$, and as ns (non-significant) when $p>0.05$.*

3.5.2.2 Immune checkpoint markers

Similar to the CD4+ T cell analysis, we assessed CD8+ T cells for changes of expression of three markers of immune checkpoint molecules PD-1, PD-L1, and LAG3 relative to CD25 in response to rSLPI under each of the three previously described conditions. In the anti-CD3/CD28 condition, rSLPI treatment did not cause any significant changes compared to the control which is

observed as the unchanging percentage of the CD8+CD25+ population in Q16 (**Figure 14A top panel**) as well as in the statistical analysis of the gMFI and frequency of PD-1 in the CD8+CD25+ population (**Figure 15A**). A similar observation was noted for PD-L1 and LAG3 in the anti-CD3/CD28 activated cells, where rSLPI treatment did not induce any significant changes (**Figure 14B, Figure 14C top panel, and Figure 15A**).

In contrast, in the OVA condition, the frequency of PD-1 in CD8+CD25+ cells increased significantly from 13% in the control to 40-45% after the addition of 1μg/mL and 2μg/mL of rSLPI (**Figure 14A middle panel, Figure 15B**). PD-L1 frequency in CD8+CD25+ cells also showed a trend towards an increase in response to 2μg/mL rSLPI in the OVA condition (**Figure 15B**) (9.62% in control vs. 22.7% with 2μg/mL rSLPI). However, PD-L1 expression represented by the gMFI in the CD8+CD25+ population significantly decreased with both 1μg/mL and 2μg/mL rSLPI. This indicates that even if the level of expression of PD-L1 in cells is decreasing, the percentage of PD-L1+ cells is increasing with rSLPI treatment. Similarly, LAG3 expression in cells did not change, but the frequency of CD8+CD25+LAG3+ cells increased dramatically with rSLPI (**Figure 14C middle panel, Figure 15B**).

In the naïve condition (IL-7), only slight shifts were observed in PD-1, PD-L1, and LAG3 frequencies within the CD8+CD25+ population, increasing from 0% in the control to 2%, 6%, and 2% after rSLPI treatment under the three conditions. In summary, rSLPI treatment did not significantly affect immune checkpoint markers PD-1, PD-L1, and LAG3 in the naïve or the anti-CD3/CD28 condition. However, in the OVA condition (cognate peptide), an increase in the frequency of PD-1+, PD-L1+, and LAG3+ cells was observed, suggesting that the effects of rSLPI on these markers in CD8+ T cells vary depending on the activation conditions and the strength of the TCR signaling.

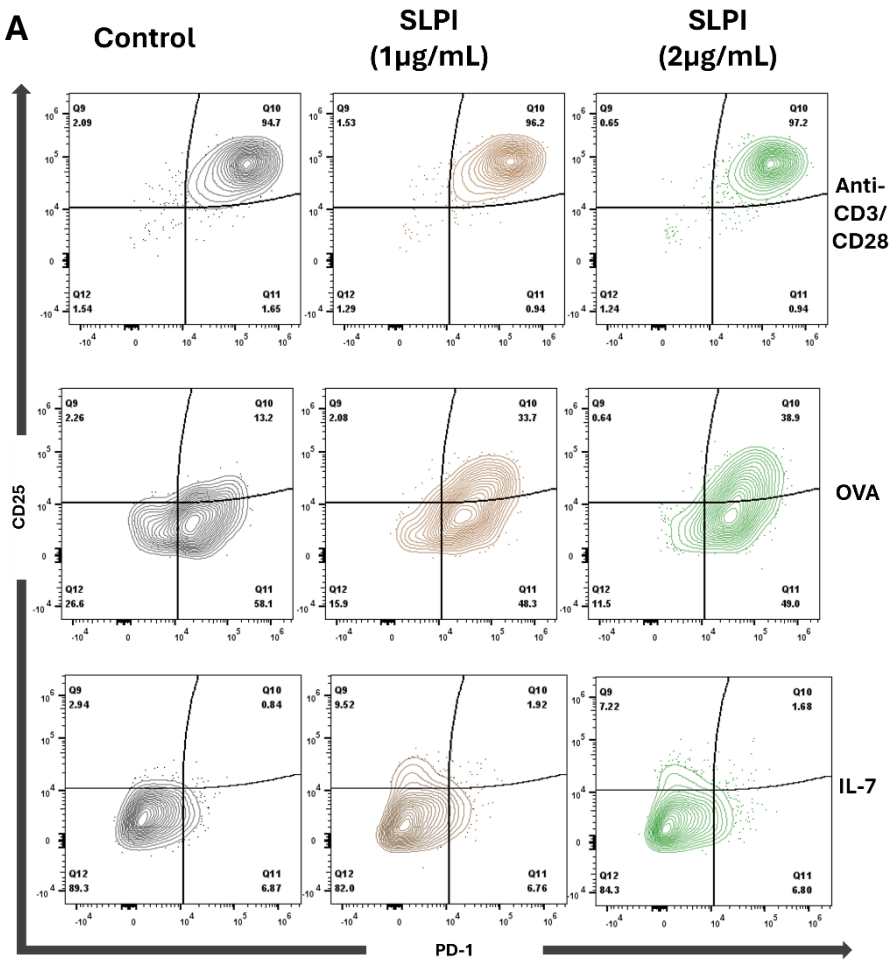
A
Control
SLPI (1μg/mL)
SLPI (2μg/mL)
Anti-CD3/CD28
OVA
IL-7
CD25
PD-1
Q9 2.09
Q10 94.7
Q12 1.54
Q11 1.65
Q9 1.53
Q10 96.2
Q12 1.29
Q11 0.94
Q9 0.65
Q10 97.2
Q12 1.24
Q11 0.94
Q9 2.26
Q10 13.2
Q12 26.6
Q11 58.1
Q9 2.08
Q10 33.7
Q12 15.9
Q11 48.3
Q9 0.64
Q10 38.9
Q12 11.5
Q11 49.0
Q9 2.94
Q10 0.84
Q12 89.3
Q11 6.87
Q9 9.52
Q10 1.92
Q12 82.0
Q11 6.76
Q9 7.22
Q10 1.68
Q12 84.3
Q11 6.80

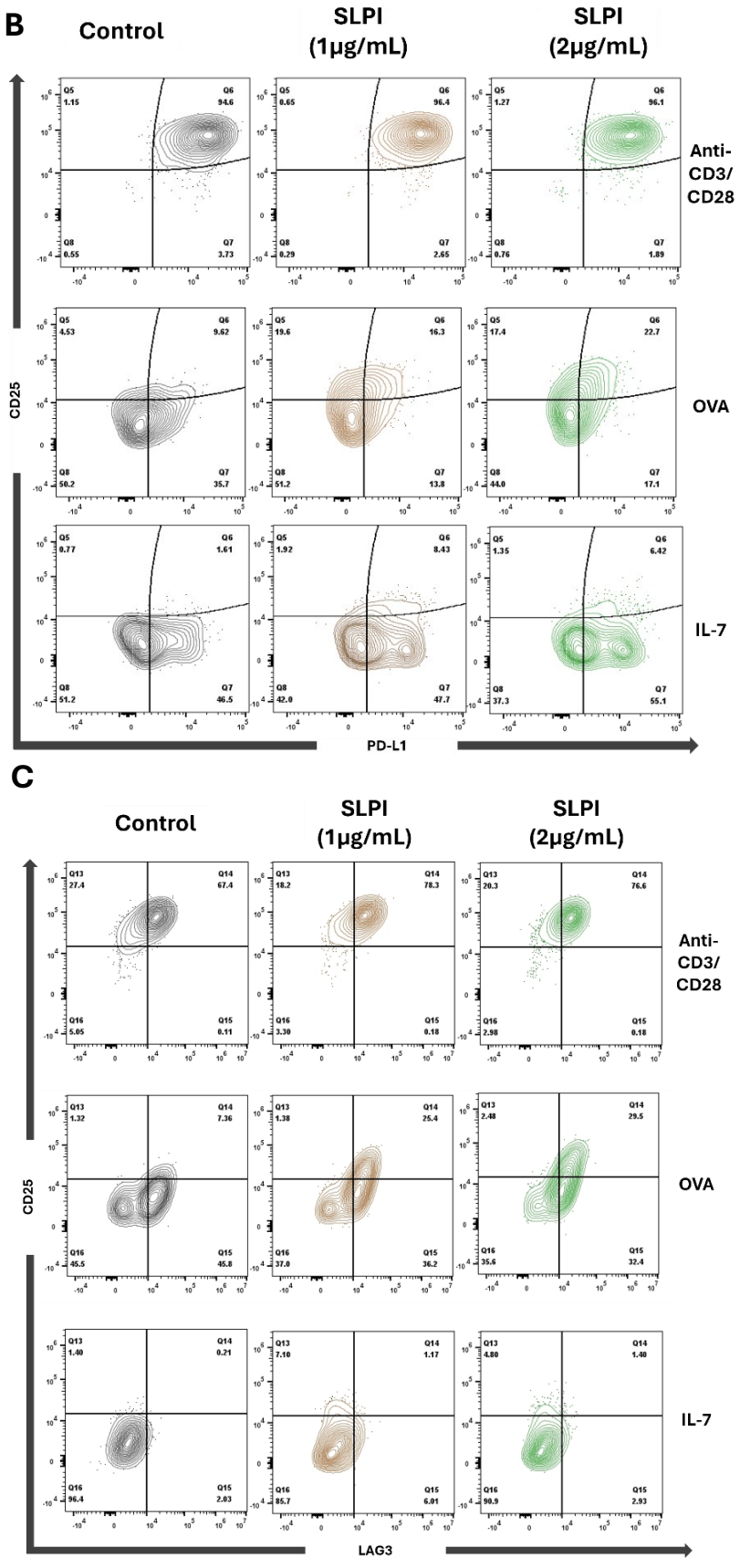
B
Control
SLPI (1μg/mL)
SLPI (2μg/mL)
Anti-CD3/CD28
OVA
IL-7
CD25
PD-L1
C
Control
SLPI (1μg/mL)
SLPI (2μg/mL)
Anti-CD3/CD28
OVA
IL-7
CD25
LAG3

Figure 14. Treatment with recombinant SLPI induces a shift in the frequency of the activation markers PD-1, PD-L1, and LAG3 in CD8+ T cells only when stimulated with both OVA and rSLPI. *Contour plots showing cell population frequencies based on the expression of (A) CD25 and PD-1 and (B) CD25 and PD-L1 in CD8+ T cells activated with anti-CD3/CD28 for 72h (top), CD8+ T cells stimulated with OVA peptide (middle), and CD8+ T cells maintained in their naïve state using IL-7 (bottom), in three conditions: control, 1ug/mL treatment with rSLPI and 2ug/mL treatment with rSLPI. Gating started by isolating lymphocytes, then single cells, followed by dead cell exclusion, and then CD8+ cells. FMOs were used for each marker to gate on the true positives.*

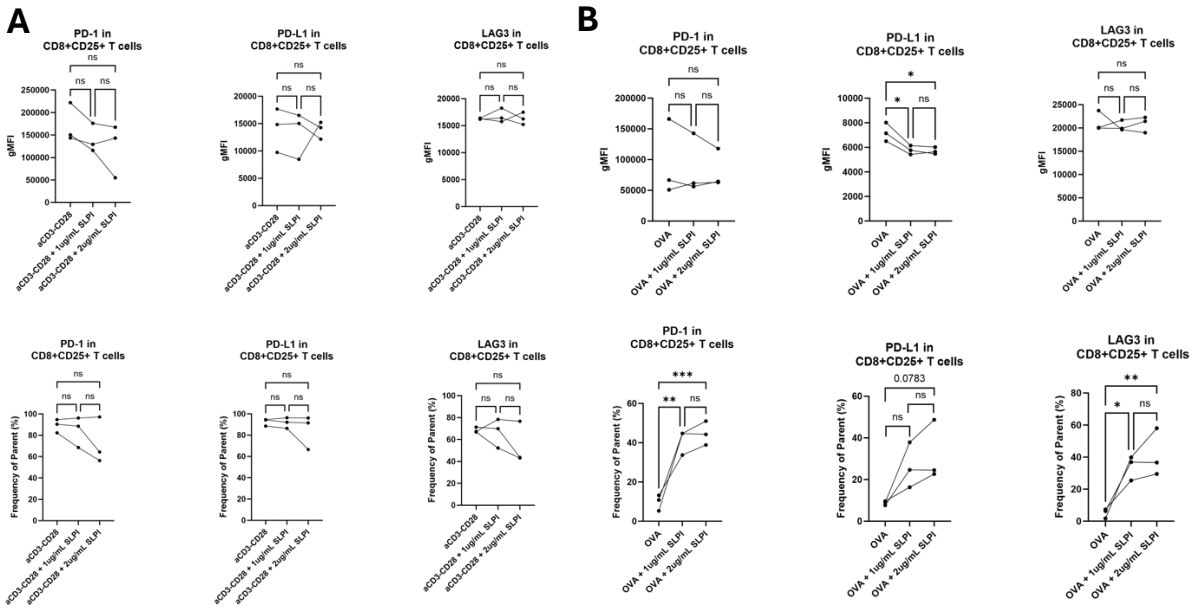

Figure 15. Quantification of the CD8+ T cell populations expressing PD-1, PD-L1, and LAG3 markers during the treatment with 1µg/mL and 2µg/mL of rSLPI *presented using their geometric mean fluorescent intensity (gMFI) and their frequency (%) when stimulated with (A) anti-CD3/28 to activate (B) OVA peptide. Statistical analysis was done using one-way ANOVA and the p-value is shown as * for p<0.05, ** for p<0.01, *** for p<0.001, value for p<0.1, and as ns for non-significant. n=3*

3.6 Development of knockout and overexpression models for SLPI

Having shown that SLPI has the potential to modify the activation/exhaustion state of T cells in vitro, I sought to determine whether those actions can modify cancer progression and the TME using mouse models of ovarian cancer. Based on their baseline levels of SLPI expression, two models were selected, MOE *Pten*^{shRNA}*KRas*^{G12V} and ID8-*Trp53-/-*, for the knockout and

overexpression of SLPI, respectively. ID8-*Trp53*-/- cells exhibit the lowest SLPI expression and MOE *Pten*^{shRNA}*KRas*^{G12V} had the highest, as shown in **Figures 5A and 5B**. In MOE *Pten*^{shRNA}*KRas*^{G12V}, *Slpi* was knocked out using three single-guide RNAs (sgRNA) using CRISPR/Cas9 technology. A control sgRNA targeting Renilla, a non-mammalian gene, was used a positive control expressing Cas9 and a guide RNA. The knockout was confirmed by western blot (**Figure 16A**) showing that sgSLPI-3 has a complete knockout of *Slpi* compared to sgSLPI-1 and sgSLPI-2 which still have some modest expression levels of SLPI. sgRenilla showed the same levels as the parental cell line (**Figure 16A**).

The overexpression of *Slpi* was carried out in ID8-*Trp53*-/- and KPCA.B cells using an expression vector generated by PCR amplifying fragments of the *Slpi* gene from genomic DNA to encode *Slpi* under the control of a CMV (cytomegalovirus) promoter. The lentivirus carrying the overexpression, or the empty vector was transduced into the cell lines that were then positively selected for puromycin resistance. The overexpression was confirmed by western blot (**Figure 16B-C**) after treating the cells with Brefeldin A to inhibit protein secretion. Cells overexpressing *Slpi* (ID8-*Trp53*-/-Slpi^{OE} and KPCA.B-*Slpi*^{OE}) had a higher SLPI abundance compared to vector-transduced and parental that had little to no detectable expression of SLPI with or without Brefeldin A treatment.

The effect of the knockout or overexpression of SLPI was first determined by assessing potential autocrine effects on cell proliferation. In the MOE *Pten*^{shRNA}*KRas*^{G12V} model, the parental, Renilla control, and *Slpi*-/- cell lines all reached the plateau after 72h with no significant difference in the cell counts (**Figure 16D**), which indicates that they all reached confluency at the same growth rate. However, at 96 hours, the parental cell line had significantly fewer cell counts than the Renilla control and the *Slpi*-/- (**Figure 16D)** due to cell death after the confluency. The

comparison between parental and Renilla controls mainly for the transduction impact on cell proliferation. When comparing the Renilla control and the *Slpi*-/-, the cell count of these cells over time was not different (**Figure 16D**). The overexpression of SLPI also did not affect the proliferation of the modified cells since there were no significant differences between the $Slpi^{OE}$ and $Slpi^{EV}$ in both ID8-*Trp53*-/- and KPCA.B (**Figure 16E-F**). $Slpi^{EV}$ controls exhibited no significant difference from the parental control over time in both ID8-*Trp53*-/- and KPCA.B cells, but the growth rate of the parentals in the latter started to slow down after 72 hours, which decreased significantly the cell count by 96 hours compared to the $Slpi^{EV}$. Overall, the knockout and overexpression modifications did not alter the proliferation rate across time in all modified cells.

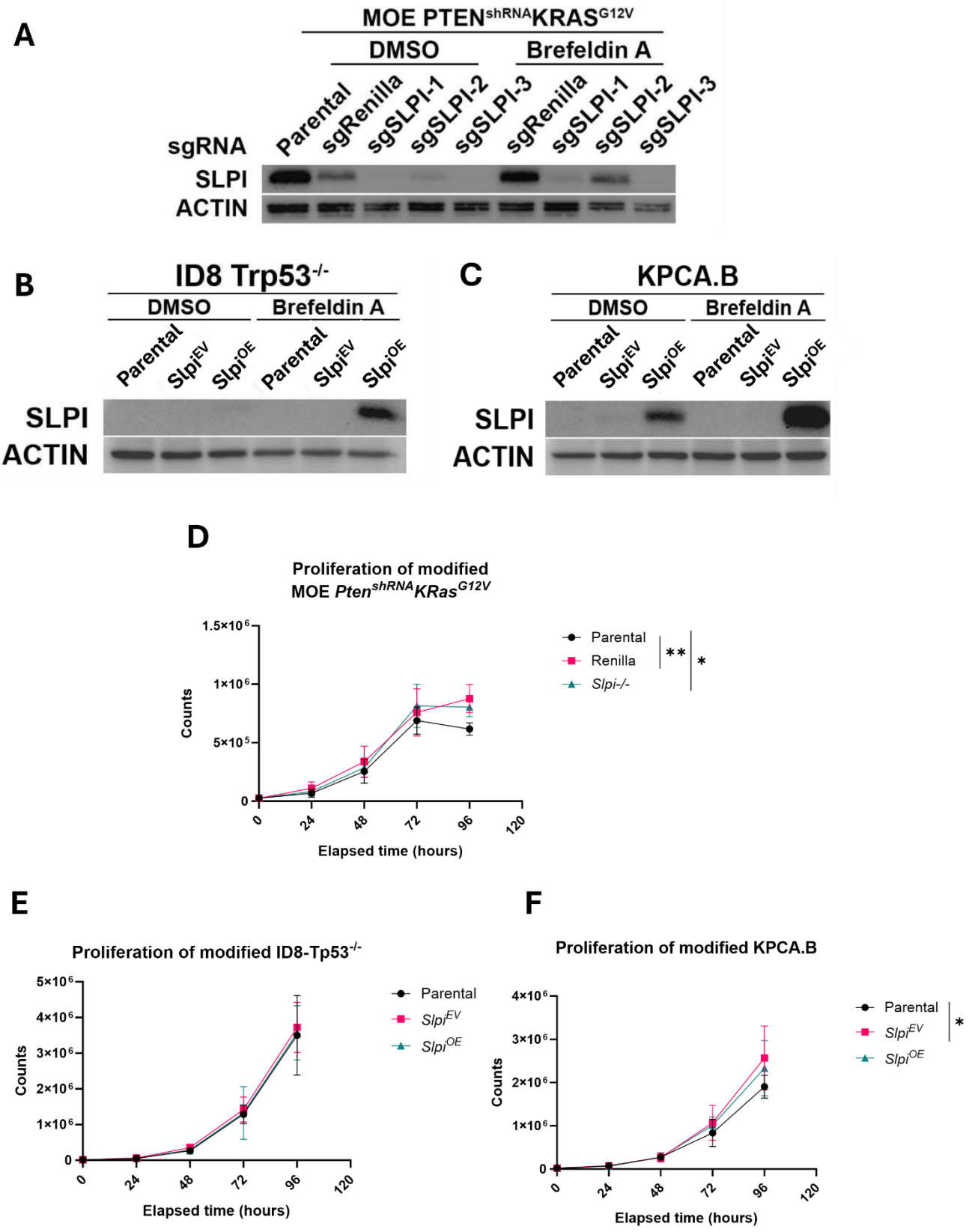
A
MOE PTEN^shRNA KRAS^G12V
DMSO
Brefeldin A
Parental
sgRenilla
sgSLPI-1
sgSLPI-2
sgSLPI-3
sgRenilla
sgSLPI-1
sgSLPI-2
sgSLPI-3
sgRNA
SLPI
ACTIN
B
ID8 Trp53-/-
DMSO
Brefeldin A
Parental
SlpiEV
SlpiOE
Parental
SlpiEV
SlpiOE
SLPI
ACTIN
C
KPCA.B
DMSO
Brefeldin A
Parental
SlpiEV
SlpiOE
Parental
SlpiEV
SlpiOE
SLPI
ACTIN
D
Proliferation of modified
MOE Ptenshrna KRasG12V
Counts
1.5×10^6
1×10^6
5×10^5
0
0
24
48
72
96
120
Elapsed time (hours)
Parental
Renilla
Slpi-/-
**
*
E
Proliferation of modified ID8-Tp53-/-
Counts
5×10^6
4×10^6
3×10^6
2×10^6
1×10^6
0
0
24
48
72
96
120
Elapsed time (hours)
Parental
SlpiEV
SlpiOE
F
Proliferation of modified KPCA.B
Counts
4×10^6
3×10^6
2×10^6
1×10^6
0
0
24
48
72
96
120
Elapsed time (hours)
Parental
SlpiEV
SlpiOE
*

Figure 16. Knockout and overexpression of Slpi do not impact cell proliferation. ***(A)*** *Western blot showing the levels of SLPI in MOE Pten^{shRNA}KRas^{G12V} cells transduced with 3 sgRNA and a control (sgRenilla) lentivirus compared to the parental cell line.* ***(B)*** *Western blot showing the levels of SLPI in ID8-Trp53-/- cells transduced with a lentiviral vector alone (empty) or overexpressing Slpi compared to the parental cell line.* ***(C)*** *Western blot showing the levels of SLPI in KPCA.B cells transduced with a lentiviral vector alone (empty) or overexpressing Slpi compared to the parental cell line.* ***(D)*** *Graph showing the proliferation of modified MOE Pten^{shRNA}KRas^{G12V} cells across time.* ***(E)*** *Graph showing the proliferation of modified ID8-Trp53-/- cells across time.* ***(F)*** *Graph showing the proliferation of modified KPCA.B cells across time. Data in D-F are shown as mean ± SD. Statistical analysis was done using one-way ANOVA and Tukey's post-hoc comparison test and the p-value was less than 0.01 or 0.05 (indicated respectively as ** and *). n=4*

3.7 Assessing the impact of SLPI's expression on mice survival

To determine the effects of SLPI on tumorigenicity and the rate of tumor progression, the modified MOE *Pten^{shRNA}KRas^{G12V}*, ID8-*Trp53-/-* and KPCA.B cells were injected intraperitoneally. All the models formed metastatic tumors within the peritoneal cavity, indicating that the presence or absence of SLPI did not affect the tumorigenicity of the three cell lines. At humane endpoint, the tumor weights in the MOE *Pten^{shRNA}KRas^{G12V}* model were not different amongst the mice with parental, Renilla control, and *Slpi*-/- tumors (**Figure 17D**). However, the ascites volume was significantly higher in the mice with parental tumors (~7mL) compared to both the Renilla control and *Slpi*-/- tumors (~2mL) (**Figure 17D**). In terms of survival rate, mice with tumors deficient in SLPI had a significantly lower median survival (46 days) than the mice with Renilla control tumors (62 days) (**Figure 17A**). This shows that the knockout of Slpi increased tumor progression which resulted in shorter survival. However, mice with tumors derived from the parental cell line had a significantly shorter period of survival (median of 37 days) compared to both the Renilla control and the *Slpi*-/- tumors. This difference between the parental and Renilla control group is possibly due to the immunogenicity of Cas9[83], reducing the amounts of ascites

that are known to have immunosuppressive cytokines/chemokines, thereby slowing tumor progression.

The models which tested the effects of overexpression of SLPI led to divergent outcomes. In the ID8-*Trp53-/-* model, mice with tumors that overexpress SLPI ($Slpi^{OE}$) had significantly prolonged survival (median of 55 days) (**Figure 17B**) and significantly lower tumor weight (**Figure 17E**) compared to the $Slpi^{EV}$ control group. The ascites volume was around 4.5mL and was not different between the two groups (**Figure 17E**). In contrast, in the KPCA.B model, the length of survival of mice with $Slpi^{OE}$ tumors was not different from mice with control and parental tumors (**Figure 17C**). Despite the similar survival, mice with $Slpi^{OE}$ tumors had a significantly higher volume of ascites (~3mL) compared to the parental group (~0.5mL), with a trend of an increase relative to the $Slpi^{EV}$ group (~1.5mL, p= 0.1008) (**Figure 17F**). The ascites volume did not have any impact on the tumor weights, which were not significantly different among the three groups (**Figure 17F**).

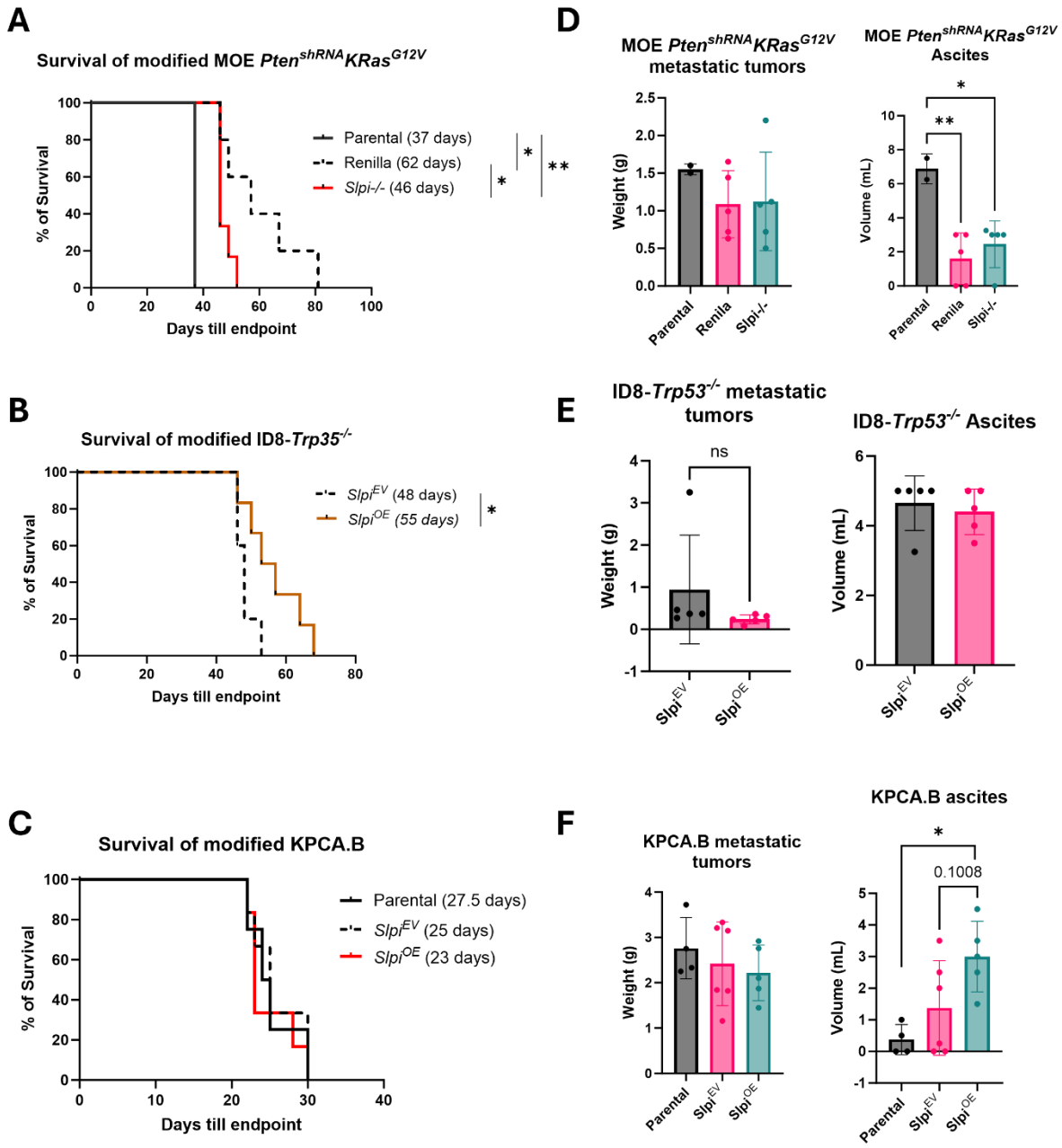

Figure 17. Survival of mice bearing tumors with modified expression of SLPI. *Kaplan-Meier plots showing the survival of A) modified MOE Pten^{shRNA}KRas^{G12V} tumor-bearing mice, B) modified ID8-Trp53-/- tumor-bearing mice, and C) modified KPCA.B tumor-bearing mice. Panel showing the tumor weight and ascites volume at the humane endpoint in D) modified MOE Pten^{shRNA}KRas^{G12V} tumor-bearing mice, E) modified ID8-Trp53-/- tumor-bearing mice, and F) modified KPCA.B tumor-bearing mice. Statistical analysis of (A-C) was done using the Log-rank (Mantel-Cox). Data in (D-F) is shown as mean +/- SD. Statistical analysis of (D-F) was done using one-way ANOVA. *p<0.05, **p<0.01.*

3.8 Assessing the impact of SLPI's expression on the TME components

3.8.1 Gating Strategy

The effects of SLPI on the composition of the ovarian TME have never been studied. Therefore, we used the modified MOE *Pten*^{shRNA}*KRas*^{G12V} and KPCA.B cells with SLPI knockout and overexpression to determine how SLPI contributes to the TME. The cell lines were injected under the bursa of syngeneic mice and the mice were monitored until the tumor formation passed 50% of development and was closer to the humane endpoint (6 days before), then collected for the TME analysis. The TME composition of these two models was analyzed using a flow cytometry panel (**Table 5**) that generated an overview of the major differences that occur with the overexpression or knockout of SLPI from cancer cells. The gating strategy (**Figure 18**) first eliminated doublets by gating on single cells, showing a linear correlation between the Forward Scatter Height (FSC-H) and Forward Scatter Area (FSC-A). We then gated on the lymphocytes based on the FSC-H and the Side Scatter Area (SSC-A) and, using our viability sample, we gated on the cells with low FSV510 staining (viable cells). From the viable population, we separated the CD45+ and CD45- populations, in which we examined the expression of PD-L1. Using the CD3 marker, we separated T cells (CD3+) from myeloid cells (CD3-), the latter of which we gated on 4 populations based on the expression levels of CD11b, CD11c, and F4/80 markers. In T cells, we gated on the CD4+ and CD8+ T cells, in which we examined the frequency of cells expressing CD25, PD-1, PD-L1, GATA3, T-Bet, and FOXP3 markers. FMO controls were used to gate on the real positive populations. In our analysis, TME was determined by the percentage of cells in that population and differences in expression levels, which were compared using the gMFI values.

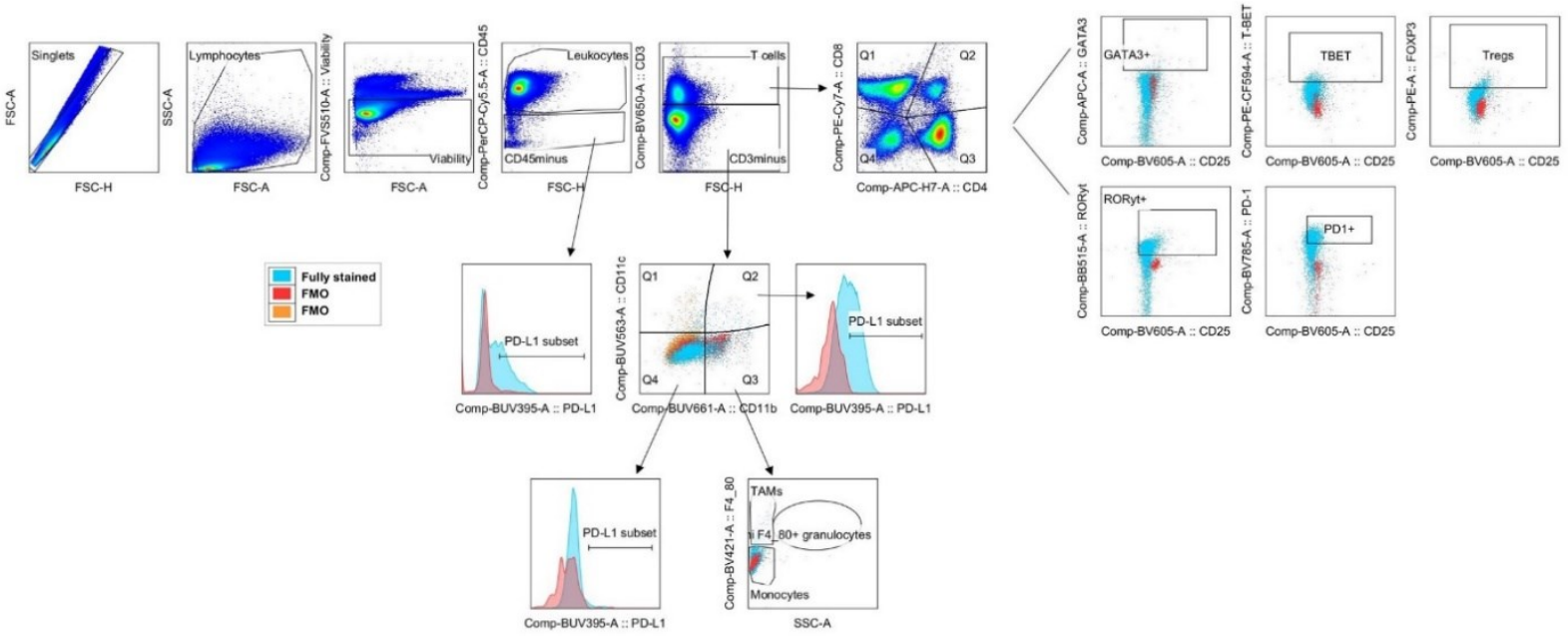

Figure 18. Gating strategy of the cell populations of interest for analysis of the TME*. The panel of antibodies used are listed in Table 5.*

3.8.2 Effect of SLPI on the ovarian TME

Because the MOE Pten^{shRNA}KRas^{G12V} has a median survival of 37 days[84], we collected tumors from the mice on day 24, which allowed us to examine the TME in growing tumors that were large enough for TME analysis. However, at day 24, both the *Slpi*-/- and Renilla control groups had not yet reached 50% of their tumor development. Consequently, some mice had no sign of tumor formation, others had a solid ovary that indicated the onset of tumor development, and a few others had tumors with a small weight (i.e. less than 0.05g) that we were able to pool together. Therefore, the number of samples that were processed was 4 for the parental tumors, 2 for the Renilla control group, and 2 for the *Slpi*-/- group. The statistical analysis done using this number mainly allows for visualization of the differences occurring within the TME at this timepoint but still needs to be confirmed with a greater number of samples.

Conversely, tumors from the KPCA.B model were collected after 50% of their median survival, by which time enough samples were available for each group. However, one of the mice from the parental group and another one from the *Slpi*^{OE} group reached the endpoint before the scheduled day of collection. Therefore, the final number of samples for each of the parental, *Slpi*^{EV}, and *Slpi*^{OE} groups was 2, 6, and 5 tumors, respectively.

3.8.2.1 Frequency of main cell populations in the TME

Differences in the frequencies of cell populations within the TME are important indicators of mechanisms contributing to tumor development. In the MOE *Pten*^{shRNA}*KRas*^{G12V} model, the presence or absence of SLPI resulted in no significant differences in terms of the frequency of CD45- (epithelial or non-immune cells) (**Figure 19A**) and the CD45+ (leukocytes) (**Figure 19B**) populations. The frequency of all 4 subsets of myeloid cells (i.e. CD11b-CD11c+, CD11b+CD11c+ representing generally dendritic cells (DCs)[85], CD11b+F4/80+ representing TAMs, and the CD11b-CD11c-) was also not different among the 3 tumor groups (**Figure 19C-F**). Similarly, the T cell subsets were not different among the tumors (**Figure 19G**), whether in terms of the CD4+ T cell population (**Figure 19J**), or the CD8+ T cell population (**Figure 19I**), or their ratio (**Figure 19H**). This suggests that the knockout of SLPI did not change the MOE *Pten*^{shRNA}*KRas*^{G12V} TME at the collected timepoint.

The overexpression of SLPI in the KPCA.B model similarly had no effect on the main cell populations in the TME. The frequency of CD45- (non-immune cells) (**Figure 20A**), myeloid cells including CD11b-CD11c+ (**Figure 20C**), CD11b+CD11c+ (**Figure 20D**) and CD11b+F4/80+ cells (**Figure 20E**) were not different among the parental, *Slpi*^{EV} and *Slpi*^{OE} tumors. Similarly, the frequency of CD4+ (**Figure 20J**) and CD8+ T cells (**Figure 20I**) as well as their ratio (**Figure 20H**) were not significantly different across all the groups. The frequency of

leukocytes was significantly higher in the *Slpi*^{OE} tumors compared to the Parental group, but not the *Slpi*^{EV} group (**Figure 20B**). The only significant difference between *Slpi*^{OE} tumors and the *Slpi*^{EV} group was a higher percentage of CD11b-CD11c- cells in SLPI-overexpressing tumors (**Figure 20F**). This suggests that SLPI does not significantly affect the overall abundance of different cell populations but may influence specific immune cell populations within the TME.

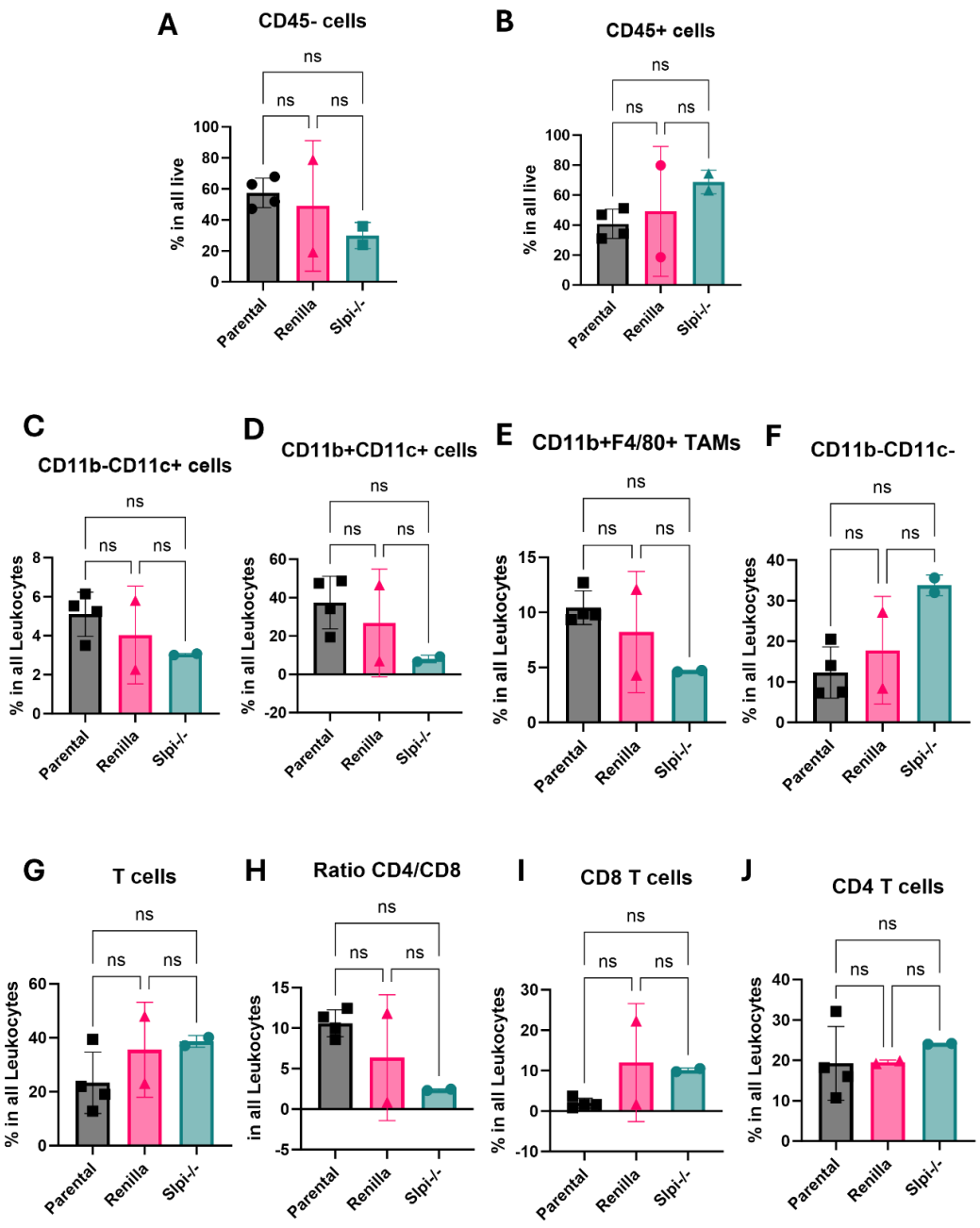

Figure 19. The abundance of cell populations within the Parental, Renilla control, and Slpi-/- tumor microenvironment of the MOE Pten^{shRNA}KRas^{G12V} model. *Tumors were collected from mice injected with 0.15x10^{6} cells under the bursa and analyzed by flow cytometry. The number of biological replicates in the parental group is 4 samples, whereas in the Renilla and Slpi-/- group, tumors with a small weight from different mice were pooled together and therefore each group had only 2 biological replicates, which are represented by dots in the graph. Data is represented as mean +/- SD. Statistical analysis was done using one-way ANOVA and Tukey's multiple comparison test. ns: non-significant.*

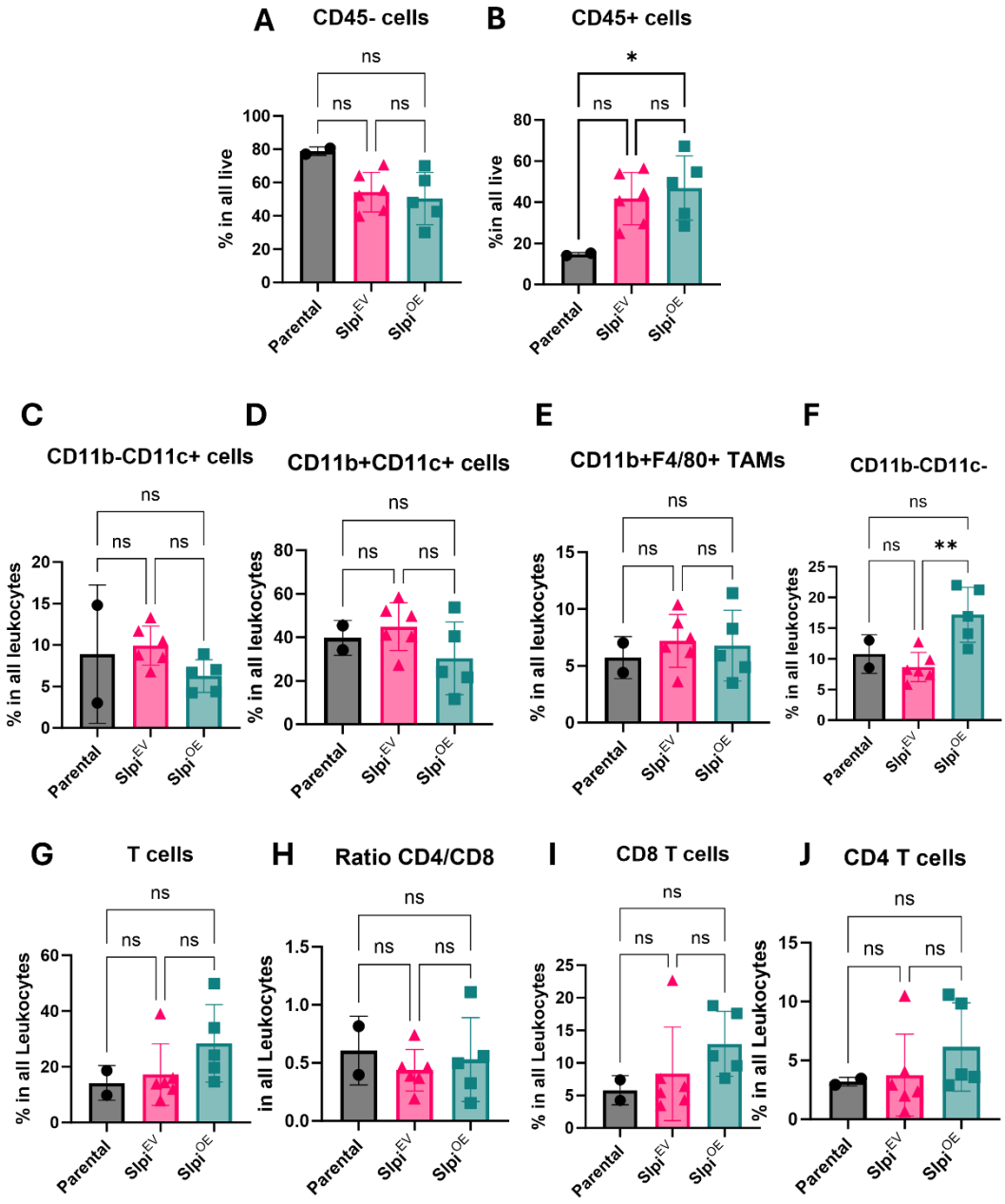

Figure 20. The abundance of cell populations within the parental, Slpi^{EV}, and Slpi^{OE} tumor microenvironment of the KPCA.B model*. Tumors were collected from mice injected with 0.15x10^{6} cells under the bursa and analyzed by flow cytometry. 2 tumor samples were used for the parental group, 6 for the Slpi^{EV,} and 5 for the Slpi^{OE}. Each biological replicate is represented by dots in the graph. Data is represented as mean +/- SD. Statistical analysis was done using one-way ANOVA. ns: non-significant.*

3.8.2.2 Assessment of PD-L1 in the CD45- and myeloid cell population

Immune evasion in tumors can occur through various mechanisms, with the upregulation of immune checkpoints, particularly PD-L1, being a common strategy[86]. To explore the role of SLPI in this process, we examined its impact on PD-L1 expression in both CD45-negative epithelial cells and myeloid cells using knockout and overexpression models. Our analysis revealed that in epithelial cells (CD45-negative), PD-L1 expression did not differ between the *Slpi*-/- and Renilla control groups (**Figure 21A**). There was also no difference in the overall expression of PD-L1 in the CD3- group (**Figure 21B**), in which the lack of SLPI did not affect the frequency of PD-L1 in its subsets (i.e. CD11b-CD11c+, CD11b+CD11c+, CD11b+F4/80+ and CD11b-CD11c-) (**Figure 21C-F**).

Similarly, the overexpression of SLPI in the KPCA.B cells did not alter the frequency of PD-L1-expressing cells in the CD45- and the CD3- groups (**Figure 22A-B**). However, the $Slpi^{OE}$ group showed a trend for an increase in the frequency of PD-L1 in the CD11b-CD11c+ population (**Figure 22C**) compared to the $Slpi^{EV}$ control group (p=0.0954). In the CD11b+CD11c+ cells, the frequency of PD-L1 was significantly higher in the $Slpi^{OE}$ group compared to the $Slpi^{EV}$ control (**Figure 22D**). A similar difference was noted in the CD11b+F4/80+ cells that had a significant increase of the PD-L1 in the $Slpi^{OE}$ tumors (**Figure 22E**). In the CD11b-CD11c- cells, the expression of PD-L1 showed a trend for an increase in the SLPI-overexpressing cells but did not reach significance (**Figure 22F**).

Overall, the $Slpi^{OE}$ tumors had an increase in the frequency of PD-L1+ myeloid cells compared to the $Slpi^{EV}$ control group, while no differences were observed in the tumors lacking SLPI.

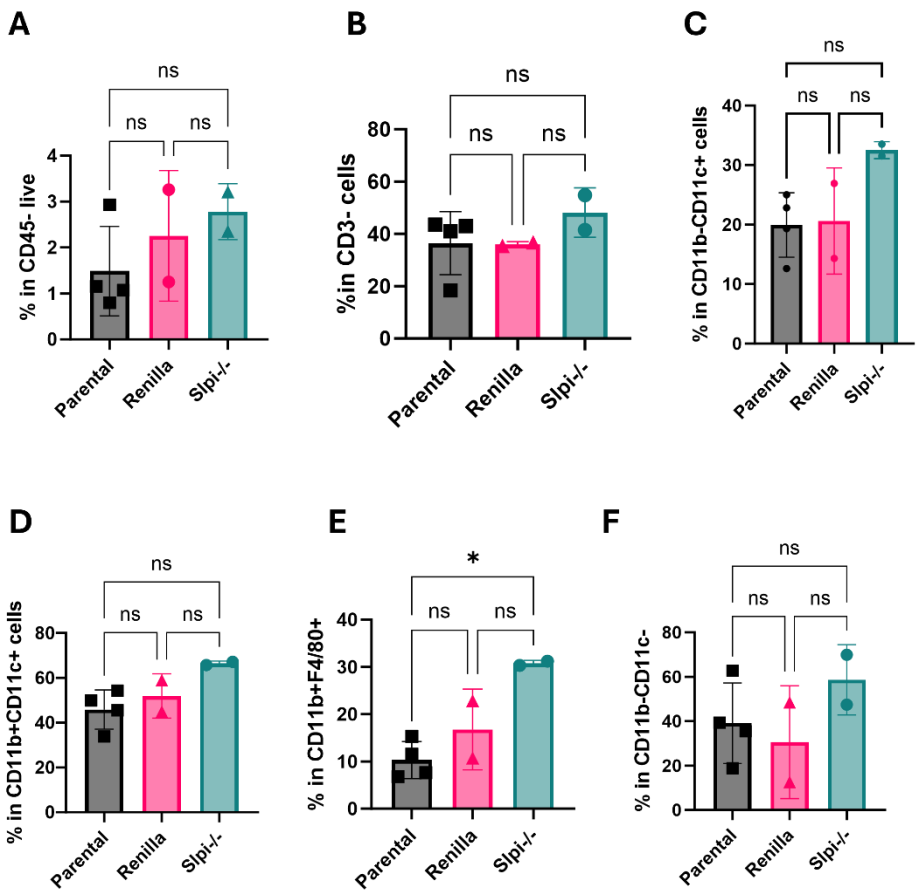

Figure 21. Expression levels of PD-L1 in cell populations within the Parental, Renilla control, and Slpi-/- tumor microenvironment of the MOE Pten^{shRNA}KRas^{G12V} model*. Tumors were collected from mice injected with 0.15x10^{6} cells under the bursa and analyzed by flow cytometry. The number of biological replicates in the parental group is 4 samples, whereas in the Renilla and Slpi-/- group, tumors with a small weight from different mice were pooled together and therefore each group had only 2 biological replicates, which are represented by dots in the graph. Data is represented as mean +/- SD. Statistical analysis was done using one-way ANOVA and Tukey's multiple comparison test. *p<0.05 and ns: non-significant.*

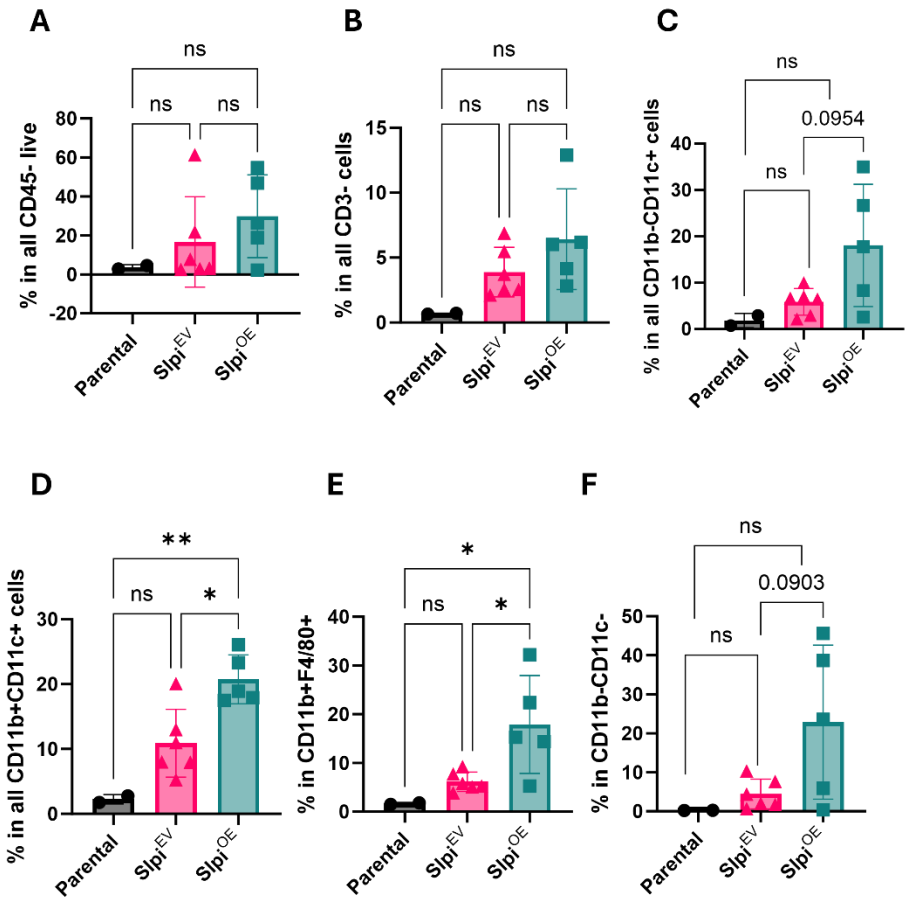

Figure 22. Expression levels of PD-L1 in the Parental, Slpi^{EV} control, and Slpi^{OE} tumor microenvironment of the KPCA.B model. *Tumors were collected from mice injected with 0.15x10^{6} cells under the bursa and analyzed by flow cytometry. 2 tumor samples were used for the parental group, 6 for the Slpi^{EV,} and 5 for the Slpi^{OE}. Each biological replicate is represented by dots in the graph. Data is represented as mean +/- SD. Statistical analysis was done using one-way ANOVA. *p<0.05, **p<0.01 and ns: non-significant.*

3.8.2.3 Assessment of the impact of SLPI on T cells

3.8.2.3.1 Activation and immune checkpoint markers

To investigate the effects of SLPI on the activity of the T-cell compartment, the expression of the activation and exhaustion markers CD25, PD-1, and PD-L1 were evaluated in CD4+ and CD8+ T cells. In the MOE *Pten^{shRNA}KRas^{G12V}* model, the knockout of SLPI did not alter the level of CD25 in either CD4+ T cells (**Figure 23A**) and CD8+ T cells (**Figure 23D**). Similarly, the

frequency of PD-L1 marker in T cells was not different between tumors whether on CD4+ T cells (**Figure 23B**) or CD8+ T cells (**Figure 23E**). However, SLPI knockout tumors exhibited a significant reduction in PD-1 expression, particularly in the CD4+T cells (**Figure 23C**) with no difference observed in CD8+ T cells (**Figure 23F**). This suggests that SLPI knockout predominantly affects PD-1 levels in CD4+ T cells.

Consistent with the MOE $Pten^{shRNA}KRas^{G12V}$ model, the $Slpi^{OE}$ tumors in the KPCA.B model showed a significantly higher frequency of the PD-1+CD4+T cells (**Figure 24C**) compared to the Parental group, however, a similar increase was observed in the $Slpi^{EV}$ *control* group. Still, no significant differences in the PD-1 levels were observed between the $Slpi^{OE}$ and the $Slpi^{EV}$ in both CD4+ and CD8+ T cell populations (**Figures 24C and 24F**). Notably, in the KPCA.B model, the $Slpi^{OE}$ tumors had a significantly higher percentage of the PD-L1 marker in the CD4+ T cells compared to the $Slpi^{EV}$ tumors (**Figure 24B**). In contrast, these changes were not observed in the CD8+ T cells, which had no significant differences in PD-L1 (**Figure 24E**) when comparing the $Slpi^{OE}$ tumors with the $Slpi^{EV}$ and the parental controls. The frequency of the CD25 in the KPCA.B model remained unchanged in both CD4+ (**Figure 24A**) and CD8+ T cells (**Figure 24D**) similar to the MOE $Pten^{shRNA}KRas^{G12V}$ model.

Overall, the analysis of T cells revealed that changes in SLPI levels impacted the frequency of cells expressing PD-1 and PD-L1 markers in CD4+ T cells, and had no impact on the CD25 marker.

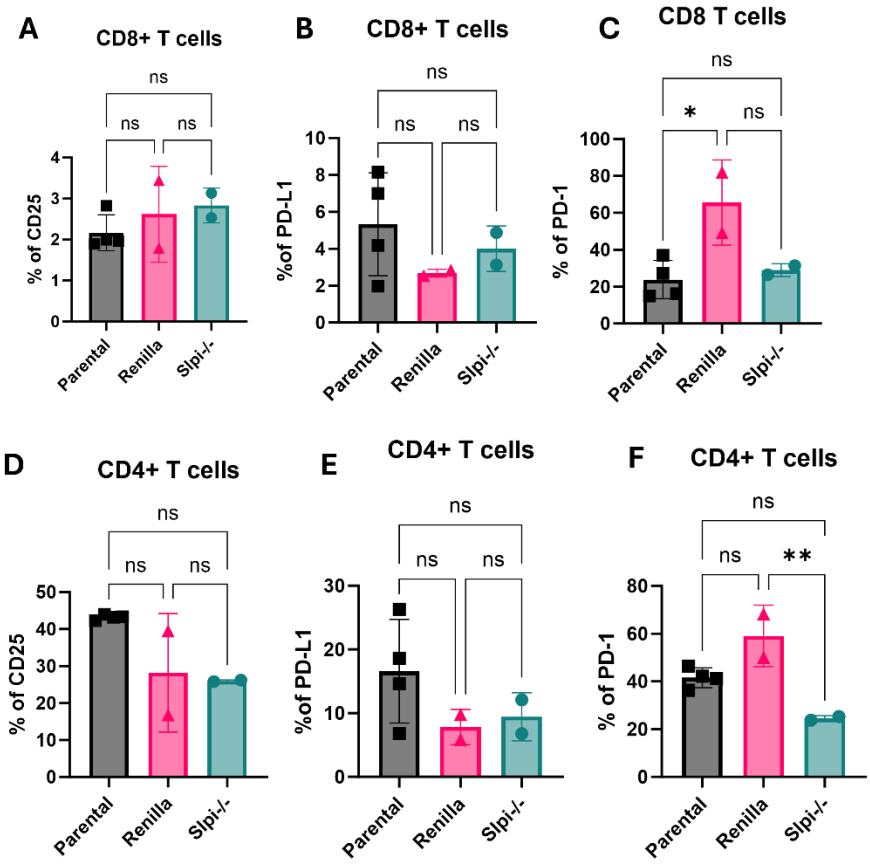

Figure 23. Expression levels of CD25, PD-L1, and PD-1 markers in T-cell subsets present within the Parental, Renilla control, and Slpi-/- tumor microenvironment of the MOE Pten^{shRNA}KRas^{G12V} model*. Tumors were collected from mice injected with 0.15x10^{6} cells under the bursa and analyzed by flow cytometry. The number of biological replicates in the parental group is 4 samples, whereas in the Renilla and Slpi-/- group, tumors with a small weight from different mice were pooled together and therefore each group had only 2 biological replicates, which are represented by dots in the graph. Data is represented as mean +/- SD. Statistical analysis was done using one-way ANOVA. *p<0.05, **p<0.01 and ns: non-significant.*

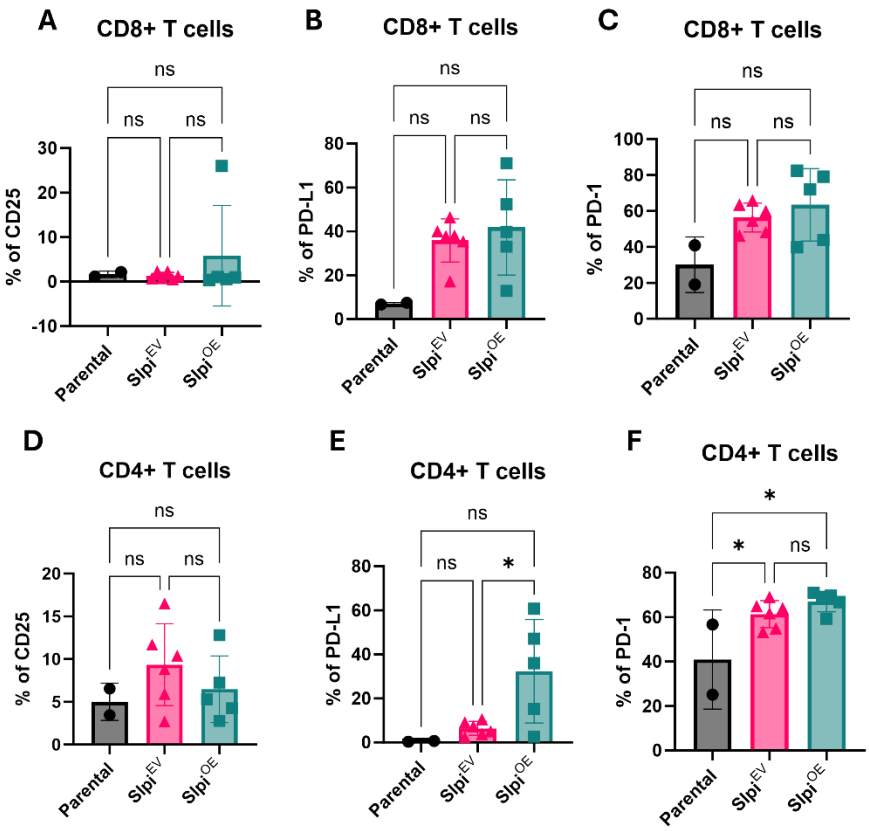

Figure 24. Expression levels of CD25, PD-L1, and PD-1 markers in T-cell subsets present within the Parental, Slpi^{EV} control, and Slpi^{OE} tumor microenvironment of the KPCA.B model. *Tumors were collected from mice injected with 0.15x10^{6} cells under the bursa and analyzed by flow cytometry. 2 tumor samples were used for the parental group, 6 for the Slpi^{EV,} and 5 for the Slpi^{OE}. Each biological replicate is represented by dots in the graph. Data is represented as mean +/- SD. Statistical analysis was done using one-way ANOVA. *p<0.05 and ns: non-significant.*

3.8.2.3.2 Impact of SLPI levels on tumor immune cell transcription factors

To identify the type of immunity driven by the knockout and overexpression of SLPI, we evaluated, by flow cytometry, the expression of 3 main transcription factors T-bet, FoxP3, RORγt, and GATA3 in T-cell compartments.

In the MOE *Pten^{shRNA}KRas^{G12V}* model, the frequency of T-bet in *Slpi-/-* tumors was significantly higher in CD8+ T cells (**Figure 25A**) compared to both the parental and empty vector

control groups. In CD4+ T cells, approximately 10% of cells in *Slpi*-/- tumors expressed T-bet, similar to the frequency in CD8+ T-bet+ cells, but this was not significantly different from the Renilla control, likely due to variability (**Figure 25E**). The GATA3+ cell population comprised less than 1% in both CD8+ and CD4+ T cells across all tumor categories (**Figure 25B and 25F**). Similar trends were observed for the RORγt transcription factor, with around 55% of RORγt+CD4+ and RORγt+CD8+ T cells in all tumors with or without SLPI expression (**Figure 25C and 25G).** Although FoxP3 expression profiles were consistent across all three tumor groups, its frequency was between 20% and 40% in CD4+ T cells and less than 6% in CD8+ T cells **(Figure 25D and 25H**), which is expected since CD4+ T cells are known to express more FoxP3 than CD8+ T cells[87].

In the KPCA.B model, the frequency of T-bet and its frequency in CD4+ and CD8+ T cells did not change with the overexpression of SLPI (**Figure 26A and 26E**) unlike the MOE *Pten*^{shRNA}*KRas*^{G12V}model. GATA3, RORγt, and FoxP3's expression profiles in both CD4+ and CD8+T cells were the same among all three tumor groups (**Figure 26B-D and 26F-H**), and therefore not affected by SLPI overexpression.

Overall, the analysis of the four key transcription factors in T cells suggests that altering SLPI levels in tumors did not influence the T-cell phenotype, as defined by transcription factor expression.

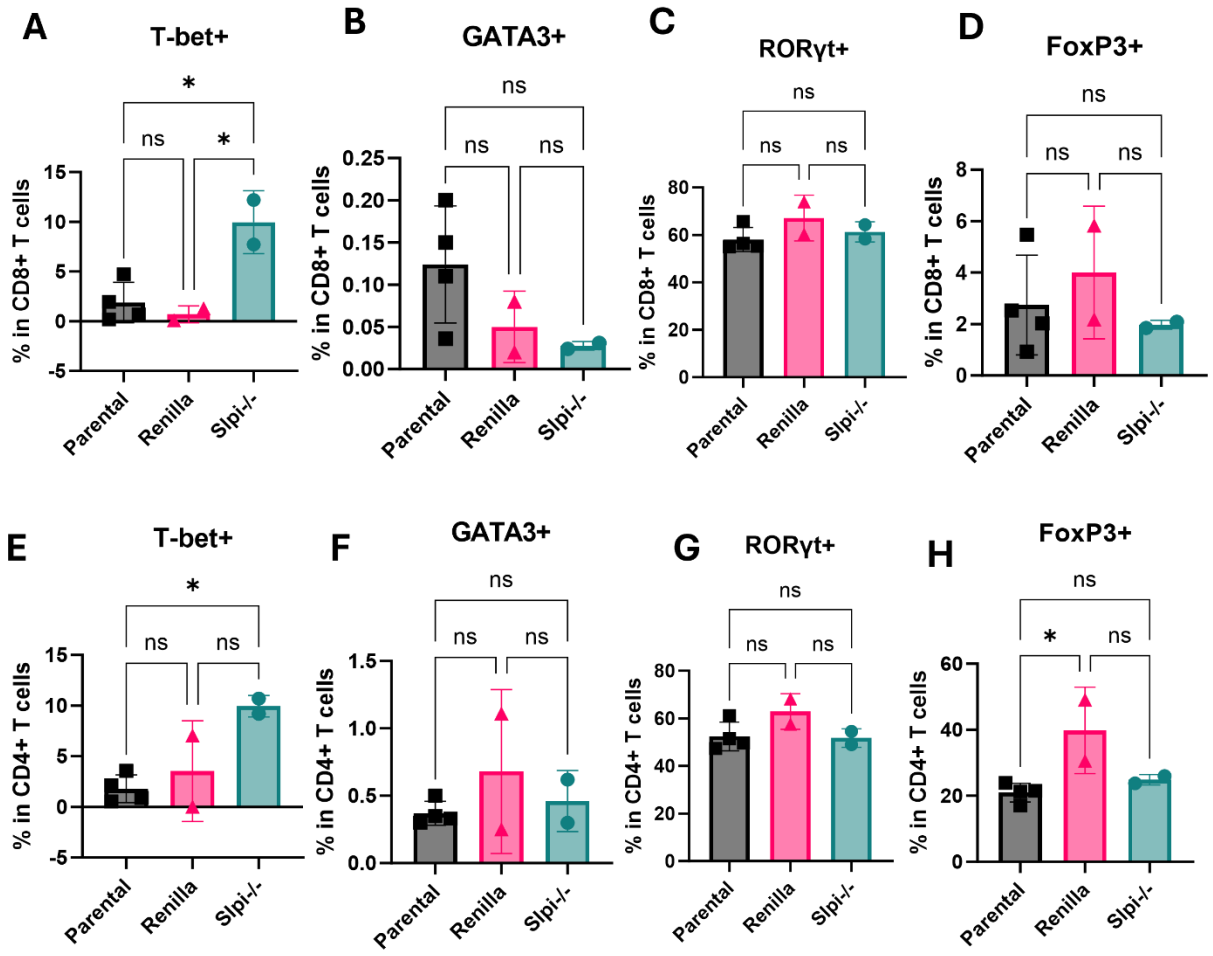

Figure 25. Expression levels of the transcription factors T-bet, GATA3, RORyt, and FoxP3 in T-cell subsets present within the Parental, Renilla control, and Slpi-/- tumor microenvironment of the MOE Pten^{shRNA}KRas^{G12V} model. *Tumors were collected from mice injected with 0.15x10^{6} cells under the bursa and analyzed by flow cytometry. The number of biological replicates in the parental group is 4 samples, whereas in the Renilla and Slpi-/- group, tumors with a small weight from different mice were pooled together and therefore each group had only 2 biological replicates, which are represented by dots in the graph. Data is represented as mean +/- SD. Statistical analysis was done using one-way ANOVA. *p<0.05 and ns: non-significant.*

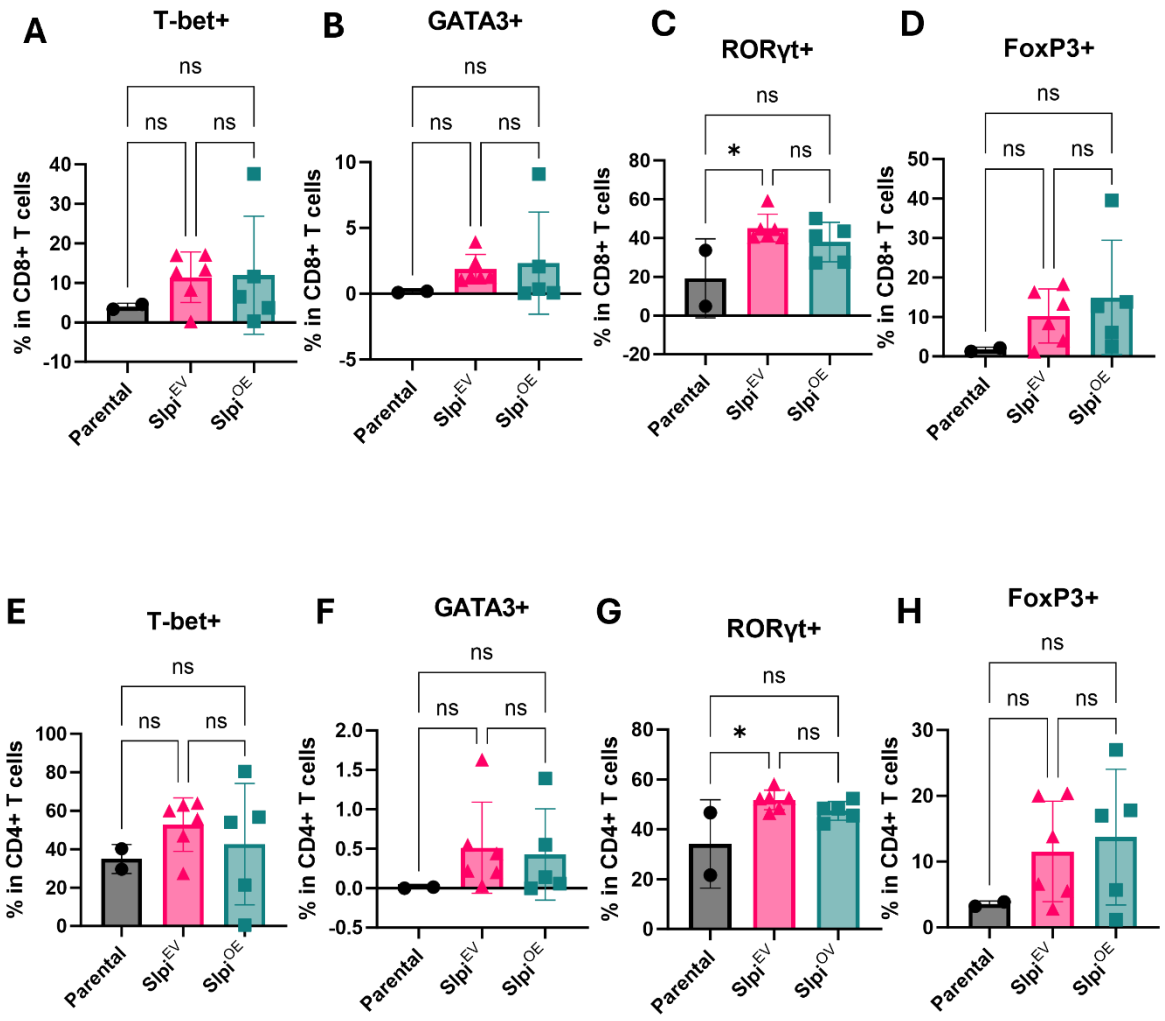

Figure 26. Expression levels of the transcription factors T-bet, GATA3, RORγt, and FoxP3 in T-cell subsets present within the Parental, Slpi^{EV} control, and Slpi^{OE} tumor microenvironment of the KPCA.B model*. Tumors were collected from mice injected with 0.15x10^6 cells under the bursa and analyzed by flow cytometry. 2 tumor samples were used for the parental group, 6 for the Slpi^{EV,} and 5 for the Slpi^{OE}. Each biological replicate is represented by dots in the graph. Data is represented as mean +/- SD. Statistical analysis was done using one-way ANOVA. *p<0.05 and ns: non-significant.*

Chapter 4: Discussion

Understanding ovarian cancer has always been challenging due to the heterogeneity of the tumors that differs not only between patients but also across different anatomical locations within the same body[39,88]. Therefore, in this study, we aimed to compare key interactions between cancer cells and immune cells by starting with a scRNA sequencing analysis.

4.1. Cell-cell communication based on EMT and discovery of SLPI

4.1.1. SLPI-CD4 as a key interaction between cancer cells and immune cells

The analysis of primary and metastatic ovarian tumor scRNA sequencing datasets revealed more similarities than differences in cell-cell communication pathways. In both primary and metastatic tumors, cancer cells strongly interact with myeloid cells, particularly monocytes and macrophages. Depending on their phenotype and their numbers, monocytes can be pro- or anti-tumorigenic[47]. They exist in various types that can modulate the immune response depending on the stage of the tumor, the tissue of origin, and the environmental signaling through cytokine secretion by other cells[89]. Their interactions become more complicated when cancer cells undergo EMT since the TME becomes more heterogeneous and immunosuppressed[37]. Studies have reported different mechanisms by which these changes happen, focusing particularly on transcription factors- or cytokine and chemokine-related mechanisms of action[37]. However, this study focused more on characterizing the TME cell-cell communication by focusing on the EMT phenotype of cancer cells, showing for the first time the stronger communication of monocytes/macrophages with mesenchymal cancer cells in both primary and metastatic tumors independently from the abundance of both. This is a novel discovery and may now have become

evident in light of the growing evidence for EMT as a plastic process in which cancer cells interconvert between all three phenotypes. Fortunately, our analysis was possible thanks to a well-defined epithelial-mesenchymal plasticity signature gene list published by Cook and Vanderhyden, 2022[70], based on which cancer cells have been classified into epithelial, partially mesenchymal, and mesenchymal.

The EMT classification allowed us to observe changes in the ligand-receptor interaction with immune cells during the transition. By looking at the monocyte-MES link, we discovered a strong interaction between a ligand secreted by cancer cells called SLPI and the CD4 receptor on monocytes. This interaction was first studied by McNeely et al.[90] in the context of human immunodeficiency virus (HIV) after having discovered that physiological concentrations of SLPI in saliva had an anti-HIV-1 function. Specifically, they reported that SLPI acts on an HIV host cell molecule (i.e. a receptor on monocytes) instead of the virus itself, which others later found to be a CD4 molecule[91,92], although McNeely *et al*. showed through a biosensor technique that SLPI does not directly interact with recombinant CD4[90]. It was confirmed by others that SLPI levels were associated with CD4+ cell counts during HIV-1 infection[93]. When exploring the molecular mechanism of action of SLPI on CD4+ cells, Py et al.[94] found that SLPI interacts with the cytoplasmic domain of a transmembrane protein called phospholipid scramblase 1 and 4 (PLSCR1 and PLSCR4) that also interacts with CD4, but they were not able to identify the functional impact of this interaction especially on the HIV-1 infection, which remains unknown, and thus keeps the mechanism of SLPI-CD4 interaction in question. To understand the SLPI-CD4 link, we need first to understand what SLPI are and CD4 and what might be their potential roles in ovarian cancer.

SLPI is a small protein (~11.7kDa) of the whey acidic protein family (WAP), thus called also WFDC4 (WAP four-disulfide protein) or WAP4[95]. In humans, this protein is located on

chromosome 20q12-13 and is composed of 107 amino acids[95,96]. SLPI performs an anti-protease activity that depends on its active site located at Leu72-Met73 of the C terminal WAP domain[97]. Some of the inhibited proteases include neutrophil elastase (NE), cathepsin G, trypsin, and chymotrypsin to prevent tissue destruction, especially in specific organs like the intestine and lungs[98–101]. Therefore, SLPI is highly produced in these tissues as well as others, in which it also plays an antimicrobial role through a mucosal defense system like saliva or genital secretions[102] and a homeostatic function regulating the immune response[103]. SLPI is known for its anti-inflammatory function induced by the inhibition of the secretion of pro-inflammatory cytokines. In monocytes for example, it was reported that SLPI inhibits toll-like receptors 2 and 4, by inhibiting NF-kB activation through the blockade of the degradation of its inhibitors[101,104]. Other studies have reported that SLPI-treated monocytes decreased the presentation of MHC II molecules and secreted IL-4, IL-6, and IL-10[105], known to be immunosuppressive cytokines[106–108]. These SLPI-treated monocytes were also found to decrease CD4+ lymphocyte proliferation but not CD8+[105]. However, this was shown only in a normal condition. It remained unclear whether SLPI abundance in the TME of ovarian cancers could impact negatively the immune response, especially since its levels were more highly expressed in the mesenchymal cancer cells, which are thought to be associated with more advanced, metastatic disease.

CD4 or cluster of differentiation 4 is a 55kDa receptor and a type 1 glycoprotein, containing 4 extracellular immunoglobin (Ig)-like domains, a transmembrane domain, and a cytoplasmic tail[109,110]. Its highest expression is found in T cells, then in monocytes and macrophages, and then in natural killers, DCs, and neutrophils[110]. CD4 is expressed on T cells that activate other immune cells, unlike CD8 which is expressed on cytotoxic T cells[111]. CD4+ T cells are also known to recognize MHC (major histocompatibility) class II molecules on APCs in contrast to CD8+ T cells

that recognize MHC I molecules[111]. Specifically, the extracellular domain D1 of the CD4 molecule stabilizes the interaction of MHC class II molecules with the T cell receptor (TCR)[110,111]. Therefore, CD4 is called a co-receptor and its signaling mechanism depends on the interaction of the TCR with the MHC class II molecule.

During T cell activation, the lymphocyte C-terminal Src kinase (Lck) binds to CD4 to prevent its endocytosis, and alternatively, Lck phosphorylates the immunoreceptor tyrosine-based activation motifs (ITAMs) present on the intracellular tails of CD3 receptor, that is essential to the TCR signaling[109,110]. Other molecules like zeta-associated protein of 70 kDa (ZAP-70) bind to the phosphorylated tails and will then phosphorylate downstream proteins like phospholipase Cy1 (PLCy1) that activates the signaling towards the protein kinase C (PKC)[109,110]. CD4 receptor is also important because it enhances the sensitivity of TCR to MHC II molecules[110]. In monocytes, the CD4 receptor plays a role in mediating their proliferation[112] and differentiation through the calcium flux and the activation of the ERK/MAPK/NF-kB signaling pathway following the ligation with MHC II[113]. All in all, the CD4 receptor plays an important role in the activation of immune cells, whether they are T cells or monocytes. Therefore, understanding the type of its interaction with SLPI and its impact on immune functionality in cancer is of great importance.

One limitation of this aspect of our study was the disproportionate number of datasets used, with 28 samples from primary tumors compared to only 6 samples from metastatic ovarian tumors. This imbalance could lead to a greater diversity of cell populations in the primary tumor samples relative to the omental metastases. Additionally, this disparity may introduce bias in the ligand-receptor analysis, as the magnitude of interactions could be influenced by the overall gene expression levels, which are correlated with the number of cells present in the dataset. Another potential limitation is that the samples used for scRNA-seq represent only a portion of the tumors

and may not fully capture the entire transcriptome. For example, the removal of adipocytes during the processing of the omental tumors may have led to the exclusion of important populations that could impact the ligand-receptor interactions.

4.1.2. Ovarian cancer mouse models exhibit an increased level of SLPI

The level of expression of SLPI as well as its role in cancer differs from one tissue to another, since it can be pro-tumorigenic in some and anti-tumorigenic in others[114]. For instance, SLPI is highly expressed in metastatic breast cancer cells compared to the epithelial breast cancer cell line[115]. Colorectal cancer also shows a high expression of SLPI[116], and its knockdown was related to reduced cell growth and migration via downregulation of AKT[117]. Similarly, SLPI is highly expressed in gastric cancer, in which it was associated with poor survival and greater tumor size[118]. In contrast to these cancers, SLPI expression is decreased in head and neck squamous cell carcinoma (HNSCC), where higher SLPI levels are associated with a better prognosis[119]. In this thesis, the analysis of ovarian cancer cells using an RNA sequencing dataset published recently showed different expression profiles of SLPI where some express significantly higher levels compared to others. Nevertheless, various studies have reported an increase in the level of SLPI in ovarian cancer and was associated with an aggressive phenotype[120–124]. It was discovered first in serum samples of patients with invasive EOC using proteomic profiling technique and was found to be increased compared to patients with benign tumors or healthy individuals[122]. Therefore, it has long been considered as a possible diagnosis biomarker and was compared to the cancer antigen 125 (CA125), a tumor marker used to diagnose various cancers[120,121]. SLPI was elevated in patients with normal levels of CA-125, and in another study, the combination of both SLPI and CA-125 tests increased the sensitivity and specificity of detection of ovarian cancer patients[120,121]. However, limiting factors like sample size and cancer subtype in ovarian cancer make it difficult

to proceed with its testing in clinical trials[121]. The variability in the expression profile of SLPI across different ovarian cancer cells based on our findings creates, furthermore, another limitation to using SLPI as a biomarker. Therefore, understanding regulation mechanisms controlling the expression of SLPI will help determine conditions where to use SLPI as a biomarker.

The expression of SLPI in mouse ovarian cancer cell lines shown by RNA-seq was quite variable but was confirmed by qPCR and western blots in a subset including MOE *Pten*^{shRNA}*KRas*^{G12V} and STOSE as cells expressing high levels compared to MOE *Pten*^{shRNA} and ID8-*Trp53*-/- expressing lower levels of SLPI as well as their respective non-cancerous control cells (OVE4 and MOSE). The differences in SLPI expression could be because they originate from different backgrounds and have different mutations. For instance, the ID8 cells derive from C57BL/6 murine ovarian surface epithelial cells[125]. None of the additional mutations that have been introduced to this cell line resulted in increased levels of SLPI, including the ones that are common in ovarian cancer like *TP53*[22], BRCA1 or BRCA2 mutations[126]. MOE cells are derived from primary cultures of murine oviductal epithelial cells from FVB/N mice, and modified to express similar pathway alterations found in HGSC patients, These included MOE *Pten*^{shRNA} and MOE *Pten*^{shRNA}*KRas*^{G12V} with PTEN silenced via shRNA and an activating mutation in KRAS G12V[78]. Like MOE cells, the STOSE cells are from an FVB/N background but differ because, like ID8 cells, they result from the spontaneous transformation of a primary culture of ovarian surface epithelial cells[77]. They resemble HGSC in the chromosomal aberrations that caused the loss of various tumor suppressors[77]. Recently, Cook et al. group[73] have found that the cells originating from the oviduct have different transcriptional profiles than those originating from the surface epithelium, impacting the activity of signaling pathways. These differences are possibly responsible for the variability observed in the level of expression of SLPI among the cell lines.

Expression of SLPI may be associated with the inefficacy of chemotherapy in patients. A recent study has shown that SLPI inhibition combined with cisplatin reduced the colorectal tumor burden in mice compared to mice receiving only cisplatin[127]. Cisplatin is a platinum-based therapy known to be effective for ovarian cancer, but resistance to its mechanisms of action is common among patients[128]. SLPI was also found to reduce the exposure and response of ovarian cancer cells to paclitaxel, a taxane chemotherapy known to target microtubules and prevent the proper formation of spindles during cellular division and induce apoptosis[129,130]. Thus far, the link between SLPI and chemotherapy resistance has only been shown with cisplatin and paclitaxel with no mechanisms describing this resistance effect. Therefore, it would be essential to determine how SLPI promotes resistance to chemotherapy and if the combination with SLPI inhibition would improve prognosis. However, it is important to first understand the factors controlling the regulation of SLPI's expression and its mechanisms of action

4.2. Regulation of SLPI expression

During this study, the level of expression of SLPI differed based on different circumstances. The first difference was observed in the human scRNA-seq analysis, where cancer cells with more mesenchymal phenotypes expressed higher levels of SLPI. The second one was observed when comparing the mouse cell lines, which showed an increase in SLPI with the addition of a KRAS mutation. Therefore, we explored both mechanisms to understand how they impact the level of expression of SLPI.

4.2.1. SLPI levels decrease during the TGFβ-dependent EMT

SLPI is a multifunctional protein that has been involved in multiple processes, but

its relationship with EMT is not clear yet, especially in ovarian cancer[131]. The higher expression of SLPI in mesenchymal cancer cells, from our human datasets, compared to the epithelial cancer cells suggests that SLPI was induced during EMT. To re-create the EMT process in ovarian cancer cells *in vitro*, they were treated cells with TGFβ, which generally caused significant increases in classical EMT markers like Vimentin, Slug, and N-cadherin, but failed to increase SLPI expression and actually resulted in a significant decrease in two cell lines, contrary to our initial expectations. One possible explanation is that the decreased *Slpi* levels may be associated with TGFβ signaling, and not necessarily the induction of EMT. Previous studies have reported a negative correlation, in which an increase in TGFβ causes a decrease in SLPI and vice versa[132,133]. The mechanism underlying this inverse relationship is not very well elucidated, especially in cancer. The only studies have shown that TGFβ1 inhibits the expression of SLPI through the activation of the SMAD signaling pathway in chronic obstructive pulmonary disease[134] and that SLPI inhibits TGFβ1 in human endometrial epithelial cells[135]. However, TNF-α, another EMT inducer[136], was reported to induce SLPI both *in vitro* and *in vivo* using mouse lung carcinoma cells and in TNF-α$^{-/-}$ mice[137]. This confirms, furthermore, that the decrease observed with TGFβ is due to its direct impact on *Slpi*'s transcription.

The process of EMT plays a huge role in cancer metastasis, and understanding the expression profile of SLPI throughout the transition is important for elucidating its potential role in the aggressive phenotype of ovarian cancer. Although the inverse relationship between SLPI and TGFβ confounds the understanding of the function of SLPI in mesenchymal cells, many studies have looked at SLPI in metastatic diseases other than ovarian cancer and have reported highly elevated expression in metastatic tumors compared to the primary tumors in breast, colorectal, and lung cancers[138]. In breast cancer cell lines, SLPI contributed to metastasis by negatively regulating

the expression of the adhesion molecule E-cadherin[139]. In triple-negative breast cancer cells, SLPI promoted metastasis by interacting with retinoblastoma tumor suppressor protein which activates FoxM1 target genes[140]. In contrast, the level of secretion of SLPI by highly metastatic liver cancer cells was low[141]. Altogether, the inconsistencies in the expression profile of SLPI in metastatic cancers and its wide-ranging mechanisms of action emphasize that the role of SLPI is clearly context specific.

4.2.2. SLPI expression depends on the activation of the MAPK pathway

Our analysis of the ovarian cancer cell lines showed that a $KRAS^{G12V}$ mutated cell line had higher expression levels of SLPI compared to the non-mutated control. A similar difference was observed in the human TCGA data, which showed higher expression of SLPI in the KRAS mutant patients. The $KRAS^{G12V}$ mutation was found to be associated with shorter overall survival in HGSC patients[142]. Since the G12V mutation is rare in HGSC, some groups have hypothesized that HGSC tumors with the G12V mutation develop from low-grade tumors that grow slowly but have a large size at diagnosis[142,143]. KRAS mutation in general is associated with oncogenic features including enhanced cell proliferation, resistance to apoptosis, increased metastasis, and altered cellular metabolism[144]. The mechanisms by which these pro-tumoral characteristics occur differ and can include different downstream pathways of KRAS. For example, proliferation has been shown to be a result of activated RAF/MEK/ERK and PI3K/AKT pathways[144]. In contrast, the resistance to apoptosis is a result of the inhibition of the pro-apoptotic Bad protein that prevents the inhibition of the anti-apoptotic proteins Bcl-2/Bcl-xl, which happens mainly through the PI3K/AKT pathway activation[144]. Therefore, inhibitors targeting different types of KRAS mutation have emerged for therapeutic purposes.

KRAS, or Kristen Rat Sarcoma protein, is a member of the RAS family, and an important oncogene known to be highly mutated in various cancers[145]. It functions as a GTPase (guanosine triphosphatase) that alters between an active state bound to GTP and an inactive state bound to GDP[145]. This process is facilitated by two enzymes, guanine nucleotide exchange-factors (GEFs) to convert GDP to GTP, and GTPase-activating proteins (GAPs) to convert GTP to GDP[146]. KRAS mutations can keep KRAS in an activated state by impeding their interaction with GAPs and their hydrolysis of GTP, which contributes to the process of carcinogenesis[147]. Most of them are known to be located at positions 12 and 13 in exon 1 of the KRAS gene[145]. Once KRAS is activated, it changes its conformation and activates the downstream effector signaling pathways; PI3K/AKT, RAF/MEK/ERK and/or RAL/NF-kB pathways[148]. In ovarian cancer, the frequency of KRAS mutations is different depending on the subtype. To date, the majority of cases diagnosed with mucinous ovarian cancer (71%) will have a KRAS mutation[149]. KRAS mutations occur less frequently in low-grade serous, then endometroid cancer and clear-cell, with 5.9% of HGSC having KRAS mutations[149]. Mutational sites differ between patients but the most common one in ovarian cancer is G12D in mucinous ovarian cancer[149].

The use of pathway-specific inhibitors allowed us to discover that SLPI expression is regulated by the activation of the MAPK pathway, but not the AKT pathway. Vroling et al. showed in dendritic cells that the inhibition of ERK by inhibition of MEK1 and MEK2 for 1 hour did not cause any changes in SLPI expression, but the expression was inhibited by the inhibition of p38, a key player of another MAPK cascade activated in response to stress stimuli and UV radiation, does[150]. Thus, SLPI expression appears to be dependent on the RAF/MEK/ERK pathway. The RNA-seq analysis of the ovarian cancer cell lines by the Vanderhyden lab also noted that SLPI was increased in STOSE cells that have an increased level of pERK[73]. Interestingly, it has also

been reported that SLPI can regulate the activation of the MEK/ERK signaling by upregulating the levels of pERK in ovarian cancer cells, which conferred resistance to paclitaxel[129]. This suggests that the regulation of SLPI in ovarian cancer may exist as a positive feedback loop that promotes ovarian cancer progression. Additional efforts to understand the role of SLPI in ovarian cancer are needed to determine what players should be targeted for therapeutic purposes.

4.3. Assessment of the impact of SLPI on immunity

4.3.1. SLPI influences CD4+ T cells by increasing their activation markers *in vitro*

To test the effects of SLPI on immune cells, we first examined the responses of CD4+ and CD8+ T cells to rSLPI *in vitro*. rSLPI enhanced CD4+ T cells activity, but not CD8+ T cells, during their CD3/CD28 receptor activation. This observation was based on an increase in the frequency of the activation markers CD25 and CD69 and a decrease in the naïve T cell marker CD62L in CD4+ T cells only. T-cell activity was induced in this study using two different approaches, the first being the use of anti-CD3 and anti-CD28 antibodies. When the CD3 antibody binds to the CD3 antigen, it signals through the TCR complex in a way that mimics its interaction with the MHC molecules, which promotes the proliferation of T cells[151]. The binding of anti-CD28 to CD28, a typical co-stimulator of the TCR complex in T cells, mimics the co-stimulatory molecules CD80 and CD86 found in antigen-presenting cells (APCs)[151]. It has minimal effect on its own, but when combined with anti-CD3 signaling, it enhances T cell proliferation and prevents cell death[152]. However, the PD-1 and PD-L1 were also increased by rSLPI in a dose-dependent manner in the CD4+ T cells. The expression of the PD-1 marker is known to be also induced during the activation of T cells, but its function during this process is to attenuate this response by

interacting with its ligand PD-L1 (or PD-L2)[153]. This inhibitory effect results in the recruitment of the Src-Homology domain-2 containing protein tyrosine Phosphatase-2 (SHP-2) in the cytoplasmic domain of PD-1, leading to a dephosphorylation of the TCR signaling molecules like ZAP-70 and PKC[153]. The increase of PD-L1 expression in T cells has been shown to cause a negative regulation of T cell response, through an autocrine or paracrine inhibition by interacting with PD-1 proteins on the T cells[154]. Therefore, we can conclude that rSLPI may promote a regulated activation of CD4+ T cells, preventing excessive immune responses.

Another approach to activating T cells involves using the OVA peptide, an epitope of the MHC class I molecule ($H2K^b$) derived from the ovalbumin protein[155]. CD8+ T cells isolated from OT-1 mice specifically recognize OVA peptides due to their TCRs, which are designed to target residues 257-264 on the ovalbumin protein[156]. The addition of rSLPI in this experiment led to a higher frequency of CD25+ cells in the CD8+ population, with no significant changes in CD69 and CD62L. However, PD-1, PD-L1, and LAG3 have increased significantly during activation with the OVA peptide in the presence of rSLPI. This raises two main questions: the first one is about the differences in the mechanism of action of anti-CD3/CD28 and of OVA peptide on CD8+ T cells in the presence of SLPI and the second one is about why this difference is observed. This raises two key questions: First, what accounts for the differences in the mechanism of action between anti-CD3/CD28 and OVA peptide activation of CD8+ T cells in the presence of SLPI? Second, why does this difference occur? The primary distinction between these activation methods lies in the specificity of TCR engagement, as the OVA peptide directly binds to the TCR, ensuring the activation of a targeted immune response[157]. While both CD3/CD28 antibodies and the OVA peptide enrich similar signaling pathways, such as TCR and MAPK signaling, the high affinity of the OVA peptide may amplify rSLPI's regulatory role. This is evident in the induced expression

of the immune checkpoints PD-1 and PD-L1, as well as the exhaustion marker LAG-3 on CD8+ T cells, which likely serves as a negative feedback mechanism to mitigate the strong activation signal and reduces T cell activation[157]. For future research, it will be important to evaluate the impact of SLPI on T cell functionality to determine whether the observed changes in immune markers have led to a reduction in the cytotoxicity of CD8+ T cells.

Another important aspect of immunomodulatory molecules is their ability to prime immune cells. The priming process, in general, aims to create an immunological memory of host defense to increase the amplitude and the speed of the immune response[158]. Priming *ex vivo* is related to physical (in terms of density of receptors and markers, for example), and phenotypical (in terms of surface receptor expression) changes that contribute to the enhancement of the activation of immune cells in the presence of activating agents[159]. In our experiments, the goal of priming with rSLPI was to evaluate if cells would be more or less susceptible to activation compared to the control condition. Priming with rSLPI had no impact on the activation of CD4+ T cells. However, priming efficiency depends on both the type of molecule and its concentration[159], so insufficient concentrations could be a reason why no changes were observed in this study.

rSLPI exhibited no effect under naïve conditions, indicating its impact is observable only during T cell activation. This behavior aligns with the homeostatic role of SLPI which is known to be significantly upregulated in similar conditions like in autoimmune diseases and inflammatory states to modulate immune cell responses. Therefore, our *in vitro* findings indicate that SLPI has a regulatory role in the activation of T cells, which was then further validated *in vivo*.

4.3.2. High levels of SLPI are associated with an increased inhibitory phenotype *in vivo*

To investigate SLPI's role in the tumor microenvironment, we generated cell lines that either overexpress or lack SLPI. This change did not impact their proliferation *in vitro*, which allowed us to investigate the impact on survival, without being confounded by an inherently different rate of cell proliferation, as has been reported for other genes. For example, the loss of p53 was reported to increase the proliferation of the ID8 cells[75], and the silencing of PTEN in MOE cells and the addition of a KRAS mutation increased their proliferation[78]. Despite similar rates of proliferation *in vitro*, cell lines with modified SLPI expression did result in different lengths of survival after IP injection into mice. Overexpression of SLPI in ID8-*Trp53-/-* cells conferred a prolonged survival compared to its controls, whereas the knockout of SLPI in MOE $Pten^{shRNA}KRas^{G12V}$ cells reduced the overall survival of the mice. This was not expected, especially since previous studies have reported that SLPI expression is associated with the worst prognosis in ovarian cancer patients[63,124]. Still, there are many unanswered questions about how SLPI contributes to survival in ovarian cancer, given its multifunctionality and the diversity of its contributions in each disease[103,131], which led us to explore further its impact on the TME.

A critical, yet unexplored question in ovarian cancer research is how the presence or absence of SLPI modulates the tumor immune microenvironment. Consequently, we collected and analyzed the immune composition of tumors derived from the *Slpi* knockout and overexpressing cell lines at mid-development and before reaching the endpoint. The frequency of non-immune cells (CD45-) was not different among the tumors and their controls. This does not necessarily mean that there was a similar amount of cancer cells because the CD45- population encompasses cancer cells, fibroblasts, endothelial cells, adipocytes, and others potentially at different ratios. On the other hand, the frequency of immune cells (CD45+) also did not change except for a significant increase in the CD11b-CD11c- cells in KPCA.B-$Slpi^{OE}$-derived tumors compared to its control.

The markers CD11b and CD11c were used to exclude monocytes/macrophages and conventional dendritic cells or other APCs[111]. Cells characterized as CD45+CD3-CD11b-CD11c- may include B cells, NK cells, or granulocytes but confirming their identity will require additional markers, such as CD19, CD20, or CD21 for B cells and CD56 for NK cells[111], which were absent from our panel. The role of both immune cells within the tumor microenvironment is important since their presence can control tumor progression. B cells, for instance, can secrete cytokines like IL-2, IFN-γ, and TNF-α, that contribute to the recruitment of effector cells, including T cells, and form a tertiary lymphoid structure (TLS)[160]. However, B cells can also secrete anti-inflammatory cytokines like IL-10 or TGF-β, which can reduce the cytotoxic response of other immune cells and promote tumorigenesis[160]. The CD11b-CD11c- population in the $Slpi^{OE}$ tumors had elevated levels of the PD-L1 marker, which may indicate the reduced ability of these cells to activate other immune cells.

The inhibitory effect induced by PD-L1 becomes worse if other cytotoxic cells express high levels of PD-1. In the case of SLPI-expressing tumors (i.e. the Renilla control in the MOE $Pten^{shRNA}KRas^{G12V}$ and $Slpi^{OE}$ in the KPCA.B model), the abundance of PD-1+CD4+ T cells was similar or higher than the SLPI-null tumors (i.e. the *Slpi-/-* in the MOE $Pten^{shRNA}KRas^{G12V}$ and $Slpi^{EV}$ in the KPCA.B model), at a percentage of more than 50%, which can control the immune response of CD4+ T cells and prevent them from activating the CD8+ T cells. Furthermore, in $Slpi^{OE}$ tumors, not only do CD11b-CD11c- cells exhibit increased PD-L1 expression compared to the control, but CD11b-CD11c+, CD11b+CD11c+, and TAMs also show elevated levels of PD-L1. All these cells are APCs that can interact with CD4+ T cells through MHC II molecules and the PD-L1 ligand, which can cause an inhibition of their immune effect. Altogether, the analysis

of PD-1 and PD-L1 markers showed that SLPI regulates the immune response within the TME by modulating the abundance of PD-1+ T cells and of PD-L1+ APCs.

The type of immunity that governs the TME depends on the expression and the activity of 4 main transcription factors: T-bet, GATA3, RORyt, and FoxP3. T-bet, or T-box transcription factor, is essential for the differentiation to Th1 or to T follicular helper cells (Tfh) in CD4+T. In CD8+ T cells, T-bet collaborates with other transcription factors to ensure their differentiation to effector T cells[161]. When Th1 is more frequent, the immune response in the environment is referred to as type 1 immunity which is characterized by an elevated secretion of IFNγ and other cytokines like TNF-α and IL-2[162]. When GATA3 increases in these cells, the immunity becomes type 2, characterized by differentiated T cells called T helper 2 and an elevated IL-4 secretion[163,164]. RORyt is another transcription factor required for the survival of immature CD4+ and CD8+ T cells, that leads to their differentiation to Th17 and Tc17 respectively. These cells contribute to type 3 immunity characterized by secretion of IL-17 and are associated with an immunosuppressive phenotype since Tc17 are usually exhausted CD8+ T cells[165,166]. FoxP3 is another transcription factor responsible for the anti-inflammatory phenotype of T cells, particularly CD4+ T cells that differentiate into regulatory T cells (Tregs). Both Tregs and CD8+FoxP3+ T cells have a suppressive function that regulates the immune response within the environment[167]. All these transcription factors along with the secreted cytokines and chemokines control the fate of the immune response. To determine the type of immunity present in the overexpressing and knockout tumors, we evaluated the expression of the transcription factors T-bet, GATA3, RORγt and FoxP3. In our tumors, T-bet was the only transcription factor that was significantly increased in the *Slpi-/-* tumors, which indicates a potential type 1 immunity in the absence of SLPI. Other

transcription factors showed no significant difference in CD4+ and CD8+ T cells, and thus SLPI does possibly not affect transcription factors.

Changes in SLPI tumor levels have all impacted myeloid cells and CD4+ T cells negatively, based on PD-L1 and PD-1 expression levels, but not CD8+ T cells. This could indicate that SLPI targets CD4+ bearing cells including myeloid cells, reducing their immune effect, and thus correlated with decreased survival. However, this was opposite to our survival study showing that high expression levels of SLPI are correlated with better prognosis. This is possibly due to some limitations that should be considered during a follow-up on this result. First, cancer cells were injected intraperitoneally during the survival study generating metastatic tumors present randomly around the peritoneal cavity where they may have different expression profiles of immune checkpoint markers, whereas the TME analysis used primary tumors generated through an intrabursal injection, with a less variant TME within the same group. Second, the sample size used for the analysis of the TME of the modified MOE $Pten^{shRNA}KRas^{G12V}$ model (only 2 per group) limits the strength of the conclusions that can be drawn from this aspect of the study. Lastly, the flow cytometry panels employed were limited to a few markers, restricting our ability to identify further subtypes and phenotypes within the immune populations present in the tumors.

Chapter 5: Conclusions

This study identified and analyzed human scRNA-seq datasets and discovered that SLPI is a factor produced predominantly by mesenchymal ovarian cancer cells. Ligand-receptor analysis indicated its association with CD4-expressing immune cells. Using mouse models of ovarian cancer and pathway-specific inhibitors to explore the mechanisms regulating SLPI expression, we identified the MEK/ERK signaling pathway as a key regulatory pathway. The association of SLPI

expression with survival differs in humans vs. mice, but the knockout and overexpression in mouse models generated consistent outcomes. SLPI secretion within the tumor microenvironment had no impact on the proportion of the various immune cell populations but was associated with an increased expression of immune checkpoint molecules, particularly PD-1 and its ligand PD-L1. Its effect is mainly observed in CD4+ T cells, whereas CD8+ T cells show no change in response to SLPI expression both *in vitro* and *in vivo.* These results suggest that SLPI should be investigated further as a potential therapeutic target to improve the immune response in ovarian cancer.

References:

1. Hanahan, D. Hallmarks of Cancer: New Dimensions. *Cancer Discov.* **12**, 31–46 (2022).

2. Hanahan, D. & Weinberg, R. A. Hallmarks of Cancer: The Next Generation. *Cell* **144**, 646–674 (2011).

3. Gebretsadik, A., Bogale, N. & Dulla, D. Descriptive epidemiology of gynaecological cancers in southern Ethiopia: retrospective cross-sectional review. *BMJ Open* **12**, e062633 (2022).

4. Canadian Cancer Society. Uterine cancer statistics. *Canadian Cancer Society* https://cancer.ca/ (2024).

5. Canadian Cancer Society. Ovarian cancer statistics. *Canadian Cancer Society* https://cancer.ca/ (2024).

6. Brenner, D. R. *et al.* Projected estimates of cancer in Canada in 2024. *CMAJ* **196**, E615–E623 (2024).

7. Canadian Cancer Society. Survival statistics for ovarian cancer. *Canadian Cancer Society* https://cancer.ca/.

8. Kim, M.-K. *et al.* A hospital-based case-control study of identifying ovarian cancer using symptom index. *J. Gynecol. Oncol.* **20**, 238–242 (2009).

9. Salehi, F., Dunfield, L., Phillips, K. P., Krewski, D. & Vanderhyden, B. C. Risk factors for ovarian cancer: an overview with emphasis on hormonal factors. *J. Toxicol. Environ. Health B Crit. Rev.* **11**, 301–321 (2008).

10. Horackova, K., Janatova, M., Kleiblova, P., Kleibl, Z. & Soukupova, J. Early-Onset Ovarian Cancer <30 Years: What Do We Know about Its Genetic Predisposition? *Int. J. Mol. Sci.* **24**, 17020 (2023).

11. Momenimovahed, Z., Tiznobaik, A., Taheri, S. & Salehiniya, H. Ovarian cancer in the world: epidemiology and risk factors. *Int. J. Womens Health* **11**, 287–299 (2019).

12. Zayyan, M. S. Risk Factors for Ovarian Cancer. in *Tumor Progression and Metastasis* (IntechOpen, 2020). doi:10.5772/intechopen.86712.

13. Types of ovarian cancer | Ovarian cancer information. *Ovarian Cancer Action* https://ovarian.org.uk/ovarian-cancer/types-of-ovarian-cancer/ (2024).

14. Arora, T., Mullangi, S., Vadakekut, E. S. & Lekkala, M. R. Epithelial Ovarian Cancer. in *StatPearls* (StatPearls Publishing, Treasure Island (FL), 2024).

15. Köbel, M. & Kang, E. Y. The Evolution of Ovarian Carcinoma Subclassification. *Cancers* **14**, 416 (2022).

16. McConechy, M. K. *et al.* Ovarian and endometrial endometrioid carcinomas have distinct CTNNB1 and PTEN mutation profiles. *Mod. Pathol. Off. J. U. S. Can. Acad. Pathol. Inc* **27**, 128–134 (2014).

17. Nakayama, K., Razia, S., Ishibashi, T. & Kyo, S. Current concept of low-grade serous ovarian carcinoma. *Transl. Cancer Res.* **13**, 6–10 (2024).

18. Nugawela, D. & Gorringe, K. L. Targeted therapy for mucinous ovarian carcinoma: evidence from clinical trials. *Int. J. Gynecol. Cancer* **33**, 102–108 (2023).

19. National Academies of Sciences,. The Biology of Ovarian Cancers. in *Ovarian Cancers: Evolving Paradigms in Research and Care.* (National Academies Press (US), 2016).

20. Kim, J. *et al.* Cell Origins of High-Grade Serous Ovarian Cancer. *Cancers* **10**, 433 (2018).

21. Duffy, M. J., Synnott, N. C., O'Grady, S. & Crown, J. Targeting p53 for the treatment of cancer. *Semin. Cancer Biol.* **79**, 58–67 (2022).

22. Zhang, Y., Cao, L., Nguyen, D. & Lu, H. TP53 mutations in epithelial ovarian cancer. *Transl. Cancer Res.* **5**, 650–663 (2016).

23. Adamson, A. W. *et al.* Genomic analyses of germline and somatic variation in high-grade serous ovarian cancer. *J. Ovarian Res.* **16**, 141 (2023).

24. Sanchez-Vega, F. *et al.* Oncogenic Signaling Pathways in The Cancer Genome Atlas. *Cell* **173**, 321-337.e10 (2018).

25. He, Y. *et al.* Targeting PI3K/Akt signal transduction for cancer therapy. *Signal Transduct. Target. Ther.* **6**, 1–17 (2021).

26. Bahar, M. E., Kim, H. J. & Kim, D. R. Targeting the RAS/RAF/MAPK pathway for cancer therapy: from mechanism to clinical studies. *Signal Transduct. Target. Ther.* **8**, 1–38 (2023).

27. Kumari, A. *et al.* TGFβ signaling networks in ovarian cancer progression and plasticity. *Clin. Exp. Metastasis* **38**, 139–161 (2021).

28. Derynck, R. & Budi, E. H. Specificity, versatility and control of TGF-β family signaling. *Sci. Signal.* **12**, eaav5183 (2019).

29. Lei, Z.-N. *et al.* Signaling pathways and therapeutic interventions in gastric cancer. *Signal Transduct. Target. Ther.* **7**, 1–38 (2022).

30. Wu, J. *et al.* Plasticity of cancer cell invasion: Patterns and mechanisms. *Transl. Oncol.* **14**, 100899 (2020).

31. Derynck, R., Turley, S. J. & Akhurst, R. J. TGF-β biology in cancer progression and tumor immunotherapy. *Nat. Rev. Clin. Oncol.* **18**, 9–34 (2021).

32. Škovierová, H., Okajčeková, T., Strnádel, J., Vidomanová, E. & Halašová, E. Molecular regulation of epithelial-to-mesenchymal transition in tumorigenesis (Review). *Int. J. Mol. Med.* **41**, 1187–1200 (2018).

33. Al Habyan, S., Kalos, C., Szymborski, J. & McCaffrey, L. Multicellular detachment generates metastatic spheroids during intra-abdominal dissemination in epithelial ovarian cancer. *Oncogene* **37**, 5127–5135 (2018).

34. Iwagoi, Y. *et al.* Omental metastasis as a predictive risk factor for unfavorable prognosis in patients with stage III–IV epithelial ovarian cancer. *Int. J. Clin. Oncol.* **26**, 995–1004 (2021).

35. Motohara, T. *et al.* An evolving story of the metastatic voyage of ovarian cancer cells: cellular and molecular orchestration of the adipose-rich metastatic microenvironment. *Oncogene* **38**, 2885–2898 (2019).

36. Loret, N., Denys, H., Tummers, P. & Berx, G. The Role of Epithelial-to-Mesenchymal Plasticity in Ovarian Cancer Progression and Therapy Resistance. *Cancers* **11**, 838 (2019).

37. Taki, M. *et al.* Tumor Immune Microenvironment during Epithelial–Mesenchymal Transition. *Clin. Cancer Res.* **27**, 4669–4679 (2021).

38. Anderson, N. M. & Simon, M. C. The tumor microenvironment. *Curr. Biol.* **30**, R921–R925 (2020).

39. Vázquez-García, I. *et al.* Ovarian cancer mutational processes drive site-specific immune evasion. *Nature* **612**, 778–786 (2022).

40. Rodriguez, G. M., Galpin, K. J. C., McCloskey, C. W. & Vanderhyden, B. C. The Tumor Microenvironment of Epithelial Ovarian Cancer and Its Influence on Response to Immunotherapy. *Cancers* **10**, 242 (2018).

41. Garlisi, B. *et al.* The Complex Tumor Microenvironment in Ovarian Cancer: Therapeutic Challenges and Opportunities. *Curr. Oncol.* **31**, 3826–3844 (2024).

42. Ribatti, D., Tamma, R. & Annese, T. Epithelial-Mesenchymal Transition in Cancer: A Historical Overview. *Transl. Oncol.* **13**, 100773 (2020).

43. Barford, D., Flint, A. J. & Tonks, N. K. Crystal structure of human protein tyrosine phosphatase 1B. *Science* **263**, 1397–1404 (1994).

44. Kondo, M. Lymphoid and myeloid lineage commitment in multipotent hematopoietic progenitors. *Immunol. Rev.* **238**, 37–46 (2010).

45. Yang, H., Parkhouse, R. M. E. & Wileman, T. Monoclonal antibodies that identify the CD3 molecules expressed specifically at the surface of porcine γδ-T cells. *Immunology* **115**, 189–196 (2005).

46. Cooper, M. A., Fehniger, T. A. & Caligiuri, M. A. The biology of human natural killer-cell subsets. *Trends Immunol.* **22**, 633–640 (2001).

47. Chen, X., Li, Y., Xia, H. & Chen, Y. H. Monocytes in Tumorigenesis and Tumor Immunotherapy. *Cells* **12**, 1673 (2023).

48. Zhang, W. *et al.* Macrophage polarization in the tumor microenvironment: Emerging roles and therapeutic potentials. *Biomed. Pharmacother.* **177**, 116930 (2024).

49. Del Prete, A. *et al.* Dendritic cell subsets in cancer immunity and tumor antigen sensing. *Cell. Mol. Immunol.* **20**, 432–447 (2023).

50. Whiteside, T. L. 3. Tumor-infiltrating lymphocytes and their role in solid tumor progression. *Exp. Suppl. 2012* **113**, 89–106 (2022).

51. Broz, M. L. & Krummel, M. F. The Emerging Understanding of Myeloid Cells as Partners and Targets in Tumor Rejection. *Cancer Immunol. Res.* **3**, 313–319 (2015).

52. Yakubovich, E., Cook, D. P., Rodriguez, G. M. & Vanderhyden, B. C. Mesenchymal ovarian cancer cells promote CD8+ T cell exhaustion through the LGALS3-LAG3 axis. *NPJ Syst. Biol. Appl.* **9**, 61 (2023).

53. Kandalaft, L. E., Dangaj Laniti, D. & Coukos, G. Immunobiology of high-grade serous ovarian cancer: lessons for clinical translation. *Nat. Rev. Cancer* **22**, 640–656 (2022).

54. Carter, J. S. & Downs, L. S. Ovarian Cancer Tests and Treatment. *Female Patient* **36**, 30–35 (2011).

55. Pawłowska, A. *et al.* Current Understanding on Why Ovarian Cancer Is Resistant to Immune Checkpoint Inhibitors. *Int. J. Mol. Sci.* **24**, 10859 (2023).

56. Kartikasari, A. E. R., Huertas, C. S., Mitchell, A. & Plebanski, M. Tumor-Induced Inflammatory Cytokines and the Emerging Diagnostic Devices for Cancer Detection and Prognosis. *Front. Oncol.* **11**, (2021).

57. Zhao, H. *et al.* Inflammation and tumor progression: signaling pathways and targeted intervention. *Signal Transduct. Target. Ther.* **6**, 1–46 (2021).

58. Huang, R.-Y. *et al.* LAG3 and PD1 co-inhibitory molecules collaborate to limit CD8+ T cell signaling and dampen antitumor immunity in a murine ovarian cancer model. *Oncotarget* **6**, 27359–27377 (2015).

59. Kozłowski, M., Borzyszkowska, D. & Cymbaluk-Płoska, A. The Role of TIM-3 and LAG-3 in the Microenvironment and Immunotherapy of Ovarian Cancer. *Biomedicines* **10**, 2826 (2022).

60. Yoon, W.-H., DeFazio, A. & Kasherman, L. Immune checkpoint inhibitors in ovarian cancer: where do we go from here? *Cancer Drug Resist.* **6**, 358–377 (2023).

61. Rotte, A. Combination of CTLA-4 and PD-1 blockers for treatment of cancer. *J. Exp. Clin. Cancer Res.* **38**, 255 (2019).

62. Farokhi Boroujeni, S. *et al.* BRCA1 and BRCA2 deficient tumour models generate distinct ovarian tumour microenvironments and differential responses to therapy. *J. Ovarian Res.* **16**, 231 (2023).

63. James, N. E., Gura, M., Woodman, M., Freiman, R. N. & Ribeiro, J. R. A bioinformatic analysis of WFDC2 (HE4) expression in high grade serous ovarian cancer reveals tumor-specific changes in metabolic and extracellular matrix gene expression. *Med. Oncol.* **39**, 71 (2022).

64. Olalekan, S., Xie, B., Back, R., Eckart, H. & Basu, A. Characterizing the tumor microenvironment of metastatic ovarian cancer by single-cell transcriptomics. *Cell Rep.* **35**, 109165 (2021).

65. Geistlinger, L. *et al.* Multi-omic analysis of subtype evolution and heterogeneity in high-grade serous ovarian carcinoma. *Cancer Res.* **80**, 4335–4345 (2020).

66. Qian, J. *et al.* A pan-cancer blueprint of the heterogeneous tumor microenvironment revealed by single-cell profiling. *Cell Res.* **30**, 745–762 (2020).

67. Hornburg, M. *et al.* Single-cell dissection of cellular components and interactions shaping the tumor immune phenotypes in ovarian cancer. *Cancer Cell* **39**, 928-944.e6 (2021).

68. Stuart, T. *et al.* Comprehensive Integration of Single-Cell Data. *Cell* **177**, 1888-1902.e21 (2019).

69. Hao, Y. *et al.* Integrated analysis of multimodal single-cell data. *Cell* **184**, 3573-3587.e29 (2021).

70. Cook, D. P. & Vanderhyden, B. C. Transcriptional census of epithelial-mesenchymal plasticity in cancer. *Sci. Adv.* **8**, eabi7640 (2022).

71. Dimitrov, D. *et al.* Comparison of methods and resources for cell-cell communication inference from single-cell RNA-Seq data. *Nat. Commun.* **13**, 3224 (2022).

72. Gu, Z., Gu, L., Eils, R., Schlesner, M. & Brors, B. circlize Implements and enhances circular visualization in R. *Bioinforma. Oxf. Engl.* **30**, 2811–2812 (2014).

73. Cook, D. P. *et al.* Comparative analysis of syngeneic mouse models of high-grade serous ovarian cancer. *Commun. Biol.* **6**, 1152 (2023).

74. Iyer, S. *et al.* Genetically Defined Syngeneic Mouse Models of Ovarian Cancer as Tools for the Discovery of Combination Immunotherapy. *Cancer Discov.* **11**, 384–407 (2021).

75. Walton, J. *et al.* CRISPR/Cas9-Mediated Trp53 and Brca2 Knockout to Generate Improved Murine Models of Ovarian High-Grade Serous Carcinoma. *Cancer Res.* **76**, 6118–6129 (2016).

76. Al-Hujaily, E. M. *et al.* Divergent Roles of PAX2 in the Etiology and Progression of Ovarian Cancer. *Cancer Prev. Res. (Phila. Pa.)* **8**, 1163–1173 (2015).

77. McCloskey, C. W. *et al.* A new spontaneously transformed syngeneic model of high-grade serous ovarian cancer with a tumor-initiating cell population. *Front. Oncol.* **4**, 53 (2014).

78. Eddie, S. L. *et al.* Tumorigenesis and peritoneal colonization from fallopian tube epithelium. *Oncotarget* **6**, 20500–20512 (2015).

79. Alwosaibai, K. *et al.* PAX2 maintains the differentiation of mouse oviductal epithelium and inhibits the transition to a stem cell-like state. *Oncotarget* **8**, 76881–76897 (2017).

80. Xu, J., Lamouille, S. & Derynck, R. TGF-β-induced epithelial to mesenchymal transition. *Cell Res.* **19**, 156–172 (2009).

81. Létourneau, S., Krieg, C., Pantaleo, G. & Boyman, O. IL-2– and CD25-dependent immunoregulatory mechanisms in the homeostasis of T-cell subsets. *J. Allergy Clin. Immunol.* **123**, 758–762 (2009).

82. Yang, S., Liu, F., Wang, Q. J., Rosenberg, S. A. & Morgan, R. A. The Shedding of CD62L (L-Selectin) Regulates the Acquisition of Lytic Activity in Human Tumor Reactive T Lymphocytes. *PLOS ONE* **6**, e22560 (2011).

83. Mehta, A. & Merkel, O. M. Immunogenicity of Cas9 Protein. *J. Pharm. Sci.* **109**, 62 (2020).

84. Rodriguez, G. M. *et al.* The Tumor Immune Profile of Murine Ovarian Cancer Models: An Essential Tool for Ovarian Cancer Immunotherapy Research. *Cancer Res. Commun.* **2**, 417–433 (2022).

85. Medoff, B. D. *et al.* CD11b+ Myeloid Cells Are the Key Mediators of Th2 Cell Homing into the Airway in Allergic Inflammation1. *J. Immunol.* **182**, 623–635 (2009).

86. Blank, C., Gajewski, T. F. & Mackensen, A. Interaction of PD-L1 on tumor cells with PD-1 on tumor-specific T cells as a mechanism of immune evasion: implications for tumor immunotherapy. *Cancer Immunol. Immunother. CII* **54**, 307–314 (2005).

87. Fontenot, J. D. *et al.* Regulatory T Cell Lineage Specification by the Forkhead Transcription Factor Foxp3. *Immunity* **22**, 329–341 (2005).

88. Yeh, C. Y. *et al.* Mapping ovarian cancer spatial organization uncovers immune evasion drivers at the genetic, cellular, and tissue level. 2023.10.16.562592 Preprint at https://doi.org/10.1101/2023.10.16.562592 (2023).

89. Olingy, C. E., Dinh, H. Q. & Hedrick, C. C. Monocyte heterogeneity and functions in cancer. *J. Leukoc. Biol.* **106**, 309–322 (2019).

90. McNeely, T. B. *et al.* Secretory leukocyte protease inhibitor: a human saliva protein exhibiting anti-human immunodeficiency virus 1 activity in vitro. *J. Clin. Invest.* **96**, 456–464 (1995).

91. Dupont, M. & Sattentau, Q. J. Macrophage Cell-Cell Interactions Promoting HIV-1 Infection. *Viruses* **12**, 492 (2020).

92. Joseph, S. B. & Swanstrom, R. The evolution of HIV-1 entry phenotypes as a guide to changing target cells. *J. Leukoc. Biol.* **103**, 421–431 (2018).

93. Nittayananta, W., Kemapunmanus, M., Yangngam, S., Talungchit, S. & Sriplung, H. Expression of oral secretory leukocyte protease inhibitor in HIV-infected subjects with long-term use of antiretroviral therapy. *J. Oral Pathol. Med.* **42**, 208–215 (2013).

94. Py, B. *et al.* The Phospholipid Scramblases 1 and 4 Are Cellular Receptors for the Secretory Leukocyte Protease Inhibitor and Interact with CD4 at the Plasma Membrane. *PLoS ONE* **4**, e5006 (2009).

95. Thompson, R. C. & Ohlsson, K. Isolation, properties, and complete amino acid sequence of human secretory leukocyte protease inhibitor, a potent inhibitor of leukocyte elastase. *Proc. Natl. Acad. Sci. U. S. A.* **83**, 6692–6696 (1986).

96. Kikuchi, T. *et al.* Structure of the Murine Secretory Leukoprotease Inhibitor (Slpi) Gene and Chromosomal Localization of the Human and Murine SLPI Genes. *Am. J. Respir. Cell Mol. Biol.* **19**, 875–880 (1998).

97. Zakrzewicz, A. *et al.* SLPI Inhibits ATP-Mediated Maturation of IL-1β in Human Monocytic Leukocytes: A Novel Function of an Old Player. *Front. Immunol.* **10**, (2019).

98. Eisenberg, S. P., Hale, K. K., Heimdal, P. & Thompson, R. C. Location of the protease-inhibitory region of secretory leukocyte protease inhibitor. *J. Biol. Chem.* **265**, 7976–7981 (1990).

99. Nugteren, S. *et al.* Expression of the immune modulator secretory leukocyte protease inhibitor (SLPI) in colorectal cancer liver metastases and matched primary tumors is associated with a poorer prognosis. *OncoImmunology* **9**, 1832761 (2020).

100. Si-Tahar, M., Merlin, D., Sitaraman, S. & Madara, J. L. Constitutive and regulated secretion of secretory leukocyte proteinase inhibitor by human intestinal epithelial cells. *Gastroenterology* **118**, 1061–1071 (2000).

101. Taggart, C. C., Greene, C. M., McElvaney, N. G. & O'Neill, S. Secretory Leucoprotease Inhibitor Prevents Lipopolysaccharide-induced IκBα Degradation without Affecting Phosphorylation or Ubiquitination *. *J. Biol. Chem.* **277**, 33648–33653 (2002).

102. Hajishengallis, G. & Russell, M. W. Innate Humoral Defense Factors. *Mucosal Immunol.* 251–270 (2015) doi:10.1016/B978-0-12-415847-4.00015-X.

103. Nugteren, S. & Samsom, J. N. Secretory Leukocyte Protease Inhibitor (SLPI) in mucosal tissues: Protects against inflammation, but promotes cancer. *Cytokine Growth Factor Rev.* **59**, 22–35 (2021).

104. Greene, C. M., McElvaney, N. G., O'Neill, S. J. & Taggart, C. C. Secretory Leucoprotease Inhibitor Impairs Toll-Like Receptor 2- and 4-Mediated Responses in Monocytic Cells. *Infect. Immun.* **72**, 3684–3687 (2004).

105. Guerrieri, D. *et al.* Serine leucocyte proteinase inhibitor-treated monocyte inhibits human CD4+ lymphocyte proliferation. *Immunology* **133**, 434–441 (2011).

106. Iyer, S. S. & Cheng, G. Role of Interleukin 10 Transcriptional Regulation in Inflammation and Autoimmune Disease. *Crit. Rev. Immunol.* **32**, 23–63 (2012).

107. Bent, E. H. *et al.* Microenvironmental IL-6 inhibits anti-cancer immune responses generated by cytotoxic chemotherapy. *Nat. Commun.* **12**, 6218 (2021).

108. Yang, W.-C. *et al.* Interleukin-4 Supports the Suppressive Immune Responses Elicited by Regulatory T Cells. *Front. Immunol.* **8**, (2017).

109. Lynch, G. W. *et al.* Marked differences in the structures and protein associations of lymphocyte and monocyte CD4: Resolution of a novel CD4 isoform. *Immunol. Cell Biol.* **84**, 154–165 (2006).

110. Vermeire, E. C. and K. The CD4 Receptor: An Indispensable Protein in T Cell Activation and A Promising Target for Immunosuppression. *Arch. Microbiol. Immunol.* **3**, 133–150 (2019).

111. Murphy, K. M. Janeway's immunobiology /. (2017).

112. Laopajon, W., Cheyasawan, P., Pata, S., Takheaw, N. & Kasinrerk, W. The ligation of CD4 molecules, expressed on monocytes by an anti-CD4 monoclonal antibody, inhibits T cell activation and monocyte mobility. *Asian Pac. J. Allergy Immunol.* (2023) doi:10.12932/AP-150123-1532.

113. Zhen, A. *et al.* CD4 Ligation on Human Blood Monocytes Triggers Macrophage Differentiation and Enhances HIV Infection. *J. Virol.* **88**, 9934–9946 (2014).

114. Xie, W. *et al.* The expression and clinical significance of secretory leukocyte proteinase inhibitor (SLPI) in mammary carcinoma using bioinformatics analysis. *Gene* **720**, 144088 (2019).

115. Sayers, K. T., Brooks, A. D., Sayers, T. J. & Chertov, O. Increased Secretory Leukocyte Protease Inhibitor (SLPI) Production by Highly Metastatic Mouse Breast Cancer Cells. *PLOS ONE* **9**, e104223 (2014).

116. Liu, G. *et al.* Expression of secretory leukocyte protease inhibitor detected by immunohistochemistry correlating with prognosis and metastasis in colorectal cancer. *World J. Surg. Oncol.* **12**, 369 (2014).

117. Wei, Z. *et al.* Targeting secretory leukocyte protease inhibitor (SLPI) inhibits colorectal cancer cell growth, migration and invasion via downregulation of AKT. *PeerJ* **8**, e9400 (2020).

118. Du, X.-Y., Liu, X., Wang, Z.-J. & Wang, Y.-Y. SLPI promotes the gastric cancer growth and metastasis by regulating the expression of P53, Bcl-2 and Caspase-8. *Eur. Rev. Med. Pharmacol. Sci.* **21**, 1495–1501 (2017).

119. Noorlag, R. *et al.* Nodal metastasis and survival in oral cancer: Association with protein expression of SLPI, not with LCN2, TACSTD2, or THBS2. *Head Neck* **37**, 1130–1136 (2015).

120. Tsukishiro, S., Suzumori, N., Nishikawa, H., Arakawa, A. & Suzumori, K. Use of serum secretory leukocyte protease inhibitor levels in patients to improve specificity of ovarian cancer diagnosis. *Gynecol. Oncol.* **96**, 516–519 (2005).

121. Carlson, A. M. *et al.* Utility of Progranulin and Serum Leukocyte Protease Inhibitor as Diagnostic and Prognostic Biomarkers in Ovarian Cancer. *Cancer Epidemiol. Biomarkers Prev.* **22**, 1730–1735 (2013).

122. Timms, J. F. *et al.* Discovery of serum biomarkers of ovarian cancer using complementary proteomic profiling strategies. *PROTEOMICS – Clin. Appl.* **8**, 982–993 (2014).

123. Devoogdt, N. *et al.* Overexpression of protease inhibitor-dead secretory leukocyte protease inhibitor causes more aggressive ovarian cancer in vitro and in vivo. *Cancer Sci.* **100**, 434–440 (2009).

124. Simpkins, F. A. *et al.* The alarm anti-protease, secretory leukocyte protease inhibitor, is a proliferation and survival factor for ovarian cancer cells. *Carcinogenesis* **29**, 466–472 (2008).

125. Roby, K. F. *et al.* Development of a syngeneic mouse model for events related to ovarian cancer. *Carcinogenesis* **21**, 585–591 (2000).

126. Neff, R. T., Senter, L. & Salani, R. BRCA mutation in ovarian cancer: testing, implications and treatment considerations. *Ther. Adv. Med. Oncol.* **9**, 519–531 (2017).

127. Wei, Z. *et al.* Inhibition of secretory leukocyte protease inhibitor (SLPI) promotes the PUMA-mediated apoptosis and chemosensitivity to cisplatin in colorectal cancer cells. *Discov. Oncol.* **14**, 1 (2023).

128. Yang, L. *et al.* Molecular mechanisms of platinum-based chemotherapy resistance in ovarian cancer (Review). *Oncol. Rep.* **47**, 1–11 (2022).

129. Rasool, N. *et al.* Secretory Leukocyte Protease Inhibitor Antagonizes Paclitaxel in Ovarian Cancer Cells. *Clin. Cancer Res.* **16**, 600–609 (2010).

130. Maloney, S. M., Hoover, C. A., Morejon-Lasso, L. V. & Prosperi, J. R. Mechanisms of Taxane Resistance. *Cancers* **12**, 3323 (2020).

131. Majchrzak-Gorecka, M., Majewski, P., Grygier, B., Murzyn, K. & Cichy, J. Secretory leukocyte protease inhibitor (SLPI), a multifunctional protein in the host defense response. *Cytokine Growth Factor Rev.* **28**, 79–93 (2016).

132. Ashcroft, G. S. *et al.* Secretory leukocyte protease inhibitor mediates non-redundant functions necessary for normal wound healing. *Nat. Med.* **6**, 1147–1153 (2000).

133. Påhlman, L. I., Jögi, A., Gram, M., Mori, M. & Egesten, A. Hypoxia down-regulates expression of secretory leukocyte protease inhibitor in bronchial epithelial cells via TGF-β1. *BMC Pulm. Med.* **15**, 19 (2015).

134. Luo, B.-L. *et al.* Downregulation of Secretory Leukocyte Proteinase Inhibitor in Chronic Obstructive Lung Disease: The Role Of TGF-β/Smads Signaling Pathways. *Arch. Med. Res.* **39**, 388–396 (2008).

135. Zhang, D. *et al.* Secretory Leukocyte Protease Inhibitor Mediates Proliferation of Human Endometrial Epithelial Cells by Positive and Negative Regulation of Growth-associated Genes *. *J. Biol. Chem.* **277**, 29999–30009 (2002).

136. Li, C.-W. *et al.* Epithelial–Mesenchymal Transition Induced by TNF-α Requires NF-κB–Mediated Transcriptional Upregulation of Twist1. *Cancer Res.* **72**, 1290–1300 (2012).

137. Devoogdt, N. *et al.* The Tumor-Promoting Effect of TNF-α Involves the Induction of Secretory Leukocyte Protease Inhibitor1. *J. Immunol.* **177**, 8046–8052 (2006).

138. Munn, L. L. & Garkavtsev, I. SLPI: a new target for stopping metastasis. *Aging* **10**, 13–14 (2018).

139. Rosso, M. *et al.* Secretory Leukocyte Protease Inhibitor (SLPI) expression downregulates E-cadherin, induces β-catenin re-localisation and triggers apoptosis-related events in breast cancer cells. *Biol. Cell* **106**, 308–322 (2014).

140. Kozin, S. V. *et al.* Secretory leukocyte protease inhibitor (SLPI) as a potential target for inhibiting metastasis of triple-negative breast cancers. *Oncotarget* **8**, 108292–108302 (2017).

141. Wang, N. *et al.* The Secretory Leukocyte Protease Inhibitor Is a Type 1 Insulin-Like Growth Factor Receptor–Regulated Protein that Protects against Liver Metastasis by Attenuating the Host Proinflammatory Response. *Cancer Res.* **66**, 3062–3070 (2006).

142. Tsang, Y. T. *et al.* KRAS (but not BRAF) mutations in ovarian serous borderline tumor are associated with recurrent low-grade serous carcinoma. *J. Pathol.* **231**, 449–456 (2013).

143. Dehari, R., Kurman, R. J., Logani, S. & Shih, I.-M. The development of high-grade serous carcinoma from atypical proliferative (borderline) serous tumors and low-grade micropapillary serous carcinoma: a morphologic and molecular genetic analysis. *Am. J. Surg. Pathol.* **31**, 1007–1012 (2007).

144. Ferreira, A. *et al.* Crucial Role of Oncogenic KRAS Mutations in Apoptosis and Autophagy Regulation: Therapeutic Implications. *Cells* **11**, 2183 (2022).

145. Jančík, S., Drábek, J., Radzioch, D. & Hajdúch, M. Clinical Relevance of KRAS in Human Cancers. *J. Biomed. Biotechnol.* **2010**, (2010).

146. Simanshu, D. K., Nissley, D. V. & McCormick, F. RAS Proteins and Their Regulators in Human Disease. *Cell* **170**, 17–33 (2017).

147. Hunter, J. C. *et al.* Biochemical and Structural Analysis of Common Cancer-Associated KRAS Mutations. *Mol. Cancer Res. MCR* **13**, 1325–1335 (2015).

148. Kim, H. J., Lee, H. N., Jeong, M. S. & Jang, S. B. Oncogenic KRAS: Signaling and Drug Resistance. *Cancers* **13**, 5599 (2021).

149. Therachiyil, L. *et al.* Role of RAS signaling in ovarian cancer. *F1000Research* **11**, 1253 (2022).

150. Vroling, A. B., Konijn, T., Samsom, J. N. & Kraal, G. The production of secretory leukocyte protease inhibitor by dendritic cells. *Mol. Immunol.* **48**, 630–636 (2011).

151. Dustin, M. L. The Immunological Synapse. *Cancer Immunol. Res.* **2**, 1023–1033 (2014).

152. Li, Y. & Kurlander, R. J. Comparison of anti-CD3 and anti-CD28-coated beads with soluble anti-CD3 for expanding human T cells: Differing impact on CD8 T cell phenotype and responsiveness to restimulation. *J. Transl. Med.* **8**, 104 (2010).

153. Shi, L., Chen, S., Yang, L. & Li, Y. The role of PD-1 and PD-L1 in T-cell immune suppression in patients with hematological malignancies. *J. Hematol. Oncol.J Hematol Oncol* **6**, 74 (2013).

154. Lin, X. *et al.* Regulatory mechanisms of PD-1/PD-L1 in cancers. *Mol. Cancer* **23**, 108 (2024).

155. Kamalov, M. *et al.* Ovalbumin Epitope SIINFEKL Self-Assembles into a Supramolecular Hydrogel. *Sci. Rep.* **9**, 2696 (2019).

156. Zöphel, D. *et al.* Heterozygous OT-I mice reveal that antigen-specific CD8 + T cells shift from apoptotic to necrotic killers in the elderly. *Aging Cell* **22**, e13824 (2023).

157. Chua, X. Y. & Salomon, A. Ovalbumin antigen-specific activation of T cell receptor closely resembles soluble antibody stimulation as revealed by BOOST phosphotyrosine proteomics. 2021.03.25.436968 Preprint at https://doi.org/10.1101/2021.03.25.436968 (2021).

158. Divangahi, M. *et al.* Trained immunity, tolerance, priming and differentiation: distinct immunological processes. *Nat. Immunol.* **22**, 2–6 (2021).

159. Kroegel, C. *et al.* Putting priming into perspective – from cellular heterogeneity to cellular plasticity. *Immunol. Today* **21**, 218–222 (2000).

160. Zhang, E. *et al.* Roles and mechanisms of tumour-infiltrating B cells in human cancer: a new force in immunotherapy. *Biomark. Res.* **11**, 28 (2023).

161. Kallies, A. & Good-Jacobson, K. L. Transcription Factor T-bet Orchestrates Lineage Development and Function in the Immune System. *Trends Immunol.* **38**, 287–297 (2017).

162. Annunziato, F., Romagnani, C. & Romagnani, S. The 3 major types of innate and adaptive cell-mediated effector immunity. *J. Allergy Clin. Immunol.* **135**, 626–635 (2015).

163. Pai, S.-Y., Truitt, M. L. & Ho, I.-C. GATA-3 deficiency abrogates the development and maintenance of T helper type 2 cells. *Proc. Natl. Acad. Sci. U. S. A.* **101**, 1993–1998 (2004).

164. Wan, Y. Y. GATA3: A master of many trades in immune regulation. *Trends Immunol.* **35**, 233–242 (2014).

165. Kim, B.-S. *et al.* Type 17 immunity promotes the exhaustion of CD8+ T cells in cancer. *J. Immunother. Cancer* **9**, e002603 (2021).

166. Hamada, H. *et al.* Tc17, a Unique Subset of CD8 T Cells That Can Protect against Lethal Influenza Challenge. *J. Immunol.* **182**, 3469–3481 (2009).

167. Liston, A. & Aloulou, M. A fresh look at a neglected regulatory lineage: CD8+Foxp3+ Regulatory T cells. *Immunol. Lett.* **247**, 22–26 (2022).